Impact of competing anions on the sorption of trivalent actinides onto clay mineral surfaces

Zur Erlangung des akademischen Grades eines
DOKTORS DER NATURWISSENSCHAFTEN
(Dr. rer. nat.)

von der KIT-Fakultät für Chemie und Biowissenschaften
des Karlsruher Instituts für Technologie (KIT) - Universitätsbereich

genehmigte
DISSERTATION

von
M.Sc. Felix Rieder
aus
Landau in der Pfalz, Deutschland

Dekan: Prof. Dr. Reinhard Fischer
Referent: Prof. Dr. Horst Geckeis
Korreferent: Prof. Dr. Petra Panak
Tag der mündlichen Prüfung: 11.10.2019

Für meine Frau Kim
und meine Eltern

“Stop giving power to people who don't believe in science.”

(Harrison Ford)

Erklärung

Hiermit versichere ich, dass ich die vorliegende Arbeit selbständig verfasst und keine anderen als die angegebenen Quellen und Hilfsmittel verwendet habe. Darüber hinaus versichere ich, dass alle Stellen der Arbeit, die wörtlich oder sinngemäß aus anderen Quellen übernommen wurden, als solche kenntlich gemacht sind und dass die Arbeit in gleicher oder ähnlicher Form noch keiner Prüfungsbehörde vorgelegt wurde. Die Satzung des Karlsruher Instituts für Technologie (KIT) zur Sicherung guter wissenschaftlicher Praxis wurde in der jeweils gültigen Fassung beachtet.

Karlsruhe, den 21.11.2019

Ort, Datum Unterschrift

Danksagung

Hiermit möchte ich mich bei allen bedanken, die durch ihren Rat, ihre Hilfe und Unterstützung zum Gelingen dieser Arbeit beigetragen haben.
Allen voran möchte ich mich bei Herrn Prof. Dr. Horst Geckeis für die hochinteressante und experimental anspruchsvolle Aufgabenstellung, die freundliche Aufnahme am Institut und die wissenschaftliche Betreuung bedanken.
Ich danke Frau Prof. Dr. Petra Panak für die Übernahme des Koreferates und die zahlreichen wissenschaftlichen Diskussionen.
Herrn Dr. Thomas Rabung danke ich für die teils lebhaften aber immer hilfreichen und lehrreichen Diskussionen zur experimentellen Umsetzung und Interpretation der im Rahmen der vorliegenden Arbeit erzielten Ergebnisse. Es war mir eine sehr große Hilfe, dass Du meine Arbeit trotz neuer Aufgaben bis zuletzt betreut hast.
Für die freundliche Aufnahme in die Abteilung der Geochemie und die Abteilung der Aquatischen Chemie möchte ich mich bei Herrn Prof. Dr. Thorsten Schäfer und Herrn Dr. Marcus Altmaier bedanken.
Herrn Dr. Andrej Skerencak-Frech, Herrn Dr. Andreas Schnurr und Herrn Dr. Tomas Kupcik danke ich für die stetige Hilfsbereitschaft, mich im praktischen Laboralltag bei der Lösung von kleinen und größeren Probleme zu unterstützen.
Für die Unterstützung bei der Bewältigung der größeren und kleineren Probleme des geochemischen Modellierens möchte ich Frau Dr. Vanessa Montoya danken. Die Diskussion rund um die Machbarkeit und Entwicklung neuer Modelle haben mir stets weitergeholfen. Herrn Dr. Michael Trumm verdanke ich einen tiefen Einblick in die Sorptionsprozesse auf molekularer Ebene. Es hat mich sehr gefreut, dass Du mir einen Zugang zu quantenchemischen Rechnungen ermöglicht hast und ich etwas besser verstehe, was die Welt (oder Tonminerale) im Innersten zusammenhält. Frau Dr. Nicole Adam möchte ich für die Einführung in die VSB Spektroskopie danken.
Herrn Dr. Dieter Schild, Herrn Dr. Nicola Fink und Frau Eva Soballa möchte ich für die Unterstützung im Bereich der Oberflächen- und Festkörperanalytik danken.
Einen großen Dank möchte ich Herrn Dr. Peter Weidler und Herrn Stefan Heißler (KIT-IFG) für die Messzeit und Unterstützung beim Nachweis der Sorption von Carbonat an Tonmineralen aussprechen.

Bei Herrn Dr. Andreas Bauer bedanke ich mich für das Vertrauen und die Interessanten Diskussionen von Tonmineralien bis Viehzucht.
Ein weiterer Dank geht für die technische Unterstützung meiner Experimente an Martina Schlieker, Volker Krepper und das gesamte Team der Werkstatt, sowie Jens Thomas, Andreas Bereswill und Erwin Schmitt. Genauso möchte ich Andreas Benzler für den unermüdlichen IT-Support danken.
Ebenfalls möchte ich „meinen“ Azubis Miriam Geiger und Jonas Rentmeister danken. Ich hatte große Freude an unserer gemeinsamen Arbeit. Nicht vergessen werden sollten an dieser Stelle Florian Steegborn, Sven Reech und Pauline Fouquet-Metivier. Ihr wart eine große Hilfe.
Gerd Christill, Thorsten Hoffmann und Ilonca Bachmann danke ich für die kompetente Beratung in Sachen Strahlenschutz und die gute Zusammenarbeit. Bernd Bummel möchte ich für die Unterstützung danken. Du hast mir meine Arbeit oft erleichtert und meist noch einen Witz parat gehabt.
Unserer Kaffeerunde, allen voran Madeleine, Martin und Christian (den anderen selbstverständlich auch!) möchte ich für die heiteren Stunden und Mittagspausen danken!
Allen Mitarbeitern des INE danke für die nette Aufnahme in ihre Reihen, das gute Arbeitsklima und die tolle Zeit.

Abschließend bedanke ich mich bei meiner Familie und meinen Freunden. Ganz besonders danke ich meinen Eltern und meiner Frau Kim. Ihr habt mich in den Höhen und Tiefen meines Lebens, Studiums und der Promotion immer unterstützt.

Abstract

Sorption processes on mineral phases are a key mechanism in the context of the safe final disposal of radioactive waste in deep geological formations. Especially clay mineral surfaces are known for their excellent adsorption properties of metal ions, like actinides and many fission products. Previous studies demonstrated their high retention abilities for diluted background electrolyte conditions (I_{max}= 0.7 M), comparable to pore water of bentonite and Opalinus clay (Switzerland), as well for saline conditions (I = 1-4 M) as described for Jurassic and lower Cretaceous clay rock layers Nnorthern Germany). The application of a geochemical model (2SPNE/CE), developed for diluted systems, was also demonstrated to be suitable for concentrated background electrolyte systems.

The influence of competing ligands on the adsorption of trivalent lanthanides and actinides onto the important natural clay minerals illite du Puy and montmorillonite was investigated within the present thesis. Sorption experiments were conducted under variation of the background electrolyte concentration, concentration of the competing ligand and the partial pressure of CO_2.

Representative competing ligands were chosen to study their impact on the An(III)/Ln(III) retention. The main focus was set on the influence of carbonate on the adsorption of trivalent lanthanides and actinides in NaCl electrolyte systems. Carbonate is omnipresent in natural groundwater. Due to the ability to form strong complexes with metal ions, carbonate is highly relevant for the geochemical behaviour of actinides. Beside carbonate, also gluconate and citrate were studied in NaCl and $CaCl_2$ background electrolyte solutions. Both ligands are model substances for cement additives. Gluconate is also studied as an analogue for isosaccharinic acid, a degradation product of cellulose. Citrate is commonly used as a decontaminant. For this reason both are part of the inventory of a repository for low and intermediate level waste.

In presence of carbonate, a somewhat increased retention of Eu(III) on clay minerals surfaces is observed in the slightly acidic and neutral pH range. Due to the formation of strong carbonate complexes, a strong decrease in retention is observed in the alkaline pH range. A variation of the applied partial pressure of CO_2 is significantly affecting the total concentration of dissolved carbonate / bicarbonate and by this the formation

of stable aquatic species. During the batch sorption studies, no indication of a significant effect of ionic strength was observed neither for the Eu(III) adsorption onto illite du Puy, nor on montmorillonite. With a combined study of quantum chemical calculations (DFT, AIMD) and spectroscopic methods (ATR-IR, TRLFS) it was possible to prove the adsorption of carbonate on the clay mineral surface. The adsorbed carbonate forms stable ternary surface complexes with Ln(III)/An(III), and, therefore, is responsible for enhancing the retention. At higher pH values a second surface sorbed complex containing an additional carbonate ligand is formed. These two carbonate stabilized surface complexes were implemented in a geochemical model (2SPNE/CE), resulting in a consistent model to accurately describe the adsorption of Eu(III) onto illite du Puy and montmorillonite for the whole pH range and under variation of ionic strength and the partial pressure of CO_2.

In presence of gluconate, the retention of Eu(III) onto illite du Puy and montmorillonite is significantly reduced between pH = 3-12.5 (up to three orders of magnitude). Using time resolved laser fluorescence spectroscopy, 3 pH regions of characteristic interactions of adsorbed and competing aquatic species were identified. The competition of aquatic species with the cation exchange was observed in the acidic pH and with inner sphere surface complexation from neutral to high pH. In presence of Ca^{2+} the existence and influence of quaternary Ca-Cm-OH-GLU could be monitored under alkaline conditions.

The presence of citrate is influencing the adsorption of Eu(III) onto clay minerals in 2 different ways. In NaCl background electrolyte solution a reduced retention is observed in the slightly acidic pH range, while the retention is increased in presence of Ca^{2+} in the same pH range. From neutral to high pH a nearly quantitative retention is observed in both systems.

Zusammenfassung

Sorptionsprozesse an Mineralphasen stellen im Kontext eines Endlagers für radioaktive Abfälle in tiefen geologischen Formationen einen wichtigen Rückhaltemechanismus für Actiniden und viele Spaltprodukte dar. Insbesondere Tonmineraloberflächen verfügen über exzellente Eigenschaften zum Rückhalt von Metallkationen wie z.B. Actiniden. Belegt wurde dies in frühere Untersuchungen ausführlich für niedrige Hintergrundelektrolytkonzentration (I_{max}= 0,7 M), wie sie z.B. im Porenwasser von Bentoniten und im Opalinuston (Schweiz, Süddeutschland) zu finden sind, sowie auch für höhere Hintergrundelektrolytkonzentrationen (I =0,1-4 M) wie sie in Porenwässern der Jura- und Unterkreidetonlagerstätten (Norddeutschland) auftreten. Ebenfalls konnte bereits erfolgreich ein geochemisches Sorptionsmodell (2SPNE/CE model) zur Beschreibung der Sorption unter ebendiesen Bedingungen entwickelt und angewandt werden.

Im Rahmen dieser Arbeit wurde der Einfluss von konkurrierenden Liganden auf die Sorption von trivalenten Lanthaniden und Actiniden an den bedeutenden natürlichen Tonmineralien Illite du Puy und Montmorillonit untersucht. Sorptionsexperimente wurden unter Variation der Hintergrundelektrolytkonzentration, der Konzentration des konkurrierenden Liganden und des CO_2-Partialdrucks durchgeführt. Die Untersuchungen wurden in Anwesenheit von repräsentativen Konkurrenzliganden durchgeführt. Der Hauptfokus der Arbeit wurde auf den Einfluss von Carbonat auf die Sorption trivalenter Lanthaniden und Actiniden in NaCl Elektrolytsystemen gelegt. Carbonat ist omnipräsent in natürlichen Grundwässern und wegen der Bildung starker Komplexe von hoher Relevanz für das geochemische Verhalten von Actiniden. Neben Carbonat wurden ebenfalls Gluconat und Citrat in NaCl und $CaCl_2$ Hintergrundelektrolyten untersucht. Beide dienen als Modellliganden für polymere Zementadditive. Gluconat wird zudem stellvertretend für das Abbauprodukt von Cellulose, die Isosaccharinsäure untersucht. Citrat wird, neben dem Einsatz als Zementadditiv, als Dekontaminationsmittel eingesetzt. Beide besitzen somit auch eine große Bedeutung als Bestandteile von schwach und mittelradioaktiven Abfällen.

Der Rückhalt von Eu(III) an Tonmineralphasen zeigt in Anwesenheit von Carbonat im leicht sauren bis neutralen pH-Bereich eine etwas erhöhte Sorption. Im alkalischen

bedingt die Bildung von stabilen aquatische Carbonatkomplexen einen massiven Rückgang der Sorption. Die Variation des CO_2-Partialdrucks beeinflusst die Gesamtkonzentration des gelösten Carbonats / Hydrogencarbonats und somit auch die Bildung stabiler aquatischer Eu-Carbonatspezies. Im Verlauf der Batchsorptionsreihen konnte kein qualitativer Unterschied des Sorptionsverhalten von Eu(III) an den Tonmineralien Illite du Puy und Montmorillonit oder durch die Variation der Konzentration des Hintergrundelektrolyten festgestellt werden. Durch eine Kombination aus quantenchemischen Berechnungen (DFT, AIMD) und spektroskopischen Untersuchungen (ATR-IR, TRLFS) konnte die Sorption von Carbonat an Tonmineraloberflächen belegt werden. Das adsorbierte Carbonat stabilisiert seinerseits Ln(III)/An(III) Oberflächenkomplexe durch die Bildung ternärer Spezies. In Abhängigkeit vom pH und der vorhandenen Carbonatkonzentration konnten zwei unterschiedliche ternäre Oberflächenkomplexe nachgewiesen werden. Die Implementierung der experimentellen Befunde in ein geochemisches Modell (2SPNE/CE) liefert ein konsistentes Modell zur Beschreibung der Sorption von Eu(III) an den Tonmineralphasen Illite du Puy und Montmorillonit über den gesamten pH-Bereich und unter Variation des Hintergrundelektrolytes und des CO_2-Partialdrucks.Die Anwesenheit von Gluconat reduziert den Rückhalt der Eu(III) Sorption an Illite du Puy und Montmorillonite um bis zu 3 Größenordnungen über den untersuchten pH Bereich von pH = 3-12.5. Durch zeitaufgelöste Laserfluoreszenzspektroskopie war es möglich, je 3 pH Regionen unterschiedlicher Einflüsse des Liganden zu definieren. Es konnte eine Konkurrenz zwischen aquatischen Spezies und Kationenaustausch sowie zwischen innersphärischen Oberflächenkomplexen aufgezeigt werden. Zusätzlich konnte die Existenz und der Einfluss von aquatischen quaternären Ca-Cm-OH-GLU Komplexen unter alkalischen Bedingungen nachgewiesen werden.

Der Einfluss von Citrat auf die Sorption von Eu(III) bedingt in NaCl Hintergrundelektrolyten eine erniedrigte Sorption im leicht sauren pH-Bereich, wohingegen eine erhöhte Sorption in $CaCl_2$ Lösungen im selben pH Bereich beobachtet wird. Im neutralen und alkalischen pH-Bereich ist eine quasi quantitative Sorption zu beobachten.

Content

1. Introduction

On 1st of January 2014 a strategy for selecting a site for nuclear waste disposal has been defined by the government of Germany in a federal law (*Gesetz zur Suche und Auswahl eines Standortes für ein Endlager für Wärme entwickelnde radioaktive Abfälle*) [1]. This law defines a timeframe for selecting a suitable repository site. There is a general global consensus that the final disposal in deep geological formations is the best option to isolate high level nuclear waste from the biosphere and from unauthorized access by third parties. Therefore, three different types of host rock formations (crystalline rock, salt and clay rock) are discussed concerning their capabilities to confine radioactive waste in the repository near-field and to inhibit radionuclide dispersion. In Germany all three types of host rock are available.

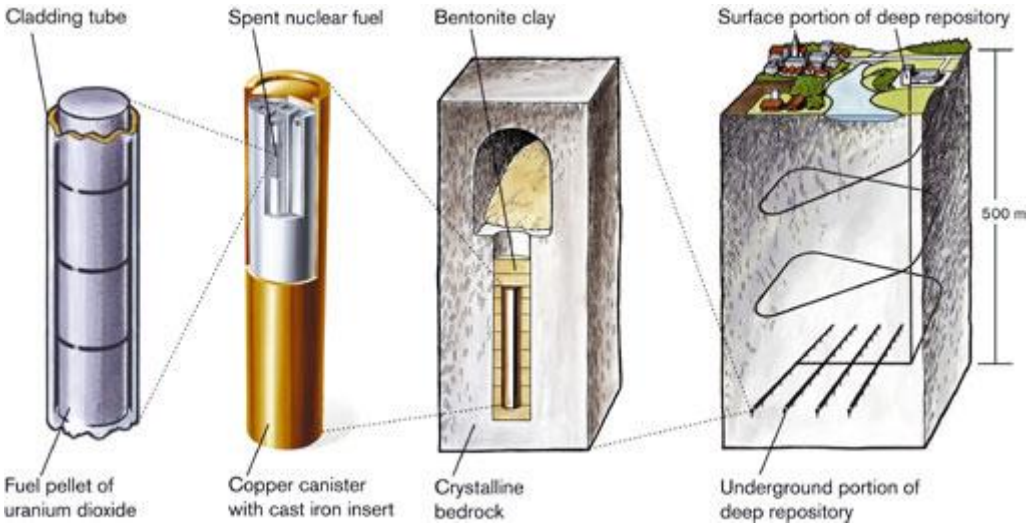

Figure 1.1: Multi-barrier-system for final nuclear waste disposal in crystalline rock (Swedish concept, KBS-3) [2].

Beside the host rock itself, different technical (e.g. waste canisters) and geotechnical barriers (e.g. engineered clay barriers) are considered to establish a so called multi-barrier system. As an example, the Swedish KBS-3 multi-barrier-concept for a nuclear waste disposal in a crystalline host rock formation is shown in Figure 1.1. This concept visualizes the principal of a multi-barrier system. The first barrier is the technical barrier and consists of the fuel matrix, the cladding tube of the fuel rods and a canister made of stainless steel covered with copper. An engineered barrier made of certain backfill

material like bentonite is planned as a geotechnical barrier and second containment. Finally the host rock itself is representing the geological barrier. Within the frame of a long term safety analysis, all events from low to high probability have to be considered and weighted due to their potential risk for a deep geological repository. Beside natural catastrophes like earthquakes or glacial periods and other events which may lead to a water ingress have to be taken into account. The application of a multi-barrier system should realize the immobilisation of radionuclides by slowing down the water intrusion and increasing the radionuclide retention.

One of the key components in the multi-barrier system for granitic host rocks is bentonite which is a clay mixture used as backfill material to fill up cavities in the near field. Its major component is smectite (mainly montmorillonite), which has the ability to swell when contacted with water. [2]. Thus, bentonite is capable to effectively seal fractures and fissures and to suppress water intrusion. A second positive characteristic of bentonite is its high retention capacity of dissolved radionuclides by physical and chemical sorption processes. Due to the strong interaction of radionuclides with the clay mineral surface a high immobilisation of radionuclides is given. Moreover the permeability of clay rock is extremely low (~ $5 \cdot 10^{-6}$ to ~ $5 \cdot 10^{-8}$ cm/s, [3]). For this reason only slow diffusive and no fast advective transport is possible [4].

Different countries consider clay deposits as host rock formations for deep geological disposal (Opalinus Clay in Switzerland [5], Boom and Ypresian clays in Belgium [6, 7], Callovo-Oxfordian and Toarcian clays in France). Also for Germany, a mapping of potential clay host rock formation took place [8]. Hoth *et al.* described two different clay deposits by regions. The Opalinus clay formation in southern Germany, comparable to formations in Switzerland [9], and a Jurassic and Cretaceous clay formation in parts of Northern Germany [10]. The northern clay rock formations are characterized by a higher salinity caused by saline ground waters nearby rock salt layers or diapirs.

Clay minerals like illite, montmorillonite or mixed layers are the most relevant components in natural claystone and also in bentonite. The sorption of radionuclides to these minerals has been investigated in detail in previous studies [11-16]. In general, these studies were carried out in diluted electrolyte solutions with an ionic strength of around I = 0.7 M or below. Only in a few studies sorption experiments at higher ionic strength were performed [17-19] to cover the conditions in clay formations with higher salinities in their pore waters.

Carbonate as an omnipresent component in natural groundwater will have a high impact on many radionuclides, especially the actinides, as they are known to form strong aqueous carbonate complexes. With some exceptions [20-25], the majority of sorption studies were performed in absence of CO_2 and none of them was performed under saline conditions and presence of CO_2. Hence, the study of trivalent actinide/lanthanide interactions with two highly relevant clay minerals illite and montmorillonite in the presence of carbonate/bicarbonate and up to high ionic strength is the first main topic of the present work.

Beside dissolved inorganic carbon, natural groundwaters may contain also higher concentrations of natural organic ligands (e.g. humic substances). In the vicinity of a future nuclear waste disposal also man-made organic anionic ligands with partly strong complexing properties can occur. Cement, which is part of the construction and container material, contains a large inventory of organic components and potential complexing ligands [26-29]. Several organic compounds are used as cement additives or admixtures, like poly-carboxylate (PCE) comb copolymers as superplasticizer [29], or sodium gluconate [28] and citric acid as retarder [26]. The second focus of this study was set on the sorption of trivalent actinides/lanthanides on illite and montmorillonite in presence of monomeric admixtures of sodium gluconate and citric acid. They are taken as representatives for cement additives and natural organic ligands, respectively Both organic ligands are known to form strong complexes with trivalent lanthanides [30-33] and actinides [34-36]. Therefore a significant impact on the retention of Ln(III) / An(III) is expected.

The presence of complexing ligands can modify the interaction of a metal cation with a solid phase by changing the aquatic speciation of the metal ion or by changing the reactivity of the mineral surface itself. The sorption of anionic, organic ligands to mineral surfaces is well known [37-40]. Adsorbed organic ligands may modify the surface reactivity depending on their structure and number of functional groups. Ligands with only one functional group can occupy and block existing mineral surface sites. Organic compounds with more than one reactive groups can act as bridging ligand generating new sorption sites. The latter process could even enhance metal ion sorption.

The interaction between Ln(III)/An(III) and clay mineral surfaces (illite, montmorillonite) in different electrolyte solutions (up to high ionic strengths) and in the presence of

competing ligands (carbonate, gluconate, citrate) is the key aspect of this thesis. Batch sorption experiments and spectroscopic speciation studies are performed to quantify the sorption reactions and to gain an understanding of the sorption mechanism on a molecular level. Based on these data, a geochemical model will be proposed to describe the experimental results. The applied model is based on the well-established 2-SPNE/CE surface complexation and cation exchange model by Bradbury & Baeyens [12-14, 16, 41, 42]. To apply a sorption model, all relevant interactions between the different compounds have to be identified and implemented.

The applicability of a modified 2-SPNE/CE surface complexation model to describe ternary (clay-radionuclide-ligand) systems up to high ionic strengths will be demonstrated for the adsorption of An(III)/Ln(III) in presence of carbonate within this study.

2. Actinide and groundwater geochemistry

A sound understanding of the transport processes of radionuclides (RNs) is a key aspect for the safety case of a nuclear waste repository. The migration of RNs with groundwater is the main route of transport between the final disposal site and the biosphere. For this reason the determination of RNs solubility (source term), complexation studies, an understanding of pH and redox potential (Eh) effects and interaction of RNs with mineral surfaces is necessary to describe the migration behaviour in its entirety. The formation of aqueous complexes with groundwater constituents like organic and inorganic ligands, formation of intrinsic and pseudo-colloids and their impact on the mobilisation or immobilisation has to be understood to provide the scientific basis for a sound nuclear waste disposal safety case.

2.1. Carbonate in groundwater

Studies on actinide behaviour under realistic groundwater conditions need to consider the presence of carbonate [43, 44]. Since dissolved carbonate is directly linked to a gaseous carbon dioxide phase, the partial pressure of CO_2 affects the dissolved carbonate concentration (and vice versa) and increases the experimental complexity of the system (Equation 1).

Equation 1

$$CO_{2(g)}+H_2O \leftrightarrow CO_{2(aq)}+H_2O \leftrightarrow (H_2CO_3) \leftrightarrow HCO_3^- + H^+ \leftrightarrow CO_3^{2-} + 2H^+$$

As described by Equation 1, an increase of dissolved carbonate takes places with increasing pH. The aqueous carbonate speciation itself is strongly pH dependent (Figure 2.1). The carbonate concentration and speciation in groundwater is defined by the partial pressure of CO_2 (p_{CO_2}) and the pH (Figure 2.2). In contrast to surface waters, which are exposed to an actual gas phase, the p_{CO_2} in aquifer groundwaters, without contact to any gas phase, is only a numeric parameter.

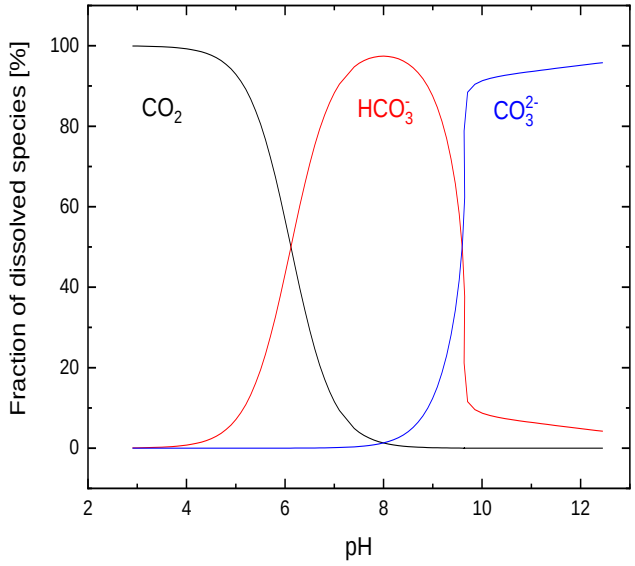

Figure 2.1: pH dependent carbonate speciation including dissolved CO_2, bicarbonate HCO_3^- and carbonate CO_3^{2-} presented as percentage.

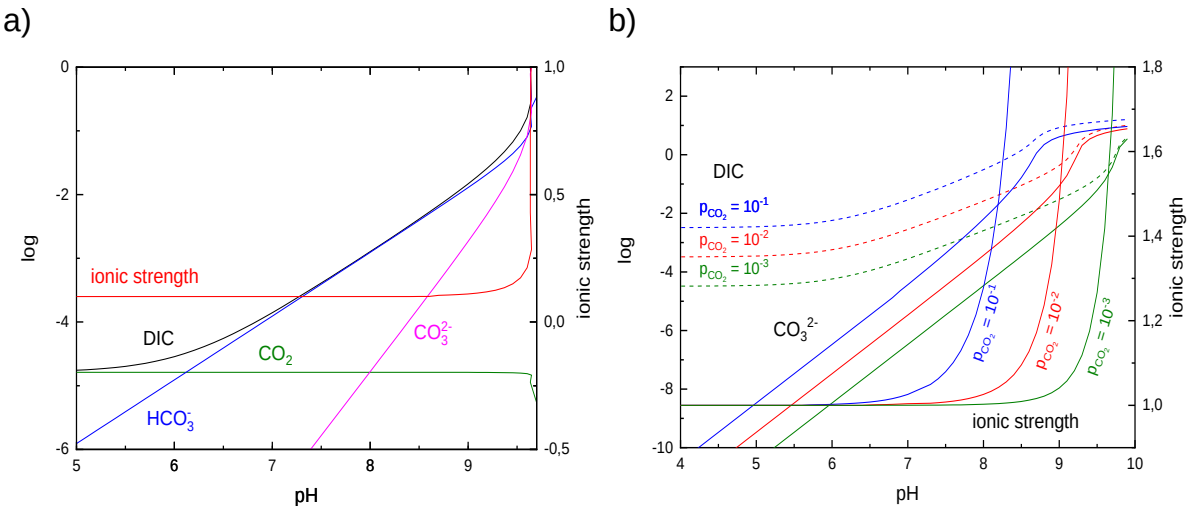

Figure 2.2: The concentration of carbonate species as a function of pH and their impact on the ionic strength for $p_{CO_2} = \mathbf{10^{-3,3}}$ bar, (a), impact of increasing partial pressure of CO_2 on the carbonate concentrating and ionic strength shown as function of pH (b). The solution speciation was calculated using *PhreeqC* [45] geochemical modelling code, the *THEREDA* database [46] and starting ionic strength of I=0.1 M.

The pH dependent speciation and concentrations are shown as logarithmic concentrations (Figure 2.2.a). The dominating species changes with increasing pH and the amount of dissolved inorganic carbon (DIC) rises. While the concentration of

bicarbonate (HCO_3^-) increases with a slope of m = 1, the carbonate concentration (CO_3^{2-}) increases with a slope of m = 2 (logarithmic scale) and controls the ionic strength above pH = 9.6 with a very steep increase.

According to the principle of *le Chatelier*, the concentrations of the carbonate anion increases at constant pH values with increasing p_{CO_2} (Figure 2.2.b). Beside this, the total dissolved inorganic carbonate concentration also rises with p_{CO_2}. For this reason the very high ionic strengths at higher pH values in equilibrium with a defined p_{CO_2} limit model calculations above a certain pH (depending on the given partial pressure of CO_2).

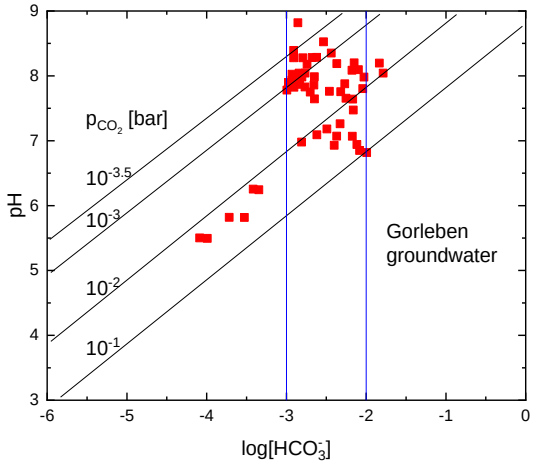

Figure 2.3: Measured bicarbonate concentrations in groundwaters from Gorleben versus pH [47]. Calculated equilibria concentrations at discrete p_{CO_2} are added as solid black lines

Between ground level (earth surface) and groundwater table (first aquifer) the CO_2 partial pressure is defined by the characteristics of the seepage, which equals the atmospheric p_{CO_2} as a first approximation. Below the groundwater level and in deep groundwater aquifers the amount of atmospheric, molecular oxygen decreases down to zero (reducing conditions) due to the exclusion of the atmosphere and microbial degradation of organic compounds. The bacterial metabolism of oxygen leads to the production of an equal amount of carbon dioxide, which increases the p_{CO_2} by a factor of ten or up to one hundred [44]. The carbonate and bicarbonate content of

groundwater is usually determined by titrations or DIC measurements. The p_{CO_2} is then calculated as function of pH [43]. This was done for the Gorleben side (Figure 2.3 [47]). The majority of tested groundwater in a range between pH = 6.5-8.5 correspond to a partial pressure of CO_2 of $p_{CO_2} = 10^{-3.5}$ to 10^{-2} bar with maximum values of 10^{-1} bar. A general problem of these measurements is outgassing during sampling.

2.2. Aquatic chemistry of actinides

Lanthanides (Z = 58-71, Cerium to Lutetium) and actinides (Z = 90-103, Thorium to Lawrencium) are members of the f-block of the periodic table. All actinides are radioactive elements and only thorium, protactinium, uranium, neptunium (traces) and plutonium (traces) are naturally occurring. The early actinides, from thorium to plutonium, show a broad variance in their oxidation state. This is also visible in a complex chemical behaviour. From americium to lawrencium trivalent oxidation states are the most stable ones. With the exception of nobelium, where the stability of No^{2+} is explained with the saturation of the 5f shell (Table 1).

Table 1: Oxidation states of actinides [48].

	Th	Pa	U	Np	Pu	Am	Cm	Bk	Cf	Es	Fm	Md	No	Lr
+1														
+2														
+3														
+4														
+5														
+6														
+7														
	Only solid state													
	In aqueous solution													
	Dominant oxidation state													
	Postulated oxidation state													

Due to these similarities, especially for trivalent oxidation states, Lanthanides are often used as non-radioactive / -toxic homologues for repository relevant actinides.
The aquatic chemistry of actinides is determined by physical parameters like pH, Eh, temperature, pressure or partial pressure of reactive gas phases (e.g. CO_2) and chemical parameters like the concentration of the actinide, and presence of complexing ligands or reactive surfaces. Tri- and tetravalent actinides occur as solvated cations at low pH and as hydrolysed species at higher pH if other ligands are absent. The oxidation states An(V) and An(VI) are forming linear oxo complexes called actinyl ions [48]. The two axial coordinated oxygen atoms direct other complexing ligands to the equatorial plane [49]. The hydrolysis of actinyl ions is starting at significantly higher pH compared to trivalent actinides (An^{3+}).

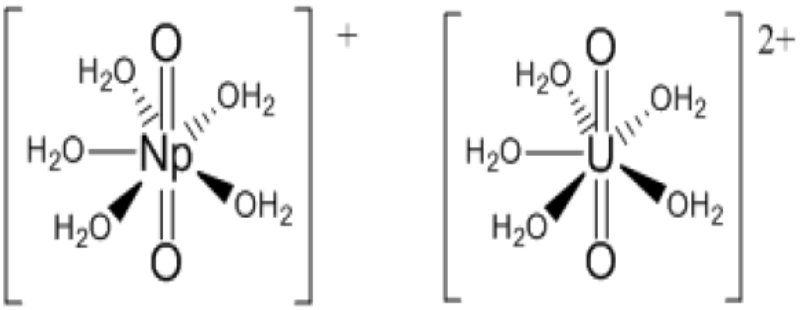

Figure 2.4: Structure of An(V) and An(VI) actinyl ions, represented by Np(V) and U(VI) [49]

Beside steric effects, the linear structure of actinyl ions with two highly electronegative oxygen atoms generates a change of the charge of the central metal atom. Thus, the effective charge Z_{eff} of $An^{V}O_2^{+}$ and $An^{VI}O_2^{2+}$ is not identical with its formal charge. The decrease of the effective charges in equatorial position is described with the following series.[50, 51].

$$Z_{eff} = \quad 4 \quad 3.3 \pm 0.1 \quad 3 \quad 2.3 \pm 0.2$$

$$An^{4+} > An^{VI}O_2^{2+} > An^{3+} > An^{V}O_2^{+}$$

Redox reactions of the actinides An(IV)/An(III) and An(VI)/An(V) are controlled by the redoxpotential in solution.

$$An^{4+} + e^- \rightarrow An^{3+}$$

$$AnO_2^{2+} + e^- \rightarrow AnO_2^{+}$$

Moreover, a transition from An(V)/An(IV) is in addition correlated with the pH.

$$AnO_2^{+} + 4\ H^{+} + e^- \rightarrow An^{4+} + 2\ H_2O$$

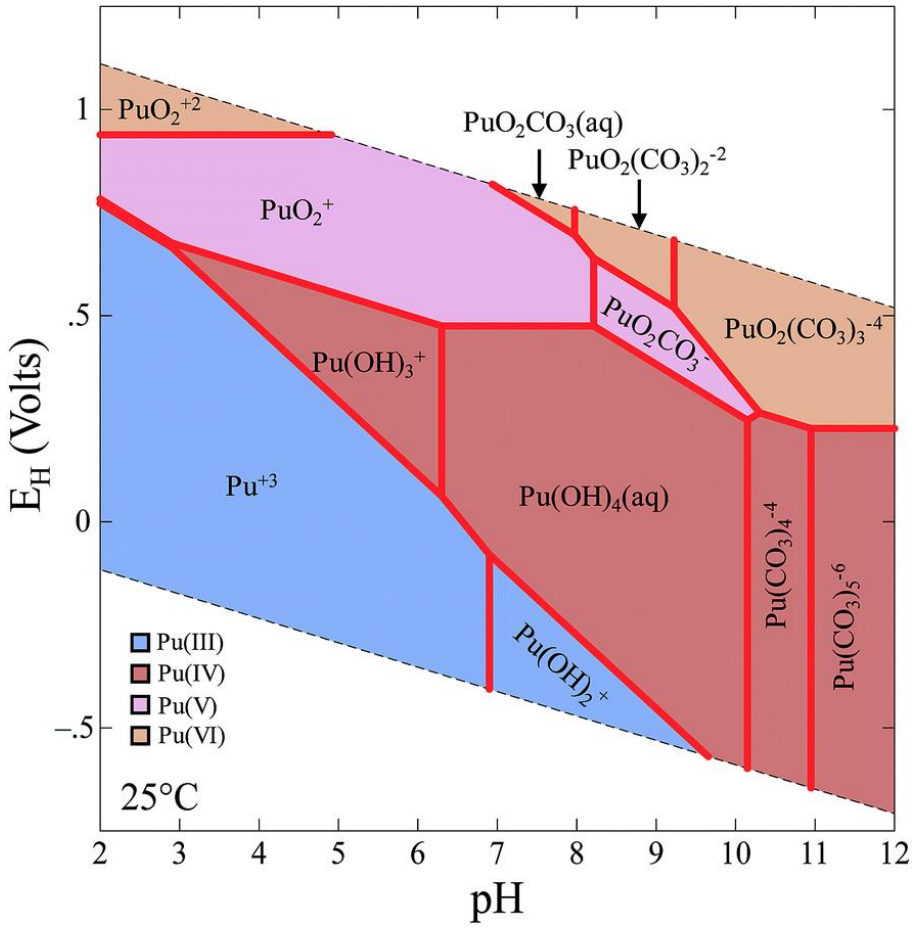

Figure 2.5: Pourbaix diagram of plutonium calculated in with equilibrium ambient CO_2 [52].

Figure 2.5 shows the redox speciation of plutonium (Eh vs. pH) under ambient comditions [52]. The relevance of the trivalent oxidation state is observed under reducing conditions from pH = 2-9 (depending on the Eh). Due to their similar chemical behaviour trivalent actinides can be compared with analogue trivalent lanthanides. Both, Ln(III) and An(III) have a low polarisability and are described as hard Lewis acids, according to the concept of hard and soft acids and bases (HSAB). As hard Lewis acids actinides and lanthanides prefer interacting with strong Lewis bases [53].

According to the HSAB concept, the stability of complexes of actinides and lanthanides with common ligands present in groundwater is summerized with decreasing stability.

$$CO_3^{2-} > OH^- > F^- \approx SO_4^{2-} \approx HPO_4^{2-} > NO_3^- > Cl^- > ClO_4^-$$

Table 2: Stability constants $\boldsymbol{\beta_n^0}$ for the formation of a $\boldsymbol{An(L)_1^{3-x}}$ complexes.

$An(L)_1^{3-x}$	CO_3^{2-}	OH^-	$HPO4^{2-}$	F^-	SO_4^{2-}	H_2PO4^-	SiO_4^{2-}	NO_3^-	Cl^-	ClO_4^-
$\lvert\log\cdot\beta_n^0\rvert$	8.3	6.8	6.2	3.4	3.3	2.5	2.3	1.3	0.2	-
Literature	[54]	[54]	[55]	[54]	[54]	[55]	[56]	[54]	[54]	[57]

A qualitative summary of the complex stability of trivalent 1:1 complexes is given in Table 2. Beside the chemo-physical properties of the ligand, the Z_{eff} is affecting the complex stability in the same way, from strong An(IV) to weaker An(VI) complexes.
A general description of the complexation of An(III) with a generic ligand L is given in Equation 2. Hereby, An^{3+} forms a binary complex with n ligands of charge x.

Equation 2

$$An^{3+}(aq) + nL^{x-}(aq) \leftrightarrow An(L)_n^{3-x\cdot n}$$

- n: number of ligands
- x: charge of the ligand

From Equation 2 a conditional complexation constant is derived, which is valid for a given temperature and ionic strength (Equation 3).

Equation 3

$$\beta_n' = \frac{[An(L)_n^{3-x\cdot n}]}{[An^{3+}(aq)]\cdot[L^{x-}(aq)]^n}$$

- β_n': complexation constant at fixed γ_i (constant ionic strength and temperature)
- [ ]: concentration

In Equation 4 a complexation constant is given for ionic strength I = 0.

Equation 4

$$\beta_n^0 = \beta_n' \cdot \frac{\gamma_{An(L)_n^{3-x\cdot n}}}{\gamma_{An^{3+}(aq)} \cdot \gamma_{L^{x-}(aq)}^n}$$

- β_n^0: complexation constant for I = 0
- γ_i: activity coefficient of species i

2.2.1. Hydrolysis

In absence of strong complexing ligands (e.g. CO_3^{2-}) and increased pH, hydrolysis is the primary reaction which determines the aquatic speciation of An and Ln. The hydrolysis depends strongly on the pH and the effective charge of the cations. In the following, An(III) and An(V) complexation is discussed and compared exemplary for actinide behaviour under reducing and oxidizing conditions. Therefore, hydrolysis of An(III) (Z_{eff}= 3) starts in the neutral pH-range, while for pentavalent An(V) ions (Z_{eff}= 2.3) hydrolysed species appear above pH = 9 [50, 51]. A calculated species distribution of Cm(III) in 1.0 M NaCl (representative for An(III)) and of Np(V) in 0.1 M NaCl (representative for An(V)) for pH = 4.5 - 13 is given in Figure 2.6.a.

The hydrolysis of An(III) in 1 M NaCl solution starts at pH > 6 with the formation of a first 1:1 (e.g. $CmOH^{2+}$). A second 1:2 species (e.g. $Cm(OH)_2^+$) forms at pH > 7,5. Above pH > 10 a neutral 1:3 species (e.g. $Cm(OH)_3$) is the dominating species. Compared to the hydrolysis of trivalent actinides, the hydrolysis of pentavalent Np(V) is much less pronounced. A first 1:1 complex appears above pH > 9,5 ($NpO_2(OH)$), and a second 1:2 ($NpO_2(OH)_2^-$) species is present above pH > 11, which is also the limiting complex.

In $CaCl_2$ containing solutions ternary $CaAm(OH)_3^{2+}$ and $Ca_2Am(OH)_4^{3+}$ species are reported by Rabung *et al.* in the hyperalkaline region [58]. A stabilizing effect of Ca^{2+} on the formation of hydrolysed species in hyperalkaline media was observed and quantified by Neck *et al.* [59].

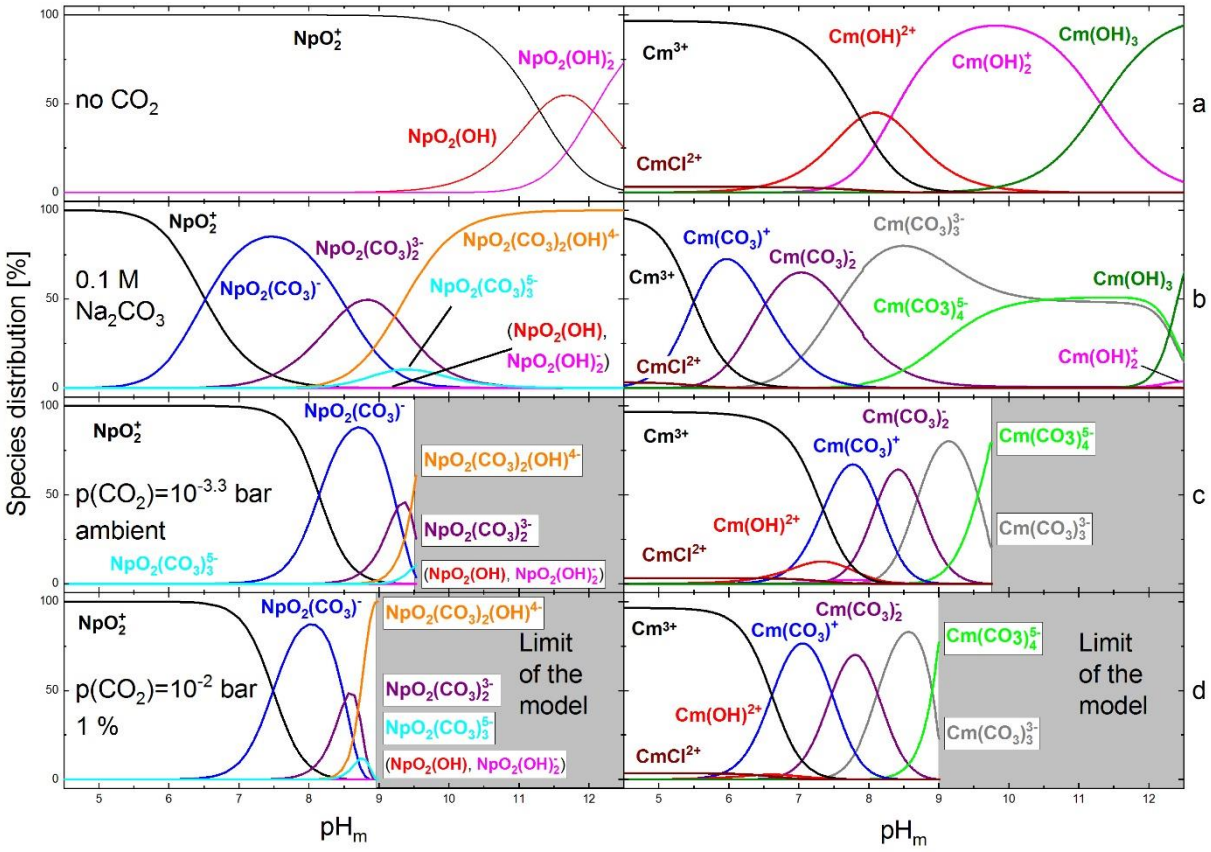

Figure 2.6: The distribution of Np(V) ($1 \cdot 10^{-7}$ M in 0.1 M NaCl, left) and Cm(III) ($1 \cdot 10^{-8}$ M in 1 M NaCl, right) species in solution (**a**) in absence of CO_2 (**b**) in presence of 0.1 M Na_2CO_3 (closed system) (**c**) at $p_{CO_2} = 10^{-3,3}$ bar (**d**) $p_{CO_2} = \mathbf{10^{-2}}$ bar as function of pH. The solution speciation was calculated using *PhreeqC* [45] geochemical modelling code and the *THEREDA* database [46].

2.2.2. Carbonate

With increasing carbonate concentrations, the formation of hydrolysed species is successively suppressed. This is visualized in some calculated species distributions for Cm(III) and Np(V) at different carbonate concentrations/CO_2 partial pressures in Figure 2.6 (also in the absence of carbonate). Figure 2.6b is describing a closed model system with a fixed carbonate concentration of 0.1 M Na_2CO_3. Two other species distributions were calculated in equilibria with a certain partial pressure of CO_2. Therefore, ambient conditions ($p_{CO_2} = 10^{-3,3}$ bar, c) and an elevated partial pressure of CO_2 ($p_{CO_2} = 10^{-2}$ bar, d) were chosen. With respect to the global increase of

atmospheric CO_2 the ambient partial pressure of CO_2 was changed from $p_{CO_2} = 10^{-3,5}$ bar (common value in literature) to $p_{CO_2} = 10^{-3,3}$ bar.

Trivalent actinides, like Cm^{3+} (Figure 2.6.b, right), form much stronger complexes with carbonate than actinides in oxidation state V as clearly visible in Figure 2.6. In presence of a constant carbonate concentration of 0.1 M Na_2CO_3 the monocarbonate complex $Cm(CO_3)^+$ is predominant at pH = 6, followed by the $Cm(CO_3)_2^-$ complex with its maximum at pH = 7 and the $Cm(CO_3)_3^{3-}$ complex with its maximum at pH = 8.5. Due to a limited amount of carbonate the fourth species, a tetracarbonate complex ($Cm(CO_3)_4^{5-}$), is not evolved to a predominant species. From pH = 9-12 both tri and tetracarbonate complexes of Cm(III) control the aquatic speciation with a contribution of about 50 %. Above pH = 12 $Cm(OH)_{3(aq)}$ and a smaller portion of $Cm(OH)_2^+$ start to form. No mixed species or complexes with bicarbonate are reported for trivalent actinides [60]. In presence of ambient CO_2 (Figure 2.6.c, right) the free Cm^{3+} is the dominant species in the acidic range, the monocarbonate complex reaches its maximum at pH = 7.75 ($Cm(CO_3)^+$). At pH = 8.4 the $Cm(CO_3)_2^-$ complex is predominant followed by the $Cm(CO_3)_3^{3-}$ species at pH = 9.1. Above pH = 9 the concentration of the tetra carbonate complex is increasing and is predominant above pH = 9.5 ($Cm(CO_3)_4^{5-}$). In equilibrium with an elevated partial pressure of CO_2 (Figure 2.6.d, right) Cm(III) start to form carbonate complexes at a lower pH value. This effect is explained by a higher carbonate concentration in solution.

The neptunyl aquo ion is stable in presence of 0.1 M Na_2CO_3 in the acidic pH range (Figure 2.6.b-d, left). In presence of ambient CO_2 NpO_2^+ remains as predominant species from the acidic range up to pH = 8. The NpO_2^+ is then replaced by $NpO_2(CO_3)^-$, with a predominance from pH = 8-9.2. In presence of elevated partial pressures of CO_2 the sequence of dominant species is comparable to the ambient CO_2 system, as described above. Due to the higher carbonate concentrations the dominance field of all species are shifted to lower pH values. The complexation of the pentavalent neptunium is less pronounced then for the trivalent curium.

2.2.3. Complexation with inorganic ligands – Cl^-, SiO_4^{2-}, PO_4^{3-}, SeO_3^{2-}

Chloride is a common ligand in groundwater and pore water of clay formations and often present in high concentrations. It forms weak complexes with An and Ln, compared to hydroxide or carbonate. According to the HASB concept, chloride prefers to interact with metal ions with a high effective charge. Trivalent curium forms significant amounts of chloro complexes at chloride concentration above [NaCl] = 4.0 mol kg^{-1} H_2O. At lower chlorine concentrations (1 M NaCl, < 5 %, Figure 2.6.a-d, right) only a small contribution of chloride complexes is formed in the acidic range. The complexation of pentavalent neptunium with chloride is significantly weaker compared to trivalent actinides.

Phosphate, silicate or selenite usually appear in trace concentrations in natural systems. These ligands show extensive protonation and deprotonation reactions, which increases the complexity of the respective aquatic system considerably. Phosphate forms with An(III) complexes of the type $An(III)H_2PO_4^{2+}$, $An(III)HPO_4^{+}$, $An(III)PO_4^{2}$ as well as the analogous complexes with a higher number of ligands. The aquatic chemistry of silicates is dominated by the formation of polynuclear species. For this reason the exact An(III) / SiO_4 speciation is not available [56]. The complexation of actinides with selenite has not been studied so far. Only a few information of the interaction of selenite with trivalent lanthanides are available [61].

2.2.4. Complexation with organic ligands – Citrate, Gluconate

Organic carboxylic acids are capable to form stable complexes with actinides. In general, the organic ligands bind to An and Ln ions via carboxylic groups in a mono- or bidentate coordination mode. Additional functional groups (e.g. OH in α-position) offer the possibility to form chelates, which increases the complexation strength distinctively. Naturally occurring polymeric ligands like humic and fulvic acids are strong ligands towards actinides and significantly influence their aquatic chemistry [62-65]. In analogy to natural macromolecules, synthetic superplasticizer also form strong

complexes with actinides [66-69]. Superplasticizer, usually poly-carboxylate (PCE) comb copolymers, are used to adjust concrete properties like hardening time or flowability during processing. Due to their strong incorporation in the cement matrix, a low mobility of superplasticizer in a nuclear waste repository is expected. Furthermore, monomeric organic compounds are used as additive to concrete mixtures to control their hardening process or rheological properties. Sodium gluconate [28] and citric acid [26] are two commonly used additives. Gluconate is also an important analogue for isosaccharinic acid, a cellulose degradation product. Citrate is a natural occurring ligand and a commercially used decontaminant. Therefore, both ligands are also highly relevant in the context of a repository for low and intermediate level radioactive waste. The chemical structures and deprotonation constants of gluconate and citrate are given in Figure 2.7 and Table 3. The complexation of gluconate [30-32, 34, 70] and citrate [33, 35, 36] with calcium and trivalent Ln/An was intensively studied. A summary of complexations reactions and stability constants is given in Table 4. Gluconate forms mono or bidentate complexes with actinides via its carboxylic group and is expected to form a five-membered chelate ring including the α-hydroxyl functional group. Citrate is able to bind with all three carboxyl groups and one hydroxyl functional group in the centre leading to the formation of six-membered chelate rings. A formation of chelating complexes including simultaneous all three carboxylic functional groups is sterically hindered.

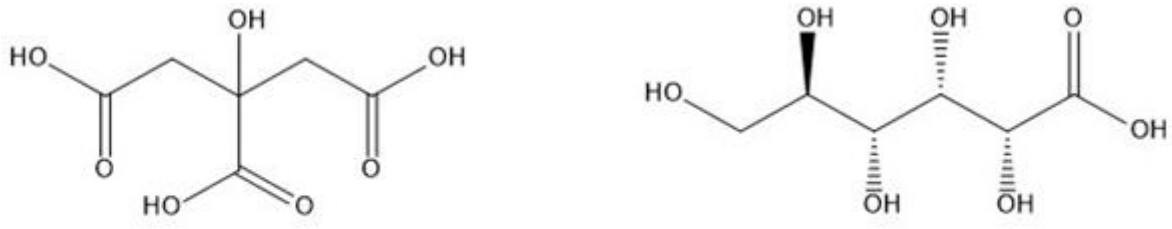

Figure 2.7: Schematic structures of citric acid (left) and D-gluconic acid (right):

Table 3: Deprotonation constant of D-gluconic and citric acid.

Deprotonated species	pK_a	Literature
H-Glu ↔Glu^- + H^+	3.86	[71]
H_3-Cit ↔ H_2-Cit^- + H^+	3.14	[72]
H_2-Cit^- ↔ H-Cit^{2-} + H^+	4.77	[72]
H-Cit^{2-} ↔ Cit^{3-} + H^+	6.39	[72]

The speciation of gluconate in solution is shown for NaCl (left) and $CaCl_2$ (right) electrolyte systems in Figure 2.8. In 0.1 M NaCl (Figure 2.8, left), gluconate is stable in its protonated form for pH < 3.86. Above this pH the deprotonated species is predominant. The presence of Ca^{2+} is leading to the formation of a binary $Ca(HGLU)^+$ species, which is occurring in the same pH range as the deprotonated species. In the alkaline range a ternary species Ca(OH)(HGLU) appears above pH = 11.

Table 4: Complexation constants for Am(III) (as an analogue for Eu(III) and Cm(III)) and Ca(III) with gluconate and citrate [73].

Complexation reactions of organic ligands with Ca(II)/Am(III)	log β^0
Gluconate	
Ca^{+2} + $HGlu^-$ = $Ca(HGlu)^+$	1.73
Ca^{+2} + $HGlu^-$ + H_2O = Ca(OH)(HGlu) + H^+	-10.4
Am^{+3} + $HGlu^-$ + 3 OH^- = $Am(OH)_3(HGlu)^-$	-19.70
Citrate	
Ca^{+2} + 2 H^+ + Cit^{-3} = $Ca(H_2Cit)^+$	12.67
Ca^{+2} + H^+ + Cit^{-3} = Ca(HCit)	9.28
Ca^{+2} + Cit^{-3} = $Ca(Cit)^-$	4.80
Am^{+3} + Cit^{-3} + H^+= $Am(HCit)^+$	12.86
Am^{+3} + Cit^{-3} = Am(Cit)	8.55
Am^{+3} + 2 Cit^{-3} + 2 H^+ = $Am(HCit)_2^-$	23.52
Am^{+3} + 2 Cit^{-3} = $Am(Cit)_2^{-3}$	13.90

The impact of gluconate on the aquatic speciation of Am(III) is shown in Figure 2.9 (0.1 M NaCl, left; 0.06 M $CaCl_2$, right). The free Am^{3+} ion is predominant from pH = 2-7. Hydrolysed species are appearing between pH = 7-8. Above pH = 8 a ternary $Am(OH)_3(HGLU)^-$ species, reported by Tits *et al.* [74], is predominant. For trivalent actinides and lanthanides no ternary or quaternary complexes including gluconate and Ca^{2+} are reported, consequently no effect of calcium on the aquatic speciation is observed. A quaternary complex like the $CaTh(OH)_4(GLU)_2$ [75] was not yet described for Ln(III)/An(III) systems.

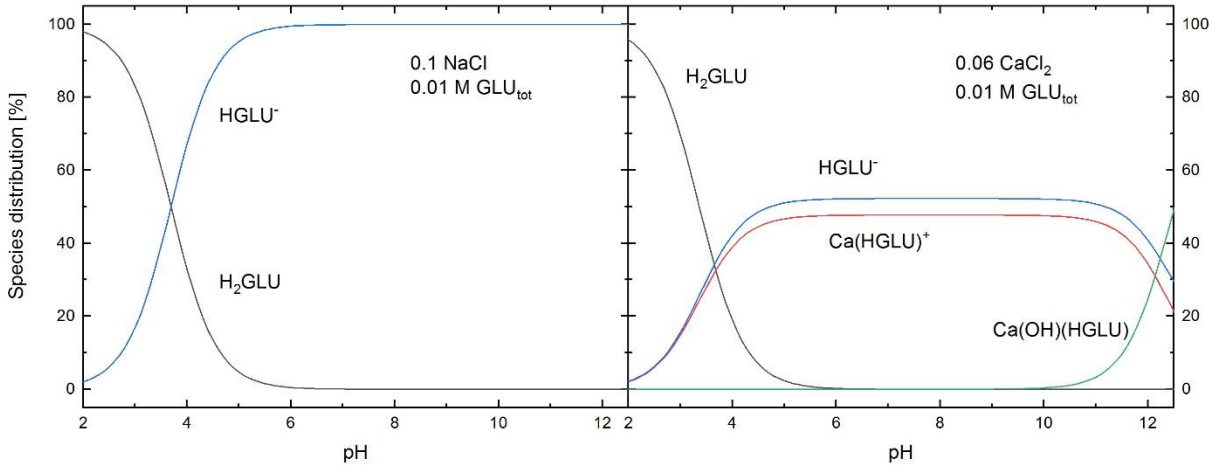

Figure 2.8: The distribution of gluconate species in solution (0.01 M GLU in 0.1 M NaCl left and 0.06 M $CaCl_2$). The solution speciation was calculated using *PhreeqC* [45] and the *Thermochimie* database [73].

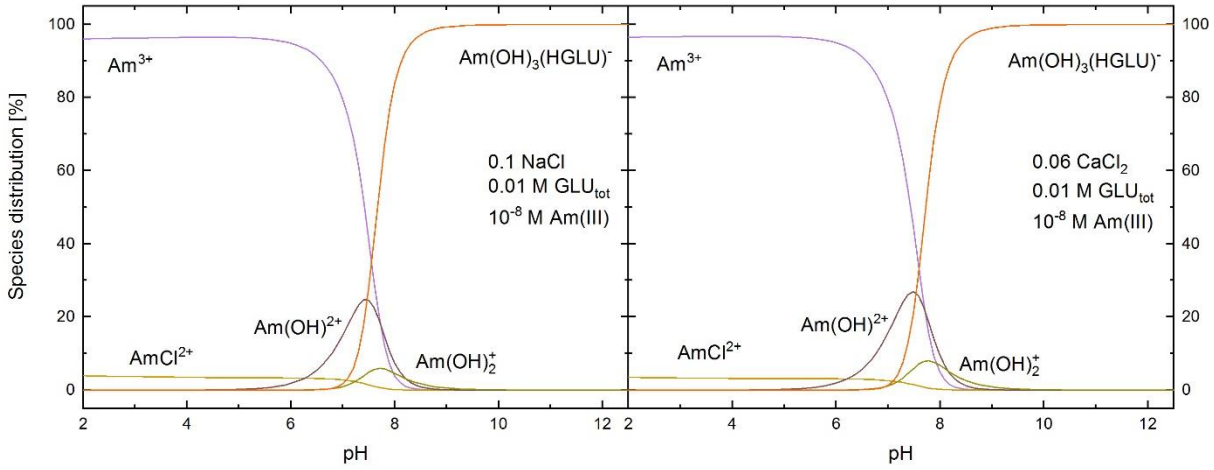

Figure 2.9: The distribution of Am(III) species in solution in presence of gluconate (10^{-8} M Am(III), 0.01 M GLU in 0.1 M NaCl left and 0.06 M $CaCl_2$). The solution speciation was calculated using *PhreeqC* [45] and the *Thermochimie* database [73].

The calculated aquatic speciation of citrate in NaCl (0.1 M, left) and $CaCl_2$ (0.06 M, right) electrolyte solutions is shown in Figure 2.10. Citric acid is stepwise deprotonated with increasing pH. Above pH = 6 citric acid is completely deprotonated and the CIT^{3-} species is dominant up to the alkaline pH range. In presence of Ca^{2+} the cationic CaH_2CIT^+ and a neutral CaHCIT species appear already in the acidic region. Above pH = 4.5 the anionic $CaCIT^-$ species is dominating the aquatic speciation.

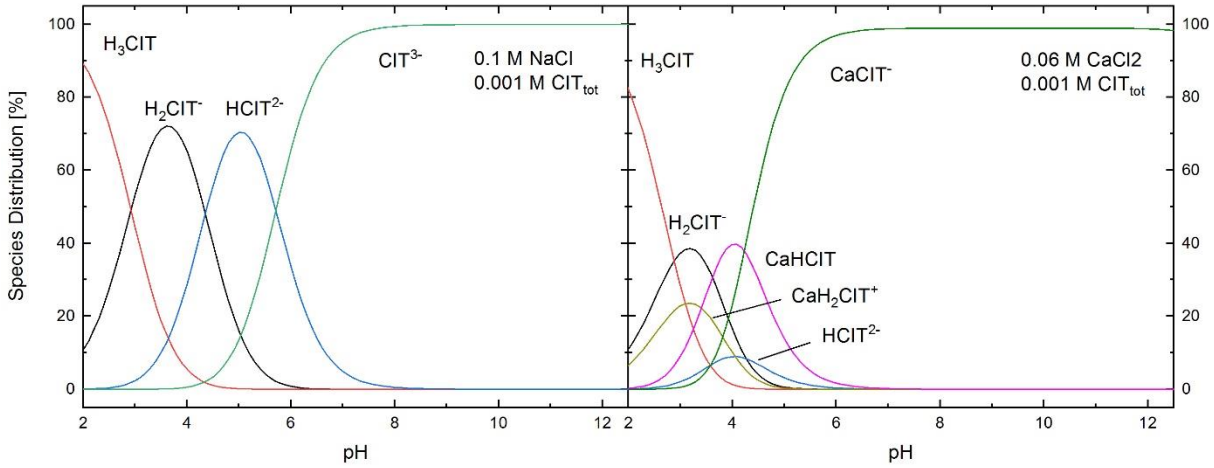

Figure 2.10: The distribution of citrate species in solution (0.001 M CIT in 0.1 M NaCl left and 0.06 M $CaCl_2$). The solution speciation was calculated using *PhreeqC* [45] and the *Thermochimie* database [73].

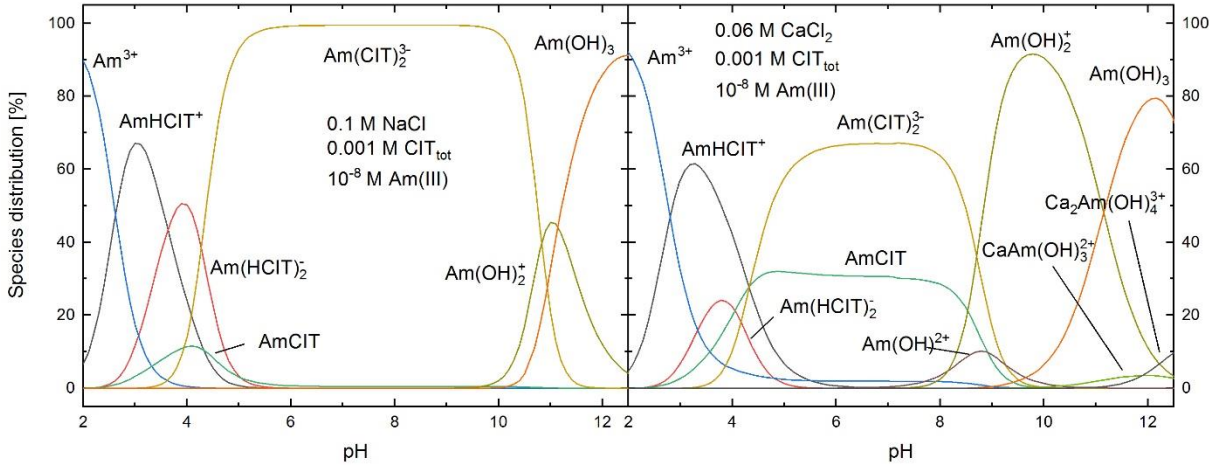

Figure 2.11 The distribution of Am(III) species in solution in presence of citrate (10^{-8} M Am(III), 0.001 M CIT in 0.1 M NaCl left and 0.06 M $CaCl_2$). The solution speciation was calculated using *PhreeqC* [45] and the *Thermochimie* database [73].

The influence of citrate on the aqueous speciation of Am(III) is shown in Figure 2.11 (0.1 M NaCl, left; 0.06 M $CaCl_2$, right). According to the deprotonation of the ligand a series of binary Am-citrate complexes are formed as function of pH. Above pH > 10 a significant amount of hydrolysed species is observed. The presence of Ca^{2+} reduces the free ligand concentration by the formation of Ca-citrate complexes. For this reason 1:2 complexes like the $Am(Cit)_2^{3-}$ are less dominant and the appearance of hydrolysed species above pH > 9 is more pronounced.

2.3. Photoluminescence of 5f-elements

Along the series of the actinides Pa(IV), UO_2^{2+}(VI), Am(III), Cm(III), Bk(III) and Cf(III) are showing fluorescence in aqueous solution [76]. Optical spectra of actinides are generated by the transition between partially occupied electronic states in the f shell and are characterized by a number of weak and sharp emission bands [77]. This was explained by the facilitation of forbidden f-f transitions (Laporte rule) by non-centrosymmetric ligand fields and concomitant mixing of electronic states [78]. Electron configuration and oxidation state of the actinides are controlling the energy of the emission.

5f electrons are shielded by inner s- and p-electron shells. Coupling between vibronic transitions of ligand molecules and the metal ion causes a lower ligand field splitting (100-1000 cm^{-1}), which cannot be resolved at room temperature [79]. Although ligand field splitting is comparatively low, it generates a shift in the emission maximum of the electronic spectra.

The contribution of 5f orbitals in chemical bindings is also increasing the spectroscopic sensitivity of actinide towards changes in their chemical environment. This can appear e.g. as a shift in emission bands and higher extinction coefficients, compared to lanthanides.

2.3.1. Fluorescence of Cm(III)

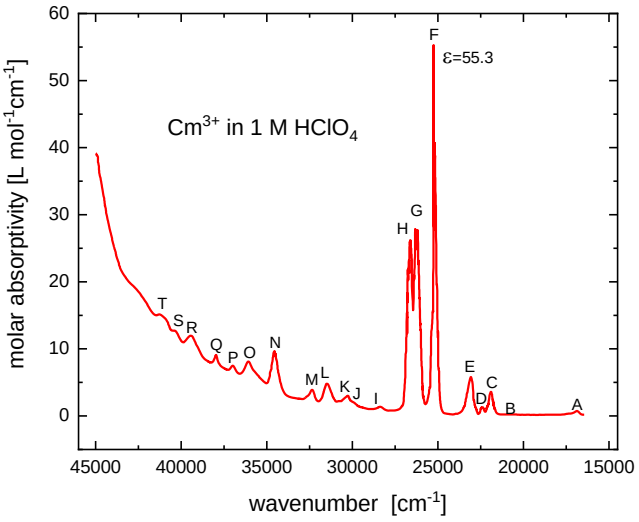

Figure 2.12: Absorption spectra of Cm(III) in 1 M $HClO_4$ adapted from Carnall *et al.* [80].

Curium was used for spectroscopic studies during this work, because of its excellent fluorescence properties. The stable oxidation state of curium in aqueous solution is the trivalent state, where the 5f orbitals are half filled with electrons ($5f^7$). An optical absorption spectra of Cm(III) in 1 M $HClO_4$ is shown in Figure 2.12. It consists of a number of sharp f-f transitions. The most intense bands are F (λ = 396.6 nm, ε = 55,3 $L \cdot mol^{-1} \cdot cm^{-1}$) G ($\lambda$ = 381.1 nm, ε = 32.6 $L \cdot mol^{-1} \cdot cm^{-1}$) and H ($\lambda$ = 375,4 nm, ε = 29,3 $L \cdot mol^{-1} \cdot cm^{-1}$). By irradiation with laser light of a wavelength of λ = 396.6 nm Cm(III) is excited from its electronic ground state Z ($^8S'_{7/2}$) to the F level (Figure 2.13, purple). This absorption process is followed by a non-radiative decay (gray) to the A level ($^6D'_{7/2}$). Level A is the first excitation state and lies 16840 cm^{-1} above the ground state. Under the emission of fluorescence a population of state Z from state A takes place (orange). A substitution of H_2O ligands in the first coordination sphere of the Cm^{3+} aquo ion by a complexing ligand causes a bathochromic shift. The stronger the ligand and the higher the number of coordinating ligands the stronger is the shift of the fluorescence light to higher wavelengths. This characteristic shift of the fluorescent wavelength allows to derive information on the chemical environment of the Cm(III) ion (mainly the first coordination sphere) and enables to derive species distributions of Cm(III) depending on different parameters as pH, nature and concentration of ligands.

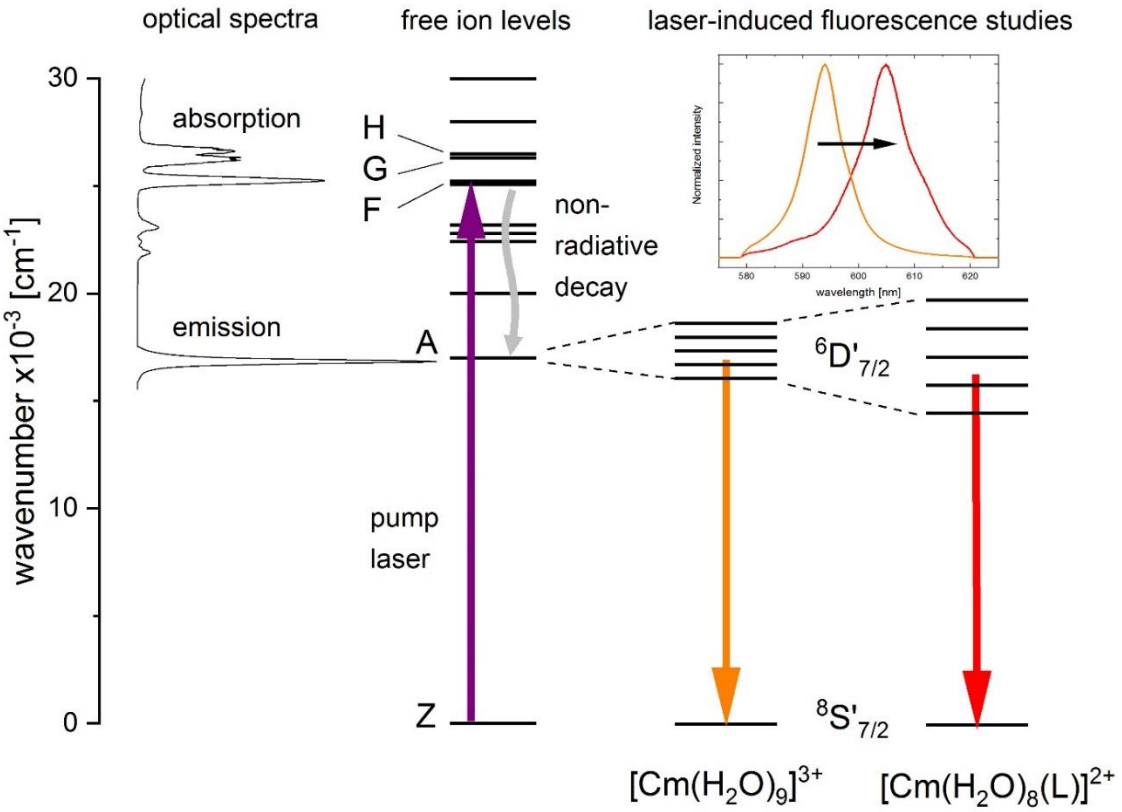

Figure 2.13: Schematic description of the Cm(III) fluorescence process according to Beitz *et al.* [81] using the absorption spectra of Crosswhite *et al.* [80] and Cm fluorescence spectra (this work).

Beside the Cm fluorescence spectra, the measurement of the fluorescence lifetime of the excited state can provide additional insights on the coordination environment of Cm(III). Like the bathochromic shift, the decay of the fluorescence lifetime from the $^6D'_{7/2}$ to $^8S'_{7/2}$ state is characteristic for each species [82]. The decay of a single species can be explained with a mono exponential decay. If different species are present in the sample, a bi- or multi exponential decay has to be considered if the lifetime of the excited state is lower than the exchange rate between ligands (which is the case for sorption reactions) [83].

Cm(III) in solution exhibits fluorescence lifetimes in a microsecond scale. This lifetime is depending on the quenching of its chemical surrounding which is mainly caused by O-H-vibrations. Substitution of water/OH ligands from the first hydration sphere of Cm(III) by other ligands reduces the quenching and the fluorescence lifetime is increasing [84]. This effect was empirically described for a H_2O/D_2O system by Kimura *et al.* [85]. According to this linear correlation, a description of the hydration of Cm(III)

in aqueous systems is possible (Equation 5). Beside a reduction of the fluorescence intensity, ligands like carbonate [60] or aromatic systems [86] are known to increase the fluorescence intensity. This effect is quantified by a fluorescence intensity factor (FI), defined as the ratio of the fluorescence intensity of the complexed Cm(III) species vs. the intensity of the Cm(III) aquo ion.

Equation 5

$$n_{H_2O} = 0.65 \cdot k_{obs} - 0.88 = 0.65 \cdot \frac{1}{\tau} - 0.88$$

- n_{H_2O}: number of H_2O in the first coordination sphere
- k_{obs}: decay rate [ms^{-1}]

2.3.2. Vibronic sideband spectroscopy

Vibronic sideband (VSB) spectroscopy is used to probe the coordination sphere of luminescent metal ions [87-90]. The observed emission bands are generated during the non-radiative decay after the laser induced excitation of the metal ion from the exited states F, H, G to lowest excited state A (Figure 2.13). The emitted VSB can be correlated with vibration modes of coordinated ligands or functional groups. The energy of vibronic sidebands is reduced by the energy of the exited state A, compared to the main emission of fluorescence (zero phonon line, ZPL) [91]. For this reason the observed energies of VBS has to be corrected according to Equation 6.

Equation 6

$$E_{Vibration}=E_{ZPL}-E_{VSB}$$

2.4. Clay minerals

2.4.1. Structure

In the framework of this thesis two different clay minerals, illite and montmorillonite, were investigated. Both are 2:1 sheet silicates consisting of periodical sheets of 2 tetrahedral silicate layers (T) and 1 octahedral alumina layer (O), called TOT layer (Figure 2.14). Isomorphic substitution of Si- and Al-ions by ions with a lower charge (e.g. T-layer: Si^{4+} replaced by Al^{3+}, Fe^{3+}; O-layer: Al^{3+} by Fe^{2+}, Mg^{2+}) generates a negative charged (x) layer surface on the basal planes [92].

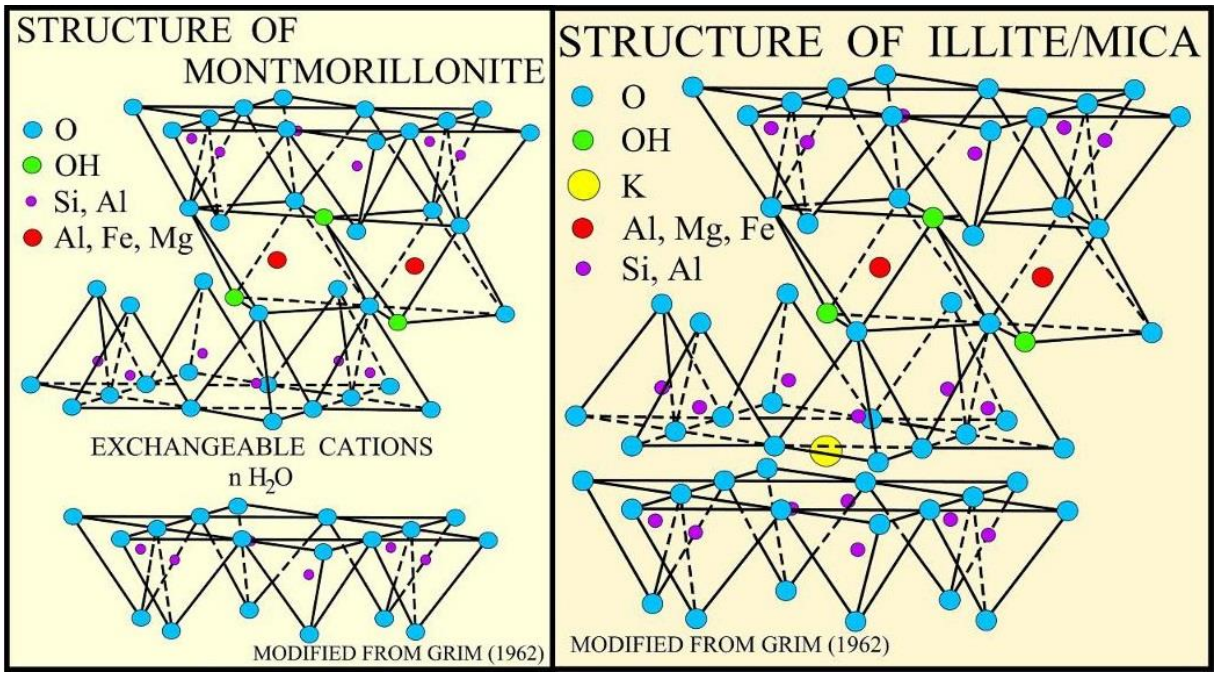

Figure 2.14: Structure of the clay minerals (a) montmorillonite and (b) illite modified from Grim et al. [93].

According to the layer charge, clay minerals are differentiated in groups with increasing charge. Montmorillonite is assigned to the smectite group (x = 0.2-0.6). Illite with a higher charge is member of the vermiculite-illite group (x = 0.6-0.9) [4]. The layer charge is compensated by cations located in the interlayer. Hydrated Ca^{2+} and Na^{+} ions are typical cations in the interlayers of the smectite group. In contrast, the

interlayer charge of clay minerals of the vermiculite-illite group is balanced by nonhydrated K^+ ions [94]. The type of interlayer cations is directly influencing the physical properties of clay minerals. Hydrated calcium and sodium enable a temporary and reversible incorporation of water molecules into the interlayer, allowing the mineral to swell when contacted with water. In contrast to montmorillonite, nonhydrated potassium in the interlayer of illite results in a collapse of the interlayer. In this case, no water molecules can enter the interlayer, this clay shows no swelling behaviour in contact with water [95, 96]. The stability of clay minerals is limited by the dissolution of the Al- and Si-layers [97-99].

2.5. Sorption phenomena

2.5.1. Cation exchange

Clay minerals are usually capable of adsorbing dissolved or gaseous substances. Adsorption processes are often driven by the surface reactivity, charge density, hydrophobic properties or the roughness of a surface. An important parameter to quantify sorption processes is the specific surface: a correlation of particle size and surface per mass. According to this relation, small platelets own a bigger specific surface then spherical particle with comparable density. Clay minerals are shaped as small platelets leading to a very high specific surface (5-500 m^2/g). 70 % of this surface are located at basal planes between the TOT layers. Only 30 % is attributed to the edge sides. Surface areas in the pore space are named inner surface. Edge sides and basal planes outside the interlayers are called outer surface [4].

As the majority of the surface area is located between the interlayers, its availability is directly connected with the access to the interlayer pore space. The availability of the reactive surface area has a major impact on the characteristic of the clay minerals studied in the present work. Montmorillonite, a mineral of the smectite group, enables hydrated ions or molecules to access its pore space. This feature is reflected by the ability of smectites to swell when contacted with water [95, 96]. After their diffusion into the pore space, hydrated ions or molecules can interact with the surface. In contrast to this, illite, as member of the vermiculite-illite group, is not able to swell and thus

hydrated ions are not able to access the pore space or only to a limited extent [100, 101]. For this reason the specific surface of illite consists only of outer surface and, thus, is significantly lower (50-200 m^2/g) compared to smectites (600-800 m^2/g) which can be completely delaminated in diluted systems [4].

In general, clay minerals which are contacted with water show a permanent negative surface charge at the basal planes. This charge is attributed to isomorphic substitution of ions in the clay structure, which induces in total a permanent und pH-independent charge [12]. In addition, amphoteric hydroxyl groups located at the edge sides can be protonated in the acidic or deprotonated in the alkaline pH range, leading to a variable pH-dependent charge [102, 103]. Further effects of variable surface charge which influence the sorption of cations are given in chapter 2.5.

The permanent surface charge of the basal planes is compensated by the adsorption of dissolved counter ions in the diffused double layer. The sum of this charge is called the cation exchange capacity (CEC). The concept of CEC describes the ability of a clay mineral to exchange adsorbed cations against each other [4]. Two physical properties are effecting the affinity of cations to adsorb. Ions with a high effective charge tend to stronger absorption on the surface, compared to ions with a lower charge (e.g. $Na^+ < Mg^{2+} < Al^{3+} < Th^{4+}$). If there is no difference in charge, the ionic radius is the key parameter ($Li^+ > Na^+ > K^+ > Rb^+ > Cs^+$) [104]. In the presence of high salt concentration, the mineral surface will be saturated with cations of the respective salt. This saturated surface is not available for a further uptake of cations [17].

2.5.2. Sorption of lanthanides and actinides

There are various processes of the retention and mobilisation of lanthanides and actinides in geochemical systems with different physicochemical reactions relations that are illustrated in Figure 2.15. The availability of radionuclides is based on their solubility, which is directly affected by redox processes and complex formation reactions. Already dissolved actinides can form aqueous complexes with various ligands or undergo sorption reactions onto mineral surfaces. In case of an oversaturation also colloids (intrinsic colloids) or a fresh precipitates can be form. [4,

105]. Each of these processes can affect the mobility and migration behaviour of actinides in the near and far field of a repository for nuclear waste. Interactions between cations and mineral surfaces are together with their solubility a key parameter in radionuclide retention. Sorption processes, consisting of adsorption and desorption reactions, are one of the most important interactions between solid phases (adsorbent) and a liquid or gaseous phase (adsorbate).

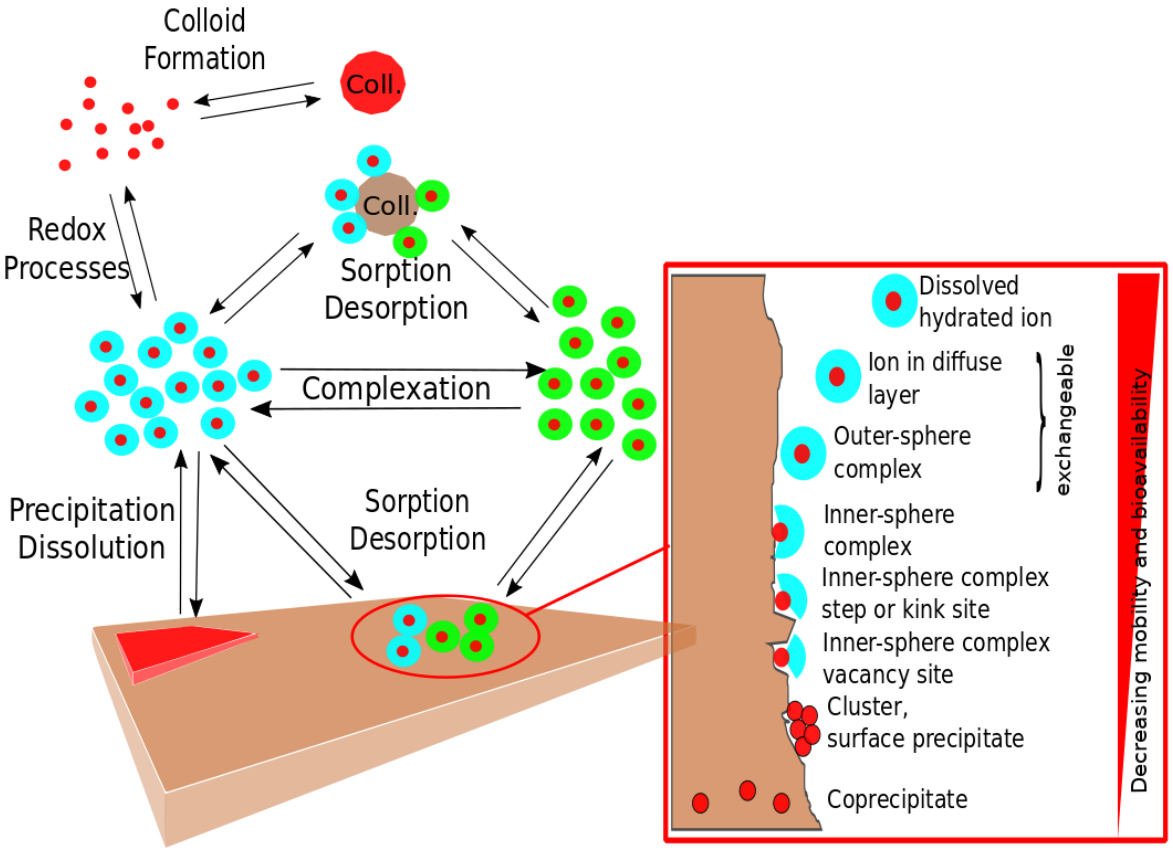

Figure 2.15: Schematic illustration of retention and release mechanisms of metal cations [4, 105].

An adsorbate enters different steps depending on the distance to the adsorbent during the sorption process (Figure 2.15, red box, [4]). Two types of interaction mechanisms are reported. Electrostatic effects are forming weak outer sphere complexes (physisorption, cation exchange), mostly at surfaces with a permanent charge. Covalent bonds are formed with reactive surface groups like the amphoteric hydroxyl

groups in clay minerals forming inner sphere complexes. In the first cases (physisorption) the bonding energy is relatively low, resulting in a fast sorption and desorption kinetic and an easy exchange with other cations. If no other retention mechanism is active, like incorporation or surface reduction, these processes are fully reversible within a relatively short period of time. Physisorption is described as ion exchange. A coordination of the adsorbate with reactive surface groups can involve covalent bonding with a significantly higher binding energy. The stronger interaction between adsorbate and adsorbents is influencing the chemical structure. Due to changes in the first coordination shell induced by the sorption reaction, desorption processes can show significantly slower kinetic. At higher adsorbate concentrations surface precipitation (at even lower concentrations than from homogeneous solutions) or cluster formation at the surface can occur. Both effects are supporting a strong retention of the sorbate. Dynamic processes at the solid-liquid interface such as dissolution-reprecipitation reactions can result in incorporation of the adsorbate [4].

In geochemical model calculations both outer and inner sphere sorption has to be described by surface complexation reactions. A cation exchange reaction for a sodium saturated clay mineral (Na-X), for example with Eu(III), can be formulated with the following equation:

Equation 7:

$$3\ Na\text{-}X + Eu^{3+} \rightarrow 3\ Na^{3+} + Eu\text{-}X_3$$

The inner sphere sorption process takes places at the amphoteric edge sites of the clay mineral. For this reason a pH dependency of the sorption site (≡S) has to be defined. According to Equation 8 and Equation 9 a protonation and deprotonation of these surface sites is can be defined.

Equation 8

$$\equiv S\text{-}OH + H^{+} \rightarrow \equiv S\text{-}OH_2^{+}$$

Equation 9

$$\equiv S\text{-}OH \rightarrow \equiv S\text{-}O^{-} + H^{+}$$

In analogy to that, the adsorption of cation (Eu^{3+}) to sorption sites can be described (Equation 10).

Equation 10

$$\equiv S\text{-}OH + Eu^{3+} \rightarrow \equiv S\text{-}O\text{-}Eu^{2+} + H^{+}$$

Further surface complexation reactions including ligand exchange reactions at the surface site itself, the addition of ligands to the central metal ion or the exchange of the central metal ion in favour of a stronger adsorbing ion can be defined in similar ways. A summary of the surface complexation reactions relevant for this study are given in section 3.3.1.

Sorption processes are getting more complex, if additional ligands like carbonate or organic acids are added to the system. On the one hand these anionic ligands are well known for building strong aquatic complexes with actinides [34, 35, 60] and on the other hand, an adsorption of the anionic ligands to mineral surface is reported at least in the acidic pH range [37, 39, 106-111]. The affinity of organic acids to mineral surfaces in cement (CSH phases) was also correlated with their affinity to Ca^{2+} as counter ions [112]. Several studies are describing a strong decrease for An(III) retention on clay minerals in the presence of carbonate [22, 113]. So far no data are available for the impact of the organic compound citrate or gluconate and their influence on the adsorption of actinides onto clay minerals. Beside inorganic or organic ligands added to the system, the competition of silicate complexation and adsorption of Ln(III)/An(III) is not completely understood.

Most of the previous studies on the complexation of SiO_4 with Cm(III) [18, 56] were performed within stability field of the clay minerals (pH = 3-10 [15]). An approach in alkaline media up to pH = 12.4 was reported by Huittinen *et al.* [114]. A similar approach is demonstrated for the clay minerals illite du puy and montmorillonite in hyperalkaline NaCl and $Ca(OH)_2$ solutions in the appendix 7.5.

2.5.3. Comparing the sorption of An(III) / An(IV) / An(V) onto clay minerals

In the low pH range (pH < 5.5), a constant contribution to the retention of actinides in oxidations states 3, 5 and 6 is given by cation exchange. For tetravalent actinide ions only inner-sphere surface complexation is found. Cation exchange is suppressed at high salt concentrations. With increasing pH the hydroxyl groups at the edge sites are successively deprotonated. Thus, at pH > 5.5 inner sphere sorption becomes the dominating sorption mechanism for trivalent actinide ions. [42]. In the frame of a deep geologic repository for nuclear waste, anoxic and reducing conditions will be established within a relatively short time after closing due to the sealing (exclusion of oxygen) and corrosion processes (consumption of oxygen). This, of course, has a strong impact on redox sensitive radionuclides, by applying reducing conditions in the repository. The following general consideration is focused on systems in absence of competing ligands.

The sorption of trivalent actinides shows a strong ionic strength dependency in the low pH range, where outer sphere sorption takes place (cation exchange) [18, 115, 116]. The retention of An(III) is reduced under saline conditions (I > 0.5). With increasing pH the uptake of trivalent actinides is increasing constantly between pH = 6-8 to an almost quantitative retention [17, 42, 117]. Above pH > 8 a nearly quantitative retention is observed.

Tetravalent actinides show a significantly higher affinity to charged surfaces, compared to trivalent actinides [118]. Already in the acidic range (pH > 3) An(IV) cations are adsorbing with high retention ratios. The sorption mechanism is dominated by inner sphere complexes up to high pH values [14].

Pentavalent actinides only start to form inner sphere complexes above pH > 8, followed by an increase in retention with increasing pH [14]. Actinyl ions like the pentavalent NpO_2^+ are bearing an effective charge of $Z_{eff} = 2.3 \pm 0.2$, compared to a low formal charge. This effects a strong impact of ionic strength on the sorption behaviour dominated by the formation of outer spherical complexes [119]. The retention of AnO_2^+ is significantly lower compared to An(III) and An(IV).

As described in previous sections, foreign ions which are incorporated in the crystal structure of natural clay rock can affect their interaction with actinides. Especially iron impurities (as Fe(II)) can influence the redox speciation and as a result of this, the sorption properties of redox sensitive radionuclides like uranium, plutonium and neptunium [120, 121]. For pentavalent neptunium a surface reduction model was applied to describe anomalies in Np(V) sorption data on the clay mineral illite. Since the reduced tetravalent form has a significantly higher affinity to the mineral surface reduced neptunium gets immediately adsorbed. This approach can explain an increase in Np sorption on iron rich clay minerals [122].

3. Experimental

All chemicals, clay minerals and analysis methods used in this work are described in the following section. The studied systems were modelled with the geochemical code *PhreeqC* [45] using the thermodynamic data given in the *THEREDA* (thermodynamic reference database) [123] or *ThermoChimie* database [73]. These model calculations were performed in order to avoid precipitation of dissolved components. (e.g. the anionic ligands tend to form stable precipitates in the presence of Ca^{2+}). The concentrations of all compounds in the experiments were at least a factor of 3 below their solubility limit. Also the contribution to the total ionic strength of competing ligands to the investigated systems was considered within the model calculations. For a more detailed description of standard analysis methods please refer to specialised literature.

3.1. Materials

3.1.1. Chemicals

The ionic strength of the electrolyte solutions was set to specific values with solid NaCl and $CaCl_2$. The pH of the samples was varied with defined addition of aliquots of NaOH, $CaOH_2$ and HCl. The concentration of the ligand was adjusted with solid Na-Gluconate, Na-Citrate and Na_2CO_3 / $NaHCO_3$. These chemicals were obtained from Merck (pro analysis) and used without further purification. The electrolyte solutions were prepared with deionized water produced by a Milli-Q® system of Millipore (resistance 18.2 MΩ/cm). Commercial buffer solutions for pH calibration were obtained by Merck. The samples in D_2O solution for FTIR investigations were prepared by dissolving the respective salts without crystal water in pure D_2O (Aldrich, > 99%). The pH was adjusted with $DClO_4$ and NaOD (Aldrich, > 99%). Electrolyte solutions were prepared using D_2O and salts without crystal water.

A ^{152}Eu stock solution ($[Eu]_{tot}$ = 6.0 10^{-4} M) was used as spike in the batch sorption experiments (Amersham International). The isotopic composition of the ^{152}Eu solution was ^{151}Eu (83%), ^{152}Eu (13%, $t_{1/2}$ = 13.33 a), ^{153}Eu (4 %). A ^{248}Cm stock solution ($[Cm]_{tot}$ = 1.3 10^{-4} M) was used as spike for time resolved laser fluorescence spectroscopy. The isotopic composition of the ^{248}Cm solution was ^{248}Cm (89.68 %), ^{246}Cm (9.38 %), ^{243}Cm (0.43 %), ^{244}Cm (0.30 %), ^{245}Cm (0.14 %) and ^{247}Cm (0.07 %).

3.1.2. Electrolyte solutions

Carbonate- / Ligand-free solutions

To carry out experimental studies without the influence of a competing ligand (e.g. carbonate, gluconate, citrate) background electrolyte solutions with different NaCl and $CaCl_2$ concentrations ([NaCl] = 0.1, 1, 3 M; [$CaCl_2$] = 0.06, 0.6, 2 M) were prepared with ionic strengths comparable to previous studies by Schnurr *et al.* [17]. The solutions were purged with $Ar_{(g)}$ for 3 h to remove O_2 and transferred into an argon atmosphere glove box (O_2 ~ 2 ppm). All experimental work was performed in protective gas atmosphere.

Carbonate solutions

Two different types of carbonate solutions were prepared with a NaCl background electrolyte concentration of [NaCl] = 0.1, 1, 3 M.

Type I (closed system): A background electrolyte solution with a constant total carbonate concentration of 0.1 M Na_2CO_3 /$NaHCO_3$ was prepared in an Ar-CO_2 glove box (99 % Ar, 1 % CO_2) with Ar-purged MilliQ water. The pH was varied from pH = 7-12.5 by addition of HCl or NaOH.

Type II (equilibrated system): For each single pH-value and salt concentration the $NaHCO_3$, Na_2CO_3, HCl and NaOH content was calculated using the geochemical code *PhreeqC* [45] and the *THEREDA* (thermodynamic reference database) [123] in equilibrium with atmospheric CO_2 (p_{CO2} = $10^{-3.3}$ bar) and at 1 % CO_2. For each pH value and partial pressure a single electrolyte batch was prepared by addition of the calculated amount of $NaHCO_3$, Na_2CO_3, HCl and NaOH to MilliQ water, which was equilibrated with the CO_2 containing atmospheres before to achieve stable initial conditions. The samples at p_{CO2} = $10^{-3.3}$ bar were prepared in contact with air and all experiments were performed under atmospheric conditions. Sample solutions in equilibrium with 1 % CO_2 were set up in an Ar-CO_2 glovebox (99 % Ar, 1 CO_2).

Gluconate / Citrate / Selenite solutions

Samples which contain gluconate, citrate or selenite were prepared by adding a defined amount of 1 M Na-Gluconate or 0.1 M Na-Citrate / Na_2SeO_3 standard solution to the electrolyte. In case of GLU two different sets of samples were studied. One set was prepared with a constant gluconate concentration of $[GLU]_{tot} = 1 \cdot 10^{-2}$ M. The second set was prepared with increasing gluconate concentration form $[GLU]_{tot} = 1 \cdot 10^{-5} - 5 \cdot 10^{-3}$ M. In case of citrate only one set of samples was prepared with a constant concentration of $[CIT]_{tot} = 1 \cdot 10^{-3}$ M. Since especially Ca-Citrate phases ($Ca_3(Cit)_2$:$4H_2O$, SI Figure 7.4) are showing a lower solubility than Na-Citrates it was necessary to reduce the total ligand concentration compared to gluconate systems from $1 \cdot 10^{-2}$ M to $1 \cdot 10^{-3}$ M. A 0.1 M NaCl solution was prepared with $3 \cdot 10^{-3}$ M Na_2SeO_3 for batch sorption experiments.

3.1.3. Clay minerals

Different natural clay minerals used in this work (Illite du Puy (Na-IdP-2), montmorillonite (Na-SWy-2)) were provided as an aquatic suspension from the Laboratory for Waste Management (LES) of the Paul Scherrer Institute (PSI). Both clays were already purified and transformed into a homoionic sodium form. This purification process [15] and pre-treatment procedures are well described in the literature [12, 15, 42, 124]. Furthermore, a synthetic iron free montmorillonite (IFM, [125]) was provided by *Laboratoire des Máteriaux Minéraux, Mulhouse, France*.

Montmorillonite

The montmorillonite type “Wyoming” (Na-SWy-2) was obtained from a clay deposit opened by the Clay Mineral Society (CMS) of the University of Missouri. Na-SWy-2 originates from the cretaceous Newcastle formation, Crook County, Wyoming (USA). A conditioned [11] clay suspension was obtained from *Labor für Entsorgung* LES-PSI (Switzerland) with a solid to liquid ratio of 11.91 g/L. Additionally, a sample of dried clay (same origin and purification) was suspended in D_2O and used for experiments

on carbonate sorption using infrared spectroscopy. Table 5 summarizes the relevant data on this clay mineral.

Table 5: Characterization of Na-SWy-2 [17, 105].

Clay	s/l ratio	CEC	N_2-BET	w-% Fe
Na-SWy-2	11.91 g/L	87.0 meq/100g	37.6 m^2/g	3.80

Illite du Puy

The clay mineral phase Illite du Puy (IdP) originates from the Le Puy en Velay, Massif Central in France. A carefully purified suspension of Na-IdP-2 was obtained by *Labor für Entsorgung* LES-PSI (Switzerland) with a solid to liquid ratio of 32.72 g/L.

Table 6: Characterization of Na-IdP-2 [15].

Clay	s/l ratio	CEC	N_2-BET	w-% Fe
Na-IdP-2	32.72 g/L	22.5 meq/100g	97 m^2/g	7.61

Iron free montmorillonite

Natural clay minerals contain variable contents of structural iron, which may lead to quenching of Cm(III) luminescence in spectroscopic sorption experiments. To avoid such effects, a synthetic iron free montmorillonite (IFM) was obtained from *Laboratoire des Máteriaux Minéraux, Mulhouse, France*. This clay mineral was synthesized using the fluorine route by Reinholdt *et al.* [125]. With this approach an iron free montmorillonite was produced with an isomorphic substitution of octahedral aluminum by magnesium. According to Soltermann *et al.* [126] the CEC properties of IFM are comparable to that of the montmorillonite Na-SWy-2.

Table 7: Characterization of IFM [17, 125, 126].

Clay	s/l ratio	CEC	N_2-BET	w-% Fe
IFM	powder	81.0 meq/100g	n.a.	0*

*below detection limit [17].

3.2. Experimental methods

3.2.1. Batch sorption experiments

Batch sorption experiments in presence of different competing ligands were performed as a function of pH. A detailed description of the experimental conditions is summarized in Table 8.

Batch sorption experiments in presence of carbonate were performed to investigate the retention of Eu(III) onto the clay minerals Illite du Puy (Na-IdP-2) and montmorillonite (Na-SWy-2) using a solid to liquid ratio of 1 g/L and different NaCl solutions ([NaCl] = 0.1, 1, 3 M, described in 3.1.2). The radionuclide concentration was limited to $2 \cdot 10^{-8}$ M. These electrolyte solutions were equilibrated either with ambient CO_2 or an Ar atmosphere with 1 % CO_2 (see 3.1.2). The stability of the pH of all electrolyte solutions was monitored for 2 weeks before used in further experiments. Furthermore, all electrolyte solutions showed stable pH values (± 0.15 pH units) over more than 4 years.

Studies in presence of gluconate ($[GLU]_{tot}$ = 0.01 M) and citrate ($[CIT]_{tot} = 10^{-3}$ M) were performed in NaCl ([NaCl] = 0.1, 1, 3 M) and $CaCl_2$ ($[CaCl_2]$ = 0.06, 0.6, 2 M) electrolyte solutions as described in section 3.1.2. In the case of gluconate an additional set of experiments with increasing ligand concentration ($[GLU] = 10^{-5}$-10^{-3} M) at pH = 9, 10.5 and 12 was performed.

Selenite was chosen as an analogue to carbonate in Eu(III) batch sorption experiments. Aim of experiments was to check for the adsorption of similar anionic ligands on clay minerals and their impact on cation sorption. The advantage of selenite compared to carbonate is the lower volatility and the easier analytical detection. Based on that a series of batch sorption experiments to study the sorption of trivalent europium onto montmorillonite in presence of 10^{-3} M SeO_3^{2-} in 0.1 M NaCl was performed as well.

In case of gluconate, citrate and selenite all studies were performed under anoxic conditions in an argon atmosphere (glove box technique). Experiments with carbonate were performed in equilibrium with different CO_2 containing atmospheres by using ambient conditions ($p_{CO2} = 10^{-3.3}$ bar) and 10^{-2} bar CO_2 (1% CO_2 99 % Ar glove box). Beside experiments where the solution was in equilibrium with the gas phase, experiments with a constant total carbonate concentration of 0.1 M Na_2CO_3 / $NaHCO_3$

were carried out in closed vessels in a 1% CO_2 99 % Ar glove box. All experiments were performed at 20 °C following the experimental routine below.

Table 8: Experimental set up of ^{152}Eu(III) batch sorption experiments

Clay mineral	**Na-IdP-2**	**Na-SWy-2**	**atmosphere**
Solid to liquid ratio	1 g/L		
^{152}Eu	$2 \cdot 10^{-8}$ M		
Equilibration time	3-5 d		
Phase separation	694000 g (90000 rpm), 1 h		
γ-Counting	3 h		
Electrolyte solutions:			
Carbonate			
In equilibrium with atm. CO_2	0.1, 1, 3 M NaCl		Ambient
In equilibrium with 1 % CO_2	0.1, 1, 3 M NaCl		1 % CO_2 99 % Ar
Const. $[CO_3^{2-}] = 0.1$ M	0.1 M NaCl	-	1 % CO_2 99 % Ar
Gluconate			
Const. [GLU] = 0.01 M	0.1, 1, 3 M NaCl 0.06, 0.6, 2 M $CaCl_2$		Ar
[GLU] = $1 \cdot 10^{-5}$–$5 \cdot 10^{-3}$ M	0.1, 1, 3 M NaCl 0.06, 0.6, 2 M $CaCl_2$		Ar
Citrate			
Const. [CIT] = 10^{-3} M	0.1, 1, 3 M NaCl 0.06, 0.6, 2 M $CaCl_2$		Ar
Selenite			
Const. $[SeO_3^{2-}] = 3 \cdot 10^{-3}$ M	-	0.1 M NaCl	Ar

-: No experiments were performed for this systems.

Batch sorption experiments were set up with a total volume of V_{tot} = 5 mL in 20 mL HDPE-Bottles (Zinsser Analytics). In a first step the clay suspension was mixed up with the electrolyte solution and a small spike of slightly acidic ^{152}Eu was added. Since the

carbonate containing electrolyte solutions were already at a fixed pH no further adjustment of the pH was needed due to the buffer capacity of carbonate. In case of the organic ligands (GLU / CIT) and selenite or in absence of competing ligands the pH was readjusted over the next days. In all experiments the pH was monitored daily. Final sampling took place 3 days after a constant pH was reached ($\Delta pH < \pm 0.1$). A volume of 4.2 mL was taken from each sample and transferred into centrifugation tubes (Quick-Seal, Beckman Coulter). The vials were welded and centrifuged for 1 h with a relative centrifugal force (rcf) of 694000 g (rotor: 90TI at 90000 rpm, Centrifuge: Beckman Coulter OPTIMA^{TM} XPN-90). After the centrifugation ~ 3 mL of the supernatant are removed and immediately acidified with 50 µL concentrated HNO_3 in order to reduce sorption to the walls of the vessel. An aliquot of 1 mL of the acidified supernatant is then measured with gamma counting for 3 h (*Wallac 1480 3“ Wizard Automatic Gamma Counter*, Chapter 3.3.3). Afterwards the logarithmic distribution coefficients *log*(K_D) are calculated.

Distribution coefficient

In general, sorption properties of cations are described by a distribution coefficient (K_D). The K_D characterizes the distribution of substances between two physically separated phases, like gaseous, liquid or solid phases or the interface between organic and aqueous liquid phases. In case of adsorption experiments the distribution between the concentration of the adsorbed species (c_{sorb}) and the aqueous species (c_{eq}) is quantified by the distribution coefficient (K_D, Equation 11). Assuming a thermodynamic equilibrium, the systems can be described by a linear adsorption isotherm, using the *Henry* adsorption constant [127].

Equation 11

$$c_{sorb} = K_D \cdot c_{aq}$$

- c_{sorb}: concentration of adsorbed species (mg/kg)
- c_{aq}: concentration of dissolved species (mg/L)
- K_D: distribution coefficient (L/kg)

This linear correlation between adsorbed and dissolved species is only valid for systems with sufficiently low concentrations of adsorbate and if only one sorption site contributes significantly to the adsorbate binding. To apply a *Henry* isotherm an adequate number of identical and independent sorption sites must be available. Onto these sorption site only a mono layer of adsorbate can be established. Approaching the saturation of sorption sites the K_D will decrease with the adsorbate concentration and can be described with a Langmuir isotherm. The K_D is defined as the distribution between adsorbed and dissolved metal ions (Equation 12).

Equation 12

$$K_D = \frac{c_{sorb}}{c_{aq}} = \frac{c_0 - c_{aq}}{c_{aq}} \cdot \frac{V}{m}$$

- c_{sorb}: total initial concentration of the adsorbate (mol/kg)
- c_{aq}: aqueous concentration of the adsorbate at equilibrium (mol/L)
- V: sample volume (L)
- m: mass of the solid / absorbent (kg)

3.2.2. Sample preparation TRLFS

Different procedures for the preparation of samples for TRLFS measurements were applied. A summary is given in Table 9: (1) Preparation of wet paste samples was done by centrifugation of the suspension. The remaining wet paste of clay was transferred into a copper sample holder and sealed airtight. (2) A reduced solid to liquid ratio of 0.25 g/L was selected for the measurement of aqueous suspensions. This was required as light scattering or light absorption effects of the incident laser beam and of the fluorescence emission would reduce the sensitivity of the measurements. (3) Aquatic solutions with no solid phase were studied and titrated directly in cuvettes. All samples were treated under anoxic or ambient conditions or under an atmosphere with a defined CO_2 partial pressure. Wet paste samples were centrifuged, the supernatant and sediment were separated and measured separately in cuvettes and solid sample holders.

Table 9: Experimental setup for Cm(III) spectroscopy.

Ligand	[Cm(III)]	Electrolyte	Clay	c*	w.p.**
CO_3^{2-} (Equilibrium ambient CO_2)	$1 \cdot 10^{-7}$ M	0.1, 1, 3 M NaCl	0.25 g/L	X	
			1 g/L		X
CO_3^{2-} (Equilibrium 1 % CO_2)		0.1, 1, 3 M NaCl	0.25 g/L	X	
			1 g/L		X
Gluconate 0.01 M		0.1 M NaCl		X	
		0.06 M $CaCl_2$	0.25 g/L	X	X
Citrate $1 \cdot 10^{-3}$ M		0.1 M NaCl		X	
		0.06 M $CaCl_2$	0.25 g/L	X	X

c*: solution / suspension in cuvette

w.p.**: wet paste

3.2.3. Sample preparation ATR-IR

Surface sensitive ATR-IR measurements were conducted to derive information on the sorption processes of carbonate onto clay mineral surfaces. Therefore, a stock suspension of 10 g/L Na-SWy-2 in D_2O with 0.1 M NaCl was prepared. Two different sets of samples were prepared: A reference system under anoxic conditions in the absence of CO_2 and a second set at a fixed concentration of 0.01 M Na_2CO_3. All chemicals were stored and handled under Ar or CO_2/Ar atmosphere. The pD was adjusted using a 0.1 M Na_2CO_3 solution in D_2O, NaOD and DCl solution. The samples were equilibrated at pH = 5.5 for 1 week. A volume of ~50 µL deuterated suspension was transferred onto an ATR crystal single bounce cell (Bruker, Platinum ATR cell, Bruker Tensor 27 FT-IR). The sample was measured in a series of 5 measurements with a delay of 2 min under ambient conditions.

3.2.4. Long term sorption experiments

The sorption behaviour of trivalent lanthanides and actinides onto clay minerals was studied over 2 years at elevated pH to check for possible phase transformations/dissolution effects/recrystallizations of the clay minerals on sorption and possible incorporation of radionuclides. Na-IdP-2, Na-SWy-2 and IFM were spiked with Eu(III) or

Cm(III) and contacted with portlandite pore water (pH=12.3). A NaCl solution at the same pH was set up as a reference system to examine a potential Ca-effect (Table 10). The sample preparation deviated from the standard batch sorption procedure: A saturated $Ca(OH)_2$ solution was prepared under anoxic conditions. After 2 weeks of equilibration time the electrolyte suspension was centrifuged with rcf of 37700 g for 30 min (rotor: 45TI at 18000 rpm, Centrifuge: Beckman Coulter OPTIMA^{TM} XPN-90) to remove any solid phase (e.g. colloidal species). The pH was determined to be pH = 12.3. A 0.1 M NaCl solution was adjusted to the same pH using 4 M NaOH.

Table 10: Experimental setup of long term experiments of Eu(III) / Cm(III) sorption onto clay minerals at cement pore water conditions.

	Eu(III)	Cm(III)
Clay	2 g/L	2 g/L
Nuclide concentration	$2 \cdot 10^{-8}$ mol/L	$1 \cdot 10^{-7}$ mol/L
V_{tot}	60 mL	6 mL
Electrolytes	Clay minerals	
$Ca(OH)_2$ sat. pH_{start} = 12.30	Na-IdP-2 Na-SWy-2 IFM	Na-IdP-2 Na-SWy-2 IFM
0.1 M NaCl pH_{start} = 12.30	Na-IdP-2 Na-SWy-2 IFM	Na-IdP-2 Na-SWy-2 IFM

The clay suspension was contacted with the slightly acidic radionuclide containing solution first (pH = 6-6.5, V ~ 1-2 mL). By stepwise addition of small aliquots of the portlandite pore water, the formation of colloidal $Cm(OH)_3$ or $Eu(OH)_3$ species was avoided. A step sequence of 4x10 µL with a 1 h sorption phase between each addition step was chosen. This procedure was repeated with 20, 50, 100, 500 µL and 1 (and 5 mL in case of Eu(III)) until the final volume of 6 mL (Cm(III) sample) or 60 mL (Eu(III) sample) were reached. During this phase, the sample was gently titrated to alkaline pH allowing the radionuclides to adsorb to the clay phase, without any risk of precipitation. These samples were monitored for 2.5 years by measuring pH, TRLFS of Cm(III) containing

samples and gamma counting of radiolabelled Eu(III) containing samples. To determine the state of clay degradation, SEM-EDS measurements were applied to study changes in the morphology and XRD analysis was performed to identify changes of the bulk structure. Experimental results are given in the appendix 7.5.

3.3. Analytical Methods

3.3.1. pH-measurement

Atmospheric and anoxic conditions

To analyse pH depending phenomena a precise determination of the pH is essential. A direct measurement of the pH is only possible for diluted systems with a low ionic strength. In saline systems with higher ionic strength, diffusion potentials and interaction between dissolved ions change the measured voltages and only an operational pH-value (pH_{ex}) can be directly determined. To compensate for these effects an empirical correction coefficient (A) was defined in previous studies [128]. As described below (Equation 13), the electrolyte composition and concentration has to be considered to convert the measured operational pH-values (pH_{exp}) into the molal proton concentration ($pH_m = -log\ m(H^+)$). Table 11 summarizes the correction coefficients for NaCl and $CaCl_2$ electrolyte systems used in this work.
The operational pH_{exp} was measured using a *Metrohm* combined class electrode and an *Orion Dual Star* pH-meter or Orion720 A+.

Equation 13

$$pH_m = pH_{exp} + A_{salt}$$

pH_m: molal proton concentration
pH_{exp}: measured operational pH-values
A: empirical correction coefficient

The ionic strength of a solution is defined by the concentration and the charge of the dissolved ions. It's defined as the sum of single species multiplied with the square of its charge (Equation 14).

Equation 14

$$I_c = \frac{1}{2} \cdot \sum_i c_i \cdot z_i^2$$

- I_c: ionic strength (depending on the ion concentration, c)
- c_i: concentration of ion i
- z_i: charge of ion i

Table 11: Empirical correction coefficient (A) valid for different background electrolytes and concentrations according to Altmaier *et al.* [128], used in this work.

[NaCl]	A_{NaCl}	[$CaCl_2$]	A_{CaCl2}
0.1 M	0	0.06 M	-0.08
1 M	0.09	0.6 M	0.15
3 M	0.49	2 M	0.85

Elevated CO_2 partial pressure

A glovebox with a defined CO_2 partial pressure (1% CO_2, 99% Ar) was used to work with equilibrated carbonate systems. To accurately measure the pH, the filling and storage solutions of the electrodes must be equilibrated with the CO_2 atmosphere prior to the measurement. Otherwise an uptake of carbonate into the filling solution would cause a drift during the pH measurement. Standard buffer solutions above pH = 4 show an in-diffusion of CO_2 leading to an acidification. For this reason every calibration was performed with fresh buffer solutions, which were stored under ambient conditions at 5°C. During a single calibration (max. 5 min), the acidification of the buffer by CO_2 in diffusion was insignificant.

3.3.2. Measurement of CO_2 gas atmospheres

The CO_2 partial pressure of the laboratory atmosphere and the glove boxes in use were measured with a *Telaire TEL-7001 CO_2 infrared sensor* and a *Zirox SGM5T-6.9A* instrument. Both instruments are based on a nondispersive infrared sensor (NDIR sensor). A schematic illustration of the setup given in Figure 3.1.

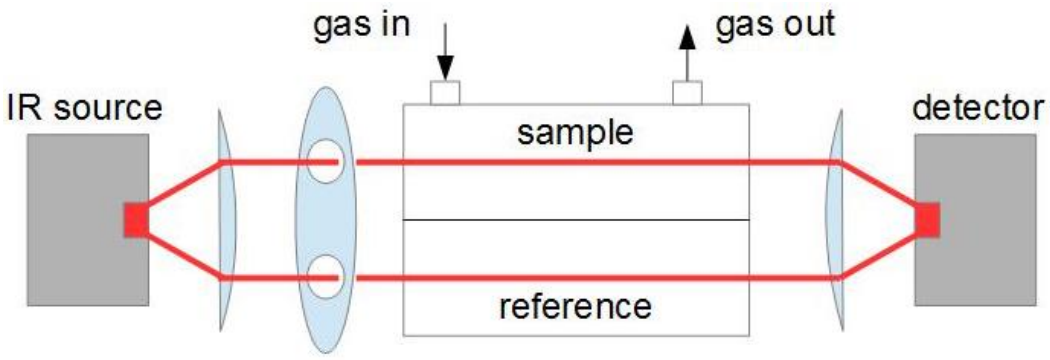

Figure 3.1: Schematic illustration of a NDIR sensor [129]

An incident infrared beam is focused onto a chopper by a lens. The beam is then sent through a reference gas or the actual gas sample. A second lens is focussing the IR beams from both pathways back into the detector. As an alternative to the mechanical chopper, a system with two detectors, one for each pathway, can also be used. This latter type was used in the present work.

The presence and quantity of CO_2 in the gas sample is determined by a transmission measurement (ratio: sample/reference). Nitrogen is commonly used as inert reference gas with no absorbance of light in the infrared. Both devices use a flow cell for continuous measurements. Beside CO_2 all infrared active gasses interfere the measurement. For experiments during this work neither organic gases nor water were present in critical concentrations.

3.3.3. γ-Counting

A precise determination of the γ-activity in solution was achieved with a *Wallac 1480 3“ Wizard Automatic Gamma Counter*. This device is based on a thallium doped NaI single crystal detector (Ø 76.2 mm) with a 75 mm lead shielding. If ionising γ radiation enters the NaI(Tl) crystal, the generated photoelectrons transfer their energy into the NaI(Tl) lattice. Excited centres of the lattice subsequently relax under emission of light. Emitted photons are multiplied (photomultiplier tube, PMT) and convert into an electronic signal. This method provides an accurate and sensitive counting of gamma emitting radionuclides with a low energy resolution.

3.3.4. Time resolved laser fluorescence spectroscopy (TRLFS)

TRLFS measurements were performed with a Nd:YAG (Continuum Surelite II, λ = 355 nm, repetition rate: 10 s^{-1}) pumped dye laser system (Radiant dyes Narrow Scan, Dye: Exalite398, Energy: 1-2 mJ), operated at a constant excitation wavelength of λ = 396.6 nm (Figure 3.2). The resulting fluorescence was detected with an optical multichannel analyser with polychromator unit (Shamrock 303i, Andor, Grating: 1200 lines/mm, Range: λ = 580-620 nm) and an ICCD-camera (iStar, Andor; Modell DH720-18F-63). Measurements were taken with a delay time of 1 µs after the laser pulse. To monitor the fluorescence lifetime, series of single spectra measurements with increasing delay time (steps: Δt = 3-100 µs) were taken.

Beside fluorescence emission, the excitation of Cm(III) with a laser beam of suitable wavelength (396.6 nm) generates a local infrared spectra representing the first coordination sphere of the central metal ion. This local infrared spectra is detected between λ ~ 600-790 nm, above the fluorescence emission. Due to the low intensity of these so called vibronic side bands (VSB) low wavenumbers are superimposed by the fluorescence emission.

As described in section 3.2.2 different types of samples were used. Measurements of clear solutions and suspensions were conducted in cuvettes, while for wet paste samples a special solid sample holder made of copper was used. Both devices are suitable for treatment of air sensitive samples.

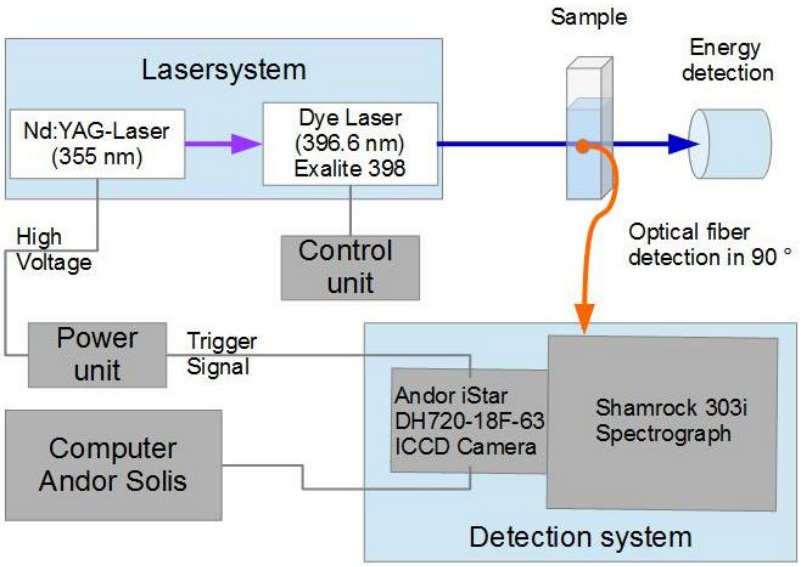

Figure 3.2: Schematic description of a Nd:YAG pumped dye laser system for time resolved laser fluorescence spectroscopy.

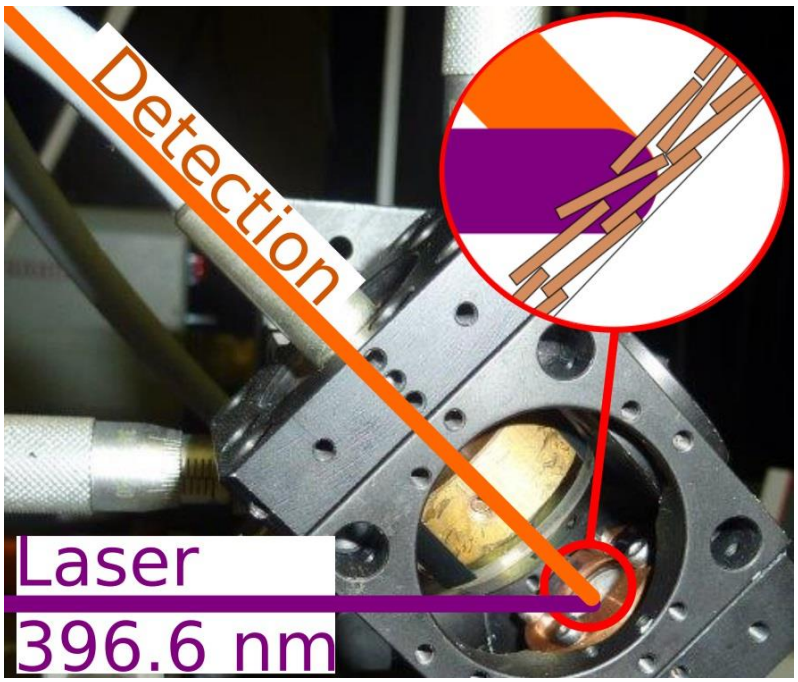

Figure 3.3: Sample holder for measuring wet pastes with TRLFS under exclusion of disturbing light entrance. In the photo, the shielding has been removed.

For the measurement of wet paste samples a new sample holder was designed (Figure 3.3). The sample holder consists of a cube (Newport Opto-Mechanics) which can be moved in x, y, z-direction and is shielded on five sides to exclude interfering light entrance. The collection of the fluorescence emission via an optical fibre takes place perpendicular to the sample surface maximizing the detection yield of the fluorescence emission. The samples were prepared as described for batch sorption experiment, using 1 g/L clay and $1 \cdot 10^{-7}$ M Cm(III). Experiments in presence of carbonate were performed in an Ar-CO_2 glove box (99 % Ar, 1 % CO_2). In the absence of carbonate a CO_2 free Ar glovebox was used (section 3.2.2).

3.3.5. Attenuated total reflection infrared (ATR-IR)

ATR-IR measurements were performed in cooperation with Dr. Peter Weidler and Stefan Heißler at the Institute of Functional Interfaces (IFG) at KIT, Karlsruhe. For measurements of carbonate adsorbed onto a clay mineral surface, a Bruker Tensor 27 coupled with a Platinum ATR cell was used. A spectral range from 4000-370 cm^{-1} was covered with 512 scans for each spectrum and a resolution of 4 cm^{-1} was obtained. All measurements were repeated 5 times with a delay of 2 min to let the suspension sediment onto the ATR crystal.

Surface sensitive infrared measurements were performed with a cell for attenuated total reflection (ATR-IR). The ATR cell consists of an infrared transparent crystal (diamond) with a high refraction index and polished surfaces. An infrared beam is coupled into the crystal at an angle of 45°. At the interface between crystal and sample the beam is totally reflected. Due to the Goos-Hänchen effect (wave properties of the incident beam) the beam is not reflected directly at the crystal plane [130]. The reflection takes place on a virtual point which is shifted into the sample media with a lower optical density. This is called an evanescent wave. It is probing the sample depending on its penetration depth (1.66 µm for diamond/water interface). After the reflection in the sample, the light is directed to a detector. As described by Figure 3.4 the infrared beam can be reflected only once (left) or multiple times (right). Single bounce cells are generating the spectral information from only one reflection, multi bounce cells are probing the sample more often during one measurement. Since every

reflection is causing a loss in intensity multi bounce cells are limited by a low signal to noise ratio. Beside different spectral properties, multi-bounce cells are vulnerable against mechanical stress (common material ZnSe). Single bounce technique provides a higher intensity and the crystal material (diamond) is much more robust against chemical and mechanical stress.

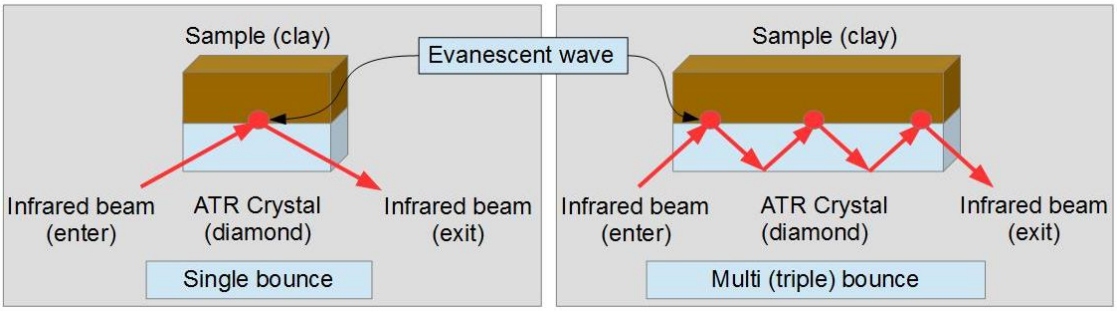

Figure 3.4: Principle of ATR measurement in single (left) and multi bounce cells.

3.3.6. X-Ray powder diffraction (XRD)

Standard XRD analysis of clay minerals were performed under ambient conditions. Clay samples were centrifuged and washed with Milli-Q water to remove the electrolyte solution and to avoid the formation of NaCl crystals. 50-150 µL of the clay suspension were dried onto a single crystal silicon wafer at room temperature and under Ar atmosphere. Radioactive samples were sealed in a special sample holder for measurements under anoxic conditions. All x-ray powder diffraction measurements were performed using a D8 Advance (Bruker) diffractometer with a Cu K-α radiation source (λ = 0.15418 nm, I = 25 mA, U = 40 kV) and an energy dispersive detector (Sol-X). Data treatment and phase identification was performed using DIFFRAC.EVA 3.0 (Bruker) and the JCPDS database.

3.3.7. Scanning electron microscopy – energy dispersive X-ray spectroscopy (SEM-EDS)

A combined SEM-EDS analysis was used to gain information on the morphology and chemical composition of clay minerals in the long term experiments. This surface sensitive imaging method was used to monitor early stage alteration, invisible for bulk characterization methods like XRD.

After a phase separation the clay was washed with Milli-Q water to remove the electrolyte and prevent the formation of NaCl crystals. 15 µL of the re-suspended sample were transferred to a polished carbon sample holder. A Quanta 650 FEG instrument (FEI) equipped with a Thermo Scientific UltraDry silicon drift X-ray detector was used to perform the SEM-EDS analysis.

3.3.8. N_2-BET specific surface area

The characterisation of the specific surface of clay minerals was performed by PSI (Switzerland) using the N_2-BET method [131]. Gaseous N_2 is passed over the sample which is cooled with liquid nitrogen. Cooling the sample generates a constant pressure. By monitoring changes in the N_2 pressure, adsorption-desorption isotherms can be measured and the specific surface derived (SI: m^2/g).

3.3.1. Theoretical calculations

For a theoretical description of sorption processes on a molecular scale a density functional model for clay edges was applied in cooperation with Dr. Michael Trumm of KIT-INE. According to Churakov *et al.* [132] the infinite clay mineral sheet was cut to obtain realistic (100) and (010) edges.

To properly account for the periodicity of the system, Gaussian and plane-waves method [133, 134], a particular implementation of density functional theory (DFT) as implemented in the CP2K software package [135] was used. With this approach it is possible to determine the local structure of different Ln(III)/An(III) surface complexes, their relative energy and vibrational spectra. For the latter, an ab initio molecular dy-

namics (AIMD) approach based on the DFT wave function was employed at room temperature. Vibrational spectra, determined from the velocity auto-correlation function of relevant atoms can directly be compared to vibronic sideband spectra (VSB) [136, 137].

3.3.1. Geochemical Modelling

Important aspects of the present work are investigations in saline media. In concentrated salt solutions, a correction of the activity coefficients e.g. of aquatic actinide complexes is needed. For this reason the ion-ion interaction has to be considered in geochemical models. Two different interaction models were used to describe concentrated electrolyte systems: The semi-empirical Pitzer approach which is especially designed for high salt concentrations [138, 139] and the SIT (specific ion interaction theory) [140] approach for lower concentrated electrolytes.

The Pitzer approach uses a Debye-Hückel term to describe ion-ion interaction in aqueous solution and is extended to take into account the short range, binary and ternary interaction between dissolved ions and neutral species into account. With the Pitzer approach a realistic description of saline and highly saline electrolytes is possible. The ionic strength is included with a Debye-Hückel term, the interaction between different species is then described by viral coefficients. The high number of parameters increases the complexity of this approach. A great effort has to be put into the determination of all these parameters. For a further description see Pitzer *et al*. [139].

Using the simplified SIT approach, the description of many systems is accessible by comparing analogue systems without the need of further experimental data [140]. The activity coefficient is described in Equation 15. The mathematical expression includes the charge of the ion (z), a Debye-Hückel term (brackets) and a sum of interaction parameters. The strength of the SIT model is the description of systems up to $I_{max} \leq 3$ M. In this range the Debye-Hückel term is dominant and the calculated activity coefficients are accurate. At higher ionic strength the simplified interaction term is causing inaccuracies and the use of a Pitzer model is advisable.

Equation 15

$$\log \gamma_i = -z_i^2 \left[\frac{A\sqrt{I}}{1+B_{a_j} 1.5\sqrt{I}} \right] + \sum \varepsilon_{ij} m_j$$

$\log \gamma_i$: logarithmic activity coefficient

z_i : charge of the ion i

m_j: concentration of the ion i

ε_{iJ}: interaction parameter of inversely charged ions

I: ionic strength (molal)

A/B_{a_j}: constants (temperature / pressure depending) 0.509 and 1.50 $kg^{1/2} \cdot mol^{1/2}$ (25 °C, 1bar)

Based on batch sorption experiments and time resolved laser fluorescence spectroscopy, a 2 site protolysis non-electrostatic surface complexation and cation exchange (2SPNE SC/CE) sorption model according to *Bradbury & Baeyens* [11, 42] was applied to model the experimental findings. This model approach describes surface complexation at two different sorption sites, strong and weak sites, and as an additional aspect an empirical cation exchange term, without considering electrostatic effects on a molecular level. In a first approach the model parameter for aqueous species (Table 12, [123]), surface hydroxyl densities, cation exchange capacities, surface complexation reactions in absence of CO_3^{2-} (Table 13, [14, 15, 117]) and surface complexation reactions in presence of CO_3^{2-} (Table 14, [113, 141]) from literature were used without modification.

Table 12: Hydrolysis and carbonate complexation constants for Am(III) as an analogue for Eu(III) and Cm(III) [123].

Hydrolysis	log β^0
$Am^{3+} + H_2O \leftrightarrow AmOH^{2+} + H^+$	-7.2±0.5
$Am^{3+} + 2\ H_2O \leftrightarrow Am(OH)_2^+ + 2\ H^+$	-15.1±0.7
$Am^{3+} + 3\ H_2O \leftrightarrow Am(OH)^0 + 3\ H^+$	-26.2±0.5
Carbonate complexation	log β^0
$Am^{3+} + CO_3^{2-} \leftrightarrow AmCO_3^+$	8.0±0.4
$Am^{3+} + 2\ CO_3^{2-} \leftrightarrow Am(CO_3)_2^-$	12.9±0.6
$Am^{3+} + 3\ CO_3^{2-} \leftrightarrow Am(CO_3)_3^{3-}$	15.0±1.0

Table 13: Model parameter for surface complexation reactions in absence of competing ligands in NaCl containing solutions [14, 15, 117].

	Na-IdP-2	Na-SWy-2
Surface sites / cation exchange capacities	n [mol/kg]	
$\equiv S^SOH$	$2.0\cdot10^{-3}$	$2.0\cdot10^{-3}$
$\equiv S^{W1,W2}OH$	$4.0\cdot10^{-2}$	$4.0\cdot10^{-2}$
CEC	$4.0\cdot10^{-1}$	$8.7\cdot10^{-1}$
Surface protolysis reactions	log $K_{protolysis}$	
$\equiv S^{S,W1}OH + H^+ \leftrightarrow \equiv S^{S,W1}OH_2^+$	4.0	4.5
$\equiv S^{S,W1}OH \leftrightarrow \equiv S^{S,W1}O^- + H^+$	-6.2	-7.9
$\equiv S^{W2}OH + H^+ \leftrightarrow \equiv S^{W2}OH_2^+$	8.5	6.0
$\equiv S^{W2}OH \leftrightarrow \equiv S^{W2}O^- + H^+$	-10.5	-10.5
Surface complexation reactions	log K_{sc}	
$\equiv S^SOH + Am^{3+} \leftrightarrow \equiv S^SO\text{-}Am^{2+} + H^+$	1.9	1.6
$\equiv S^SOH + Am^{3+} + H_2O \leftrightarrow \equiv S^SO\text{-}AmOH^+ + 2\ H^+$	-4.6	-5.9
$\equiv S^SOH + Am^{3+} + 2\ H_2O \leftrightarrow \equiv S^SO\text{-}Am(OH)_2^0 + 3\ H^+$	-12.8	-14.2
$\equiv S^SOH + Am^{3+} + 3\ H_2O \leftrightarrow \equiv S^SO\text{-}Am(OH)_3^- + 4\ H^+$	-25.3	-25.3

Table 14: Model parameter for carbonate containing ternary surface complexation reactions [113, 141].

	Na-SWy-2	Na-IdP-2
Surface complexation reactions	log K_{sc}	
$\equiv S^SOH + Am^{3+} + CO_3^{2-} \leftrightarrow \equiv S^SO\text{-}AmCO_3^0 + H^+$	8.3	9.8
$\equiv S^SOH + Am^{3+} + CO_3^{2-} + H_2O \leftrightarrow \equiv S^SO\text{-}Am(OH)CO_3^- + 2\ H^+$	-0.25	1.4

In a second step a modified model approach considering carbonate sorption onto the clay mineral surface and resulting in a (partly) carbonate coated surface was used instead of formation of ternary carbonate surface complexes as shown in Table 14. According to Su & Suarez aluminium and iron oxides/hydroxides show similar surface reactions with carbonate. Since there is no thermodynamic data for the sorption of carbonate onto clay minerals or aluminium oxides/hydroxides, studies on iron oxides from Van Geen *et al.* were used as an analogue system (Table 15, [109]). Following this approach, the clay mineral surface is covered with carboxyl groups and exhibits new sorption properties after the interaction with carbonate. A detailed description of the modified surface and the resulting surface reactions is given in section 4.1.5. Since there is no other data available, the constants from the diffuse layer model of Van Geen *et al.* were taken as a first approximation for this modified 2-SPNE/CE approach.

Table 15: Model parameters for carbonate sorption on goethite surfaces [109], used as a model compound for clay mineral surfaces (this work).

Surface complexation reactions	log K_{sc}
$\equiv SOH + HCO_3^- \leftrightarrow \equiv S\text{-}O\text{-}CO_2H + OH^-$	20.78
$\equiv SOH + CO_3^{2-} \leftrightarrow \equiv S\text{-}O\text{-}CO_2^- + OH^-$	12.71

4. Results and discussion

The two clay minerals Illite du Puy and Montmorillonite, which are studied in the present work, show comparable sorption properties towards Ln(III) and An(III) at low as well as high ionic strength [13-15, 17, 22, 113, 119, 142, 143]. For this reason, results obtained for both clay minerals are described and discussed together.

4.1. Impact of carbonate on the sorption of Eu(III) and Cm(III) onto clay minerals

The retention of trivalent lanthanides and actinides on clay minerals was studied in equilibrium with different partial pressures of CO_2: (1) Ambient CO_2 ($p_{CO_2}=10^{-3.3}$ bar) under oxic conditions (laboratory atmosphere) and (2) elevated partial pressure of CO_2 ($p_{CO_2}=10^{-2}$ bar) under anoxic conditions (99 % Ar, 1 % CO_2) and in presence of a constant concentration of 0.1 M HCO_3^-/CO_3^{2-} (closed system). The equilibrated systems are containing an increasing carbonate concentration with increasing partial pressure of CO_2. Due to the complexity of a system which contains a solid phase, a liquid phase and a gaseous reactant, a broad range of different analytical methods was applied to study the sorption processes.

4.1.1. Batch sorption experiments

Ambient CO_2 conditions ($p_{CO_2}=10^{-3.3}$ bar)

The sorption behaviour of trivalent actinides and lanthanides, represented by Eu(III), onto the clay minerals Illite du Puy and Montmorillonite was studied in diluted and concentrated NaCl solutions in the presence of ambient CO_2 conditions. In case of Montmorillonite similar experiments were also performed in the absence of CO_2.
The sorption edges of Eu(III) are presented as logarithmic distribution coefficients (log K_D) versus pH_m (Figure 4.1) for Na-IdP-2 (left) and Na-SWy-2 (right). Experimental

data from diluted to concentrated electrolyte solutions are shown (I-1 / M-1: 0.1 M NaCl, black symbols; I-2 / M-2: 1 M, red symbols and I-3 / M-3: 3 M NaCl, blue symbols). The composition of each electrolyte solution was separately calculated and prepared.

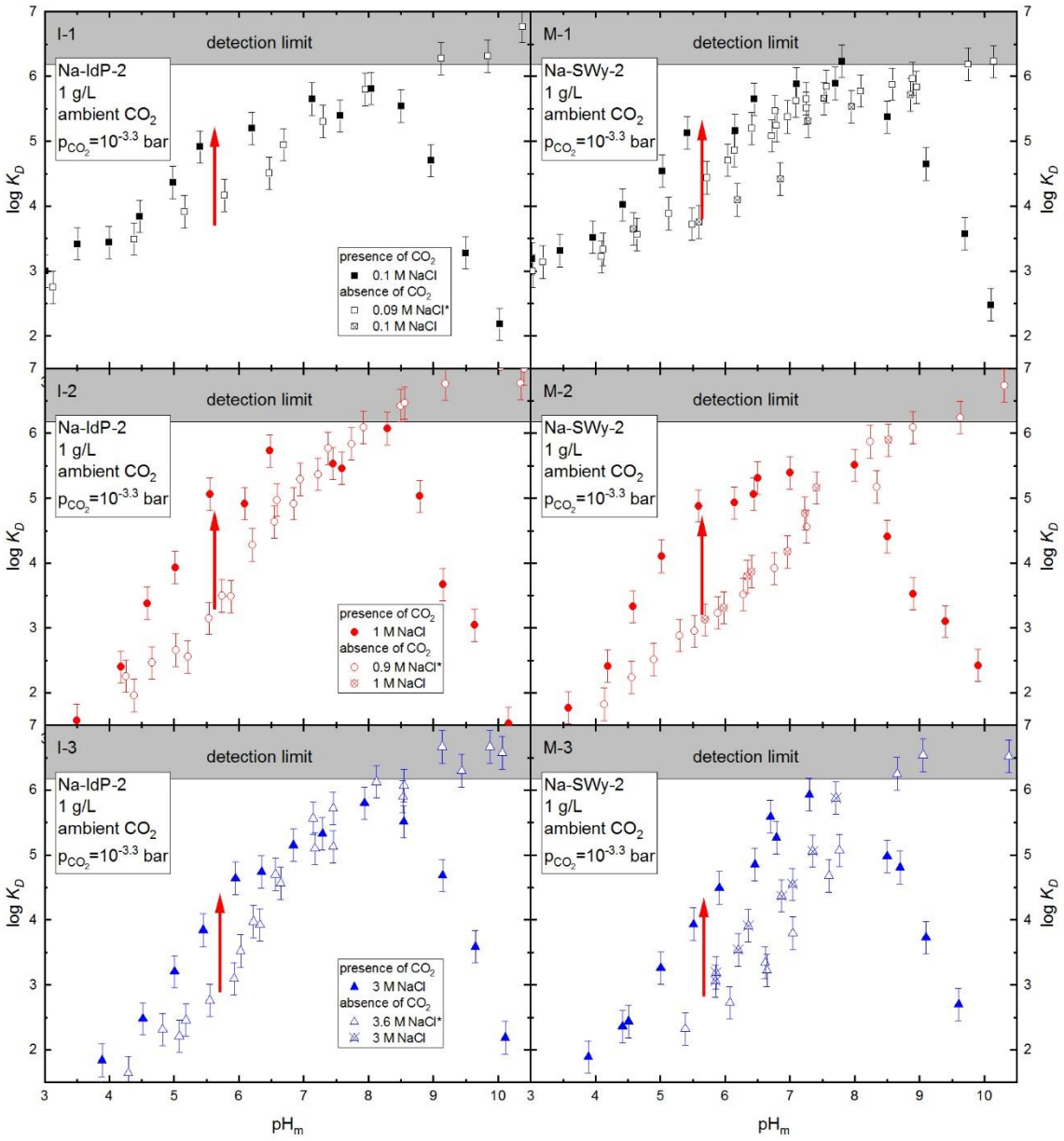

Figure 4.1: Eu(III) sorption edges for Na-IdP-2 (left) and Na-SWy-2 (right), in equilibrium with ambient CO_2 (closed symbols) and in absence of CO_2 (open symbols). * literature data (Schnurr *et al.* [17]), in different saline media ([NaCl] = 0.1 M black I/M-1, 1 M red I/M-2, 3 M blue I/M-3) and in the absence of CO_2 (crossed symbols, 0.1, 1, 3 M NaCl, this work).

Available literature sorption data at similar ionic strength conditions and in absence of carbonate were added (open symbols, 0.09, 0.9, 3.6 M NaCl, Schnurr *et al.* [17]) to estimate the impact of carbonate and to compare with own data in case of Montmorillonite (crossed symbols 0.1, 1, 3 M NaCl, in absence of CO_2).

The retention of Eu(III) increases in the pH range from 3 to 8 in presence of CO_2. At low ionic strength (0.1 M NaCl) the log K_D increases from log K_D ~ 3 to 6. The sorption edges of systems with high ionic strength start at log K_D ~ 1.5 and rise up to log K_D ~ 6. For pH > 8 a strong decrease in retention is observed in all systems with only minor impact of ionic strength. Overall, the log K_D is reduced by about 4 orders in magnitude in the selected alkaline pH range. In case of the Eu(III) sorption onto montmorillonite (right), this decrease shows a slight difference between high ionic strength (earlier and more pronounced decrease) and low ionic strength. The effect of cation exchange sorption for Eu(III) is supressed under saline conditions by adsorption of Na^+ being present in large excess. For this reason the retention of Eu(III) in the lower pH range is generally reduced in presence of high NaCl concentrations (1 M, 3 M NaCl).
An interesting feature which is obvious in Figure 4.1 is, that between pH ~ 4.5-6.5 the adsorption of Eu(III) is increased in the presence of CO_2 (closed black symbols) compared to literature and own data in absence of CO_2 (open black symbols). This effect is apparent for both studied clays for all investigated ionic strengths. At I=0.1 M NaCl the enhancement appears to be less pronounced than at higher ionic strength. For both clays a maximum difference of Δ_{max}log K_D ~ 1-1.5 is observed at pH ~ 5.5 (red arrow). The increase was further validated by batch sorption experiments in the absence of CO_2 by using the identical batch of purified montmorillonite (crossed symbols). The derived log K_D values are comparable or slightly below the data of Schnurr *et al.* [17] and supporting the experimental findings.
This increase of the log K_D values raises the hypothesis that carbonate may enhance trivalent lanthanide and actinide sorption to the clay mineral surface in the slightly acidic pH-range. These effect was not observed before.

A comparison of the results of the present work with studies by Marques *et al.* [22, 113] also performed in the presence of atmospheric CO_2 is displayed in Figure 4.2 The log K_D values of Marques *et al.* are very comparable to those obtained in the present work in the neutral to high pH region (pH ≥ 7.5). However, Marques *et al.* observed no

increase in the retention of Eu(III) adsorbed onto Illite du Puy (Figure 4.2, left) nor onto Montmorillonite (Na-SWy-2, Figure 4.2, right) between pH = 3-7 where only two data points are reported in the slightly acidic pH range. Possible explanations for this deviation could be an incomplete equilibration with the CO2 containing gas phase or effects of outgassing in the acidic range. In the present work great efforts are made to reach and maintain equilibrium conditions especially in the acidic pH range: (1) The partial pressure of CO_2 under ambient and elevated (next section) conditions was monitored during the experimental procedure. (2) The composition of the different electrolyte solutions was calculated using the geochemical code *PhreeqC* [45] considering the measured prevailing CO_2 partial pressure of the laboratory ($p_{CO_2}=10^{-3.3}$ bar). Each electrolyte solution was separately prepared by adding $NaHCO_3$ / Na_2CO_3 and checked for pH stability over a period of at least 2 weeks.

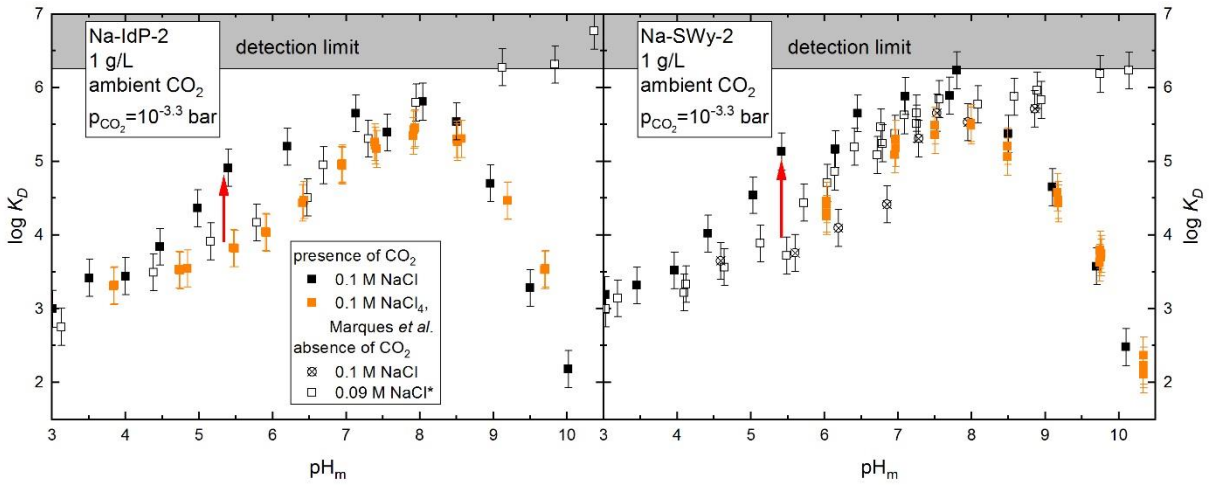

Figure 4.2: A comparison between Eu(III) sorption edges derived in the present work and literature data (closed orange symbols, Marques *et al.* [22, 113]): Eu(III) adsorbed onto Na-IdP-2 (left) and Na-SWy-2 (right), in equilibrium with ambient CO_2 (closed symbols) and in absence of CO_2 (open symbols, *Schnurr *et al.* [17], crossed symbols, this work).

Elevated CO_2 conditions ($p_{CO_2}=10^{-2}$ bar)

To study conditions which are comparable to deep groundwater conditions, batch sorption experiments were performed at an elevated partial pressure of CO_2. Batch samples were prepared in equilibrium with an atmosphere containing 1 % CO_2, to consider the higher carbonate content in deep geological aquifers. For this, a glovebox was used with an atmosphere of 99 % Ar and 1 % CO_2 ($p_{CO_2}=10^{-2}$ bar). The retention of Eu(III) on Illite du Puy (left) and Montmorillonite (right) was investigated in equilibrium with 1 % partial pressure of CO_2 and at low to high ionic strength. The log K_D is shown as a function of pH in Figure 4.3 for Na-IdP-2 (left) and Na-SWy-2 (right) for [NaCl] = 0.1 M in black, 1 M in red and 3 M in blue (closed symbols in the presence of CO_2). log K_D values in CO_2-free aqueous solution (open symbols: 0.09, 0.9, 3.6 M NaCl, Schnurr *et al.* [17]; crossed symbols: 0.1, 1, 3 M this work) are added in the graph for comparison.

As already noticed in experiments with $10^{-3.3}$ bar CO2, an enhanced retention of Eu(III) is observed in equilibrium with an atmosphere containing 1 % CO_2 in the acidic to neutral pH range (pH ~4-6) compared to own (crossed symbols) and literature data in the absence of CO_2 (open symbols, *Schnurr *et al*. [17]). In case of the Eu(III) adsorption onto illite, a less pronounced increase in Eu(III) retention is observed and the maximum of this effect is observed at lower pH values in equilibrium with 1 % CO_2 compared to ambient conditions.

The enhanced retention of Eu(III) is observed for Illite du Puy and Montmorillonite for all selected ionic strengths. Depending on the subsystem a general difference of $\Delta_{max}\log K_D$ ~ 0.5-1 is observed.

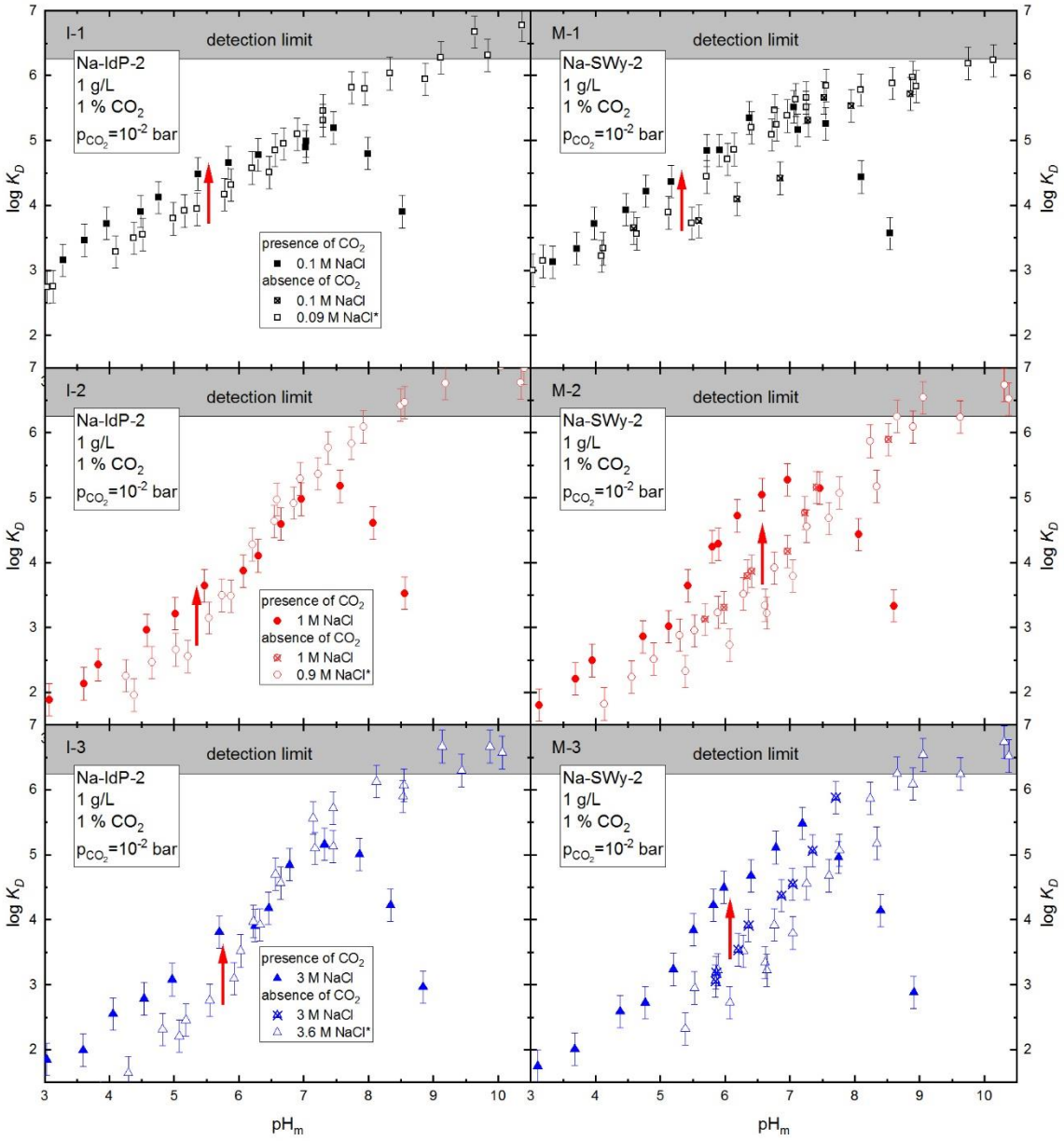

Figure 4.3: Eu(III) sorption edge on Na-IdP-2 (left) and Na-SWy-2 (right), in equilibrium with an elevated partial pressure of CO_2 (1 % CO_2, closed symbols) and in absence of CO_2 (open symbols, *Schnurr *et al*. [17]) and this work (crossed symbols), in different saline media ([NaCl] = 0.1 M black I / M-1, 1 M red I / M-2, 3 M blue I / M-3).

"Analogue" selenite (SeO_3^{2-}) system

Sorption experiments in presence of carbonate are bearing the potential of outgassing notably in the acidic pH range and might lead to experimental artefacts. To confirm and test the hypothesis of an enhanced Eu(III) sorption in presence of carbonate in the acidic pH range an analogue system was studied. SeO_3^{2-} was selected as a substitute for CO_3^2, due to the structural analogy a similar chemical behaviour of CO_3^{2-} and SeO_3^{2-} is expected. Hiemstra *et al.* [107] have reported a similar sorption behaviour of CO_3^{2-} and SeO_3^{2-} contacted with the iron oxide mineral goethite. Further on, Missana *et al.* have published batch sorption experiments and a corresponding geochemical model to describe the adsorption of SeO_3^{2-} onto the clay mineral phases illite and montmorillonite, proven that selenite is adsorbing in the slightly acidic pH range [144]. In addition to the investigation of binary systems, containing only the solid phase and the inorganic ligand, a ternary system was also studied: Shi *et al.* have reported an enhanced Eu(III) sorption onto TiO_2 in presence of SeO_3^{2-} [61]. The available literature data indicate a similar sorption behaviour of CO_3^{2-} and SeO_3^{2-} onto mineral surfaces, as well as stabilizing effects of the anionic ligand on the adsorption of metal cations. Therefore, the sorption of Eu(III) onto montmorillonite in presence of SeO_3^{2-} was studied in a diluted NaCl electrolyte solution ([NaCl] = 0.1 M). The logarithmic distribution coefficient is plotted as function of pH in Figure 4.4 (closed symbols). The data are compared with experimental Eu(III) sorption data in absence of CO_2 (open symbols, *Schnurr *et al.* [17]) and in equilibrium with ambient CO_2. The retention of trivalent europium in presence of selenite increases from log K_D =3.1-5.5 between pH = 3.5-6 and reaches nearly quantitative retention above pH > 6.5. A stabilizing effect of selenite on adsorbed Eu(III) is observed. This is in good agreement with studies on the effect of carbonate on the Eu(III) retention in clay minerals.

The sorption behaviour of Eu(III) in presence of both similar inorganic anions, selenite and carbonate, has been proven to be congruent under the selected experimental conditions. This is a further clear indication that carbonate (or other similar inorganic ligands) can enhance the sorption of trivalent actinides on clay minerals in the slightly acidic pH range. This general enhancing effect of complexing anions on metal ion sorption in the acid pH range is also well known for a variety of organic ligands [119].

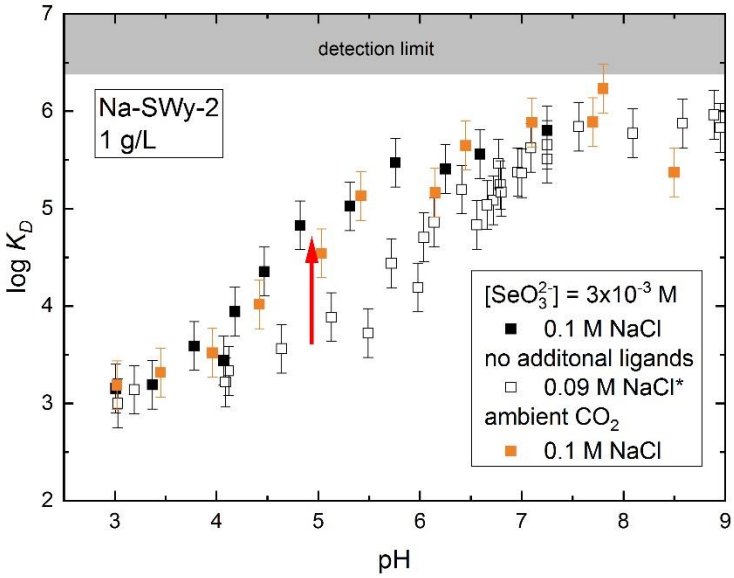

Figure 4.4: Eu(III) sorption edge for montmorillonite in presence of $3 \cdot 10^{-3}$ M SeO_3^{2-} (closed, black symbols), in equilibrium with ambient CO_2 (closed, orange symbols) and in absence of SeO_3^{2-} (open symbols, *Schnurr *et al.* [17]), in 0.1 M NaCl.

Constant carbonate concentration – 0.1 M $NaHCO_3/Na_2CO_3$

The total dissolved carbonate of in deep aquifer systems is limited by the solubility of carbonate mineral phases. An equilibration with a CO_2 containing gas phase leading to an increased carbonate concentration with increasing pH as assumed in the previously described experiments is, thus, not to be expected. Rather a more or less constant carbonate concentration in solution will be expected in aquifers. In order to study the pH dependent sorption of Eu(III) at a constant total inorganic carbon (TIC) concentration an experimental series was started at a fixed total carbonate concentration of 0.1 M $NaHCO_3/Na_2CO_3$ in the range of pH = 7-12.5 (Figure 4.5, closed red symbols).

The results of the experiments are presented as logarithmic distribution coefficient as function of the pH. It is evident that the variation of Eu(III) sorption with pH is completely different from those studies, where the solutions are equilibrated with a CO_2 containing gas phase. The retention of Eu(III) decreases almost linearly from log K_D =4 to 3 between pH = 7-10.5 and increases again at pH > 10.5. The decrease in sorption is

explained by formation and competition of non-adsorbing aqueous Eu(III) carbonate complexes with surface complexes. Previous results of experiments related to the sorption of Eu(III) in equilibrium with ambient CO_2 (green symbols), with an elevated partial pressure of 1 % CO_2 (orange symbols) and in absence of CO_2 (open black symbols, Schnurr *et al.* [17]) are added to Figure 4.5. Compared to studies performed in equilibrium with a gas phase with a given partial pressure of CO_2, Eu(III) sorption never decreases to values below log K_D = 3 at 0.1 M Na_2CO_3/$NaHCO_3$. This finding is explained by the carbonate concentration steeply increasing with increasing pH when in contact with the ambient atmosphere. At pH=10 a more than ten times higher total carbonate concentration establishes as compared to that in experiments with 0.1 M TIC and results in the predominant formation of non-adsorbing aqueous Eu(III) carbonate complexes. The following calculation illustrates this effect: When keeping the total carbonate concentration constant, the related calculated partial pressure of CO_2 is decreasing from 4.3 % (pH = 7, $p_{CO_2}=10^{-1.57}$ bar) to $5.5 \cdot 10^{-8}$ % (pH = 12.5, $p_{CO_2}=10^{-9.3}$ bar). The observed increase in retention above pH > 10.5 is caused by the progressing formation of inner sphere Eu(III) surface complexes.

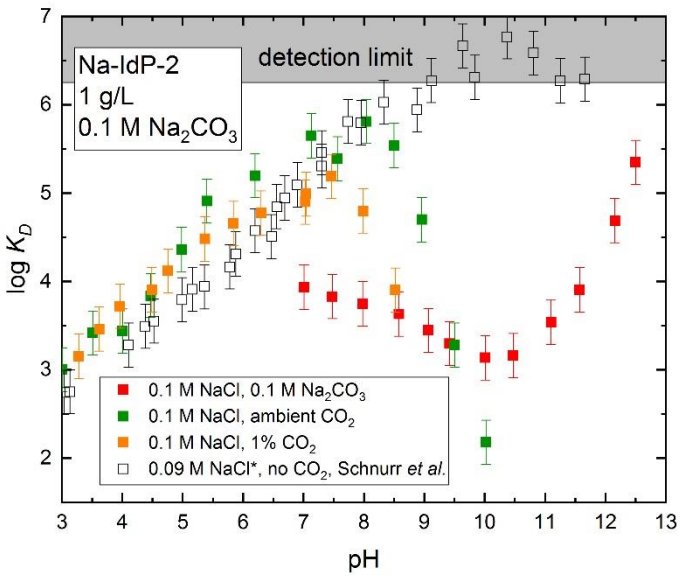

Figure 4.5: Eu(III) sorption edge on Na-IdP-2 at a constant TIC concentration of 0.1 M (closed, red symbols), in comparison to different constant partial pressures of CO_2 (closed symbols: ambient CO_2 green, 1 % CO_2 orange) and in absence of CO_2 (open symbols, *Schnurr *et al.* [17]), in 0.1 M NaCl.

4.1.2. Attenuated total reflection infrared spectroscopy (ATR-IR)

One explanation for the enhanced Eu(III)-sorption to clay minerals in the acidic range in the presence of CO_2 could be that carbonate is adsorbing at aluminol groups and acts as an additional metal binding ligand. Identifying and quantifying carbonate sorption by batch experiments, however, is difficult. Experimental problems are due to the volatility of CO_2 and the relatively low sorption extent. So far the adsorption of carbonate to mineral surfaces in the acidic pH range is reported in the literature only for minerals like iron or aluminium oxides and hydroxides being positively charged at $pH < pH_{pzc}$ (~6-9) [106-109, 145-149]. At present, no direct experimental proof on carbonate adsorption onto clay mineral surfaces is available. This is the first study of carbonate sorption onto montmorillonite edge sites using ATR-IR spectroscopy. The irreversible intercalation of CO_2 was already reported by Romanov *et al.* [150].

Montmorillonite was suspended in a 3 M NaCl / D_2O solution. The use of D_2O was necessary to suppress the H_2O scissor vibration interfering with carbonate stretching vibrations. A suspension of 10 g/L montmorillonite was placed on an ATR crystal. After a sedimentation time of 10 min, the spectra were recorded. The infrared spectra of montmorillonite in absence of CO_2 (grey pD = 6.34) and presence of 1 % CO_2 (red pD = 5.29, blue pD = 6.36, green pD = 8.41) are displayed as normalized intensity against wavenumber in Figure 4.6. The intensity is normalized to the Si-O vibration of the clay mineral at 1043 cm^{-1} [151]. A solvent spectra (D_2O, in orange) was added for comparison. The vibration band at 1204 cm^{-1} is attributed to the D_2O scissor vibration and in agreement with the pure solvent (orange line).

The absorption band at 1456 cm-1 is observed only in presence of carbonate and the intensity increases while clay particles sediment at the ATR crystal so that carbonate association to the solid phase can be assumed. After 10 min of sedimentation no further changes were observed. Vibrational bands at similar positions are reported for adsorbed carbonate on iron oxides [106, 107] and alumina oxides surfaces [146, 152]. Although a splitting of the vibrational bands is reported in these studies. According to Wijnja *et al.* [146] hydration effects on the coordinated carbonate can decrease the

splitting of the observed vibrational bands. With increasing pD and the related increase in the carbonate concentration the vibration band intensity is increasing from pD = 5.29-6.36. At pD ≥ 6.36 no further increase is observed up to pD = 8.41. This observation and the finding that a carbonate containing D2O solution yields a very low CO_3^{2-} stretching vibration signal shows that the band at 1456 cm-1 can be mainly assigned to surface bound carbonate species. A monodentate coordination of carbonate onto Al-OH surface groups was related to a vibrational band at 1455 cm-1 by Wijnja *et al.* [146]. All those findings provide for the first time spectroscopic evidence for the carbonate adsorption taking place at clay mineral edge site and point to the relevance of this effect in a slightly acidic and neutral pD range.

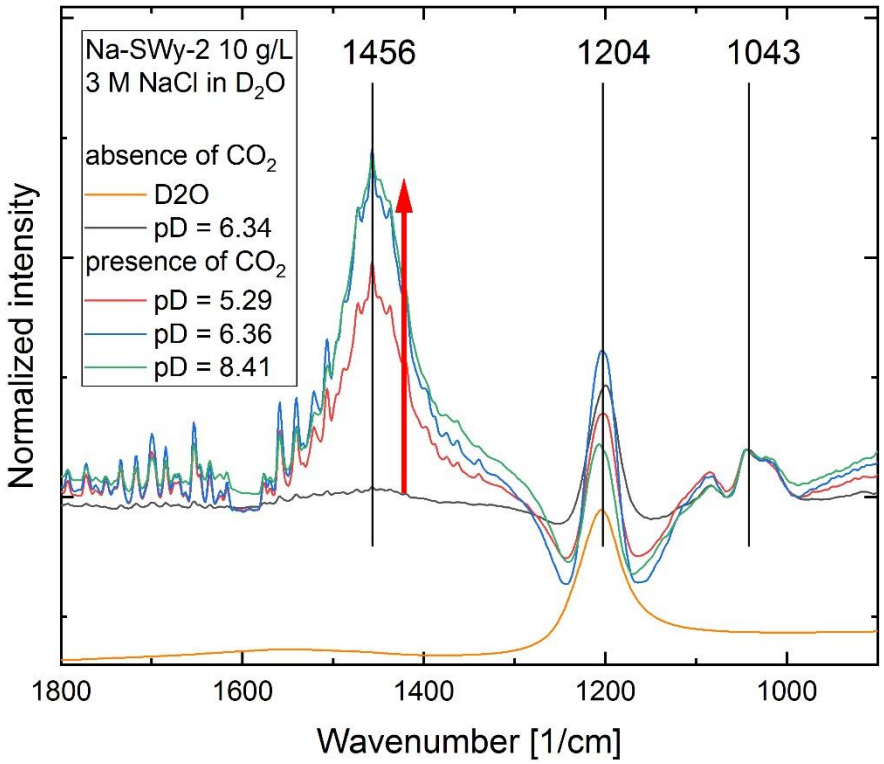

Figure 4.6: ATR-IR spectra of Na-SWy-2 suspended in D_2O in presence and absence of ambient CO_2 in saline media (3 M NaCl) as function of the pD.

4.1.3. Time resolved laser fluorescence spectroscopy (TRLFS)

In order to provide insight into changes in the coordination sphere of the adsorbing metal ion, Cm(III)-TRLFS was performed. Time resolved laser fluorescence spectroscopy is a well-established method to gain insights into sorption mechanisms and speciation of aquatic or surface complexes of Cm(III) and has been used for a variety of mineral phases including illite and montmorillonite. The sorption of Cm(III) onto montmorillonite (Na-SWy-2) within this work was studied in NaCl electrolyte solutions. In aqueous solution Na-SWy-2 forms intermediately stable suspensions. Due to its ability to swell when contacted with water, the clay mineral is easily re-suspended after centrifugation or drying. The samples were prepared as described in section 3.2.2. These physical properties make the spectroscopic significantly easier compared to non-swelling clay minerals like illite.

Emission spectra and fluorescence lifetime measurements

A series of wet paste samples were prepared by centrifugation of suspensions at different pH values (pH = 3.16-8.03) in a 3 M NaCl solution in equilibrium with a partial pressure of 1 % CO_2 and a Cm(III) concentration of $1 \cdot 10^{-7}$ M. Measuring only the solid precipitate allows to obtain spectra of adsorbed Cm(III) with only small contributions of dissolved species in adhering solution films. A summary of area normalized fluorescence spectra is given in Figure 4.7. Two series of spectra were taken at 1 µs (left) and 121 µs delay time (right). A spectrum of the pure Cm^{3+} aquo-ion was added as reference. The adsorbed Cm(III) shows fluorescence spectra similar to the $Cm(III)_{aq}$ ion between pH_m = 3.16-4.19 for the short delay time of 1 µs. Around pH_m = 4.46 a shoulder at λ = 600 nm starts to form. With increasing pH_m this feature gets more significant (pH_m = 4.46-8.03). The peak position at λ = 593.6 nm is attributed to traces of Cm_{aq}^{3+} in the leftover aqueous phase but mainly to cation exchange bound species, a physisorbed Cm_{aq}^{3+} with a completely remaining first hydration sphere. For this reason both species can't be distinguished by a bathochromic shift, but by fluorescence lifetime measurements [105, 116, 153]. Physisorbed species on

montmorillonite surfaces exhibit a short lifetime around 30 µs most likely due to quenching by structurally bound Fe. To gain more information on the second feature around λ = 600 nm, the same samples were measured at a delay time of 121 µs (Figure 4.7, right). Due to its short lifetime the physisorbed species becomes significantly less dominant at this delay time. At pH = 3.16 the cation exchange species at λ ~ 594 nm is still the main component. Starting from pH_m = 3.43 a second peak at λ ~ 600 nm increases and shifts towards λ ~ 603 nm between pH_m = 4.46-8-03.

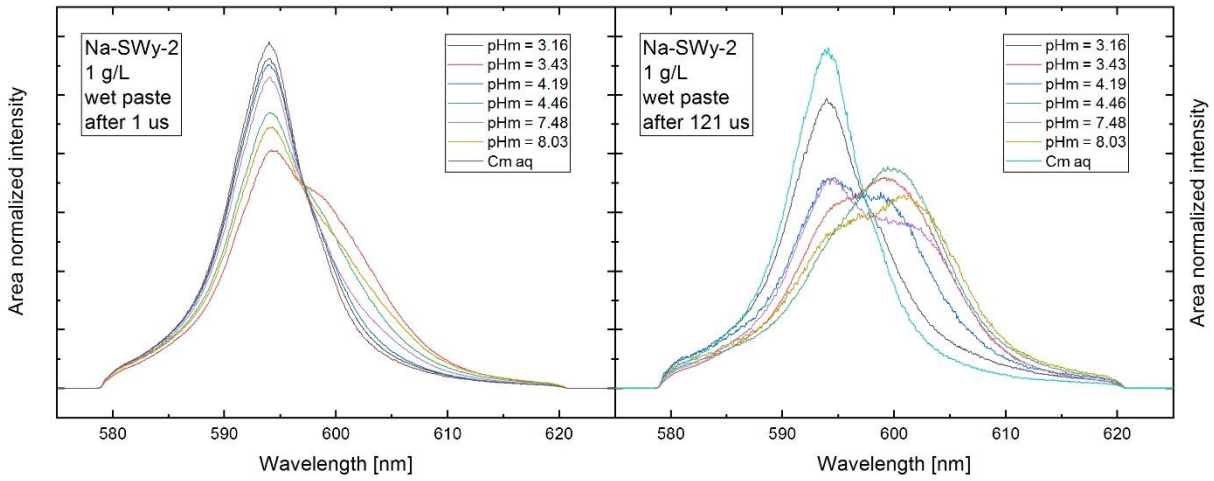

Figure 4.7: Fluorescence spectra of Cm(III) adsorbed onto montmorillonite in presence of 1 % CO_2 presented as area normalized intensities at different delay times (left 1 µs, right 121 µs) measured as wet paste sample at high ionic strength (3 M NaCl).

As reported by Schnurr *et al.* in a TRLFS study conducted in the absence of CO_2 and in suspension, a first inner sphere surface species starts to form at pH_m = 5.5 causing a bathochromic shift to λ = 598.5 nm. A second species appears above pH_m = 6.5 with λ = 602.5 nm. The different peak maxima observed for adsorbed Cm(III) species in presence and absence of CO_2 point to different prevailing surface species. The complexation of Cm(III) in presence of dissolved carbonate takes place at significantly lower pH. This is another indication for the formation of a different species.

To derive further information on the sorption of Eu(III) on Na-Swy-2 in presence of carbonate, a peak deconvolution was applied to spectra measured at a delay time of 121 µs. For this purpose single species spectra, starting from the spectrum of $Cm^{3+}_{(aq)}$, were deconvoluted from the mixed spectra (Figure 4.8, left). In total three different

fluorescence lifetimes (Figure 4.8, right) could be derived from spectra measured at pH_m = 4.46, 7.48 and 8.03. A short one τ = 32 ± 6 µs, an intermediate lifetime with τ = 130 ± 5 and a long lifetime with τ = 430 ± 5. According to Hartmann *et al.* the short lifetimes can be assigned to a physisorbed Cm(III) [116]. It can be assumed that the intermediate and long fluorescence lifetime both correspond to an inner sphere sorption species. In earlier studies a set of two similar lifetimes was reported for adsorbed species in carbonate containing systems [24, 154]. These studies were performed with different clay mineral phases at significantly higher pH (kaolinite at pH = 8.4, t < 20 K, montmorillonite, Na-STx-1 at pH = 9). Within the present study, the species with τ = 128-135±10 µs were also found from a slightly acidic to neutral pH range. The third species with a longer lifetime is found at neutral pH. This is the first investigation of the adsorption of Cm(III) onto a clay minerals in presence of carbonate over a pH range from pH = 3-8.

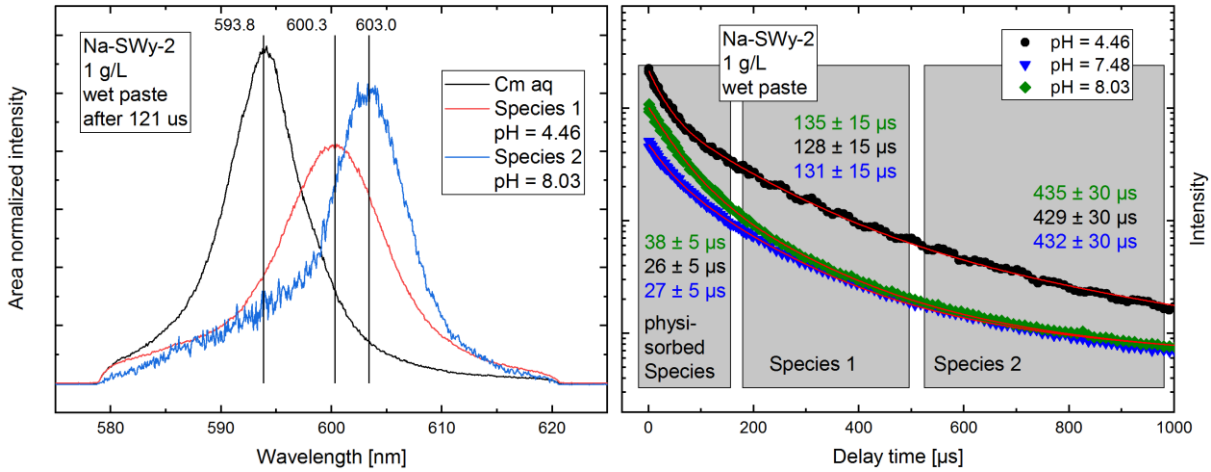

Figure 4.8: Deconvolution of Cm(III) TRLFS spectra to derive single species spectra of ternary Cm(III) carbonate complexes (left), fluorescence lifetime measurements (right). Measurements were performed as wet paste samples in equilibria with 1 % CO_2 at high ionic strength (3 M NaCl).

According to Kimura *et al.* the fluorescence lifetime of species 1 can be correlated with $n(H_2O)$ = 4.2 ± 0.7 and the lifetime of species 2 with $n(H_2O)$ = 0.64 ± 0.2 water molecules in the first coordination sphere (Section 2.3.1, Equation 5 [85]). Lifetimes for species 1 in presence of carbonate are not deviating much from those reported for adsorbed Cm(III) in the absence of carbonate and suggest the similar number of

ligands in the first coordination sphere [17]. However, compared to studies in the absence of CO_2, the first inner sphere surface species appears at lower pH which is an indication for a stabilizing effect for clay mineral surface adsorbed Cm(III) by carbonate. This interpretation is supported by the stronger red-shift for the emission band of species 1 as compared to species 1 in absence of carbonate. The long fluorescence lifetime of species 2 can only be explained by a reduction of the number of coordinated water molecules of Cm(III) to 1 or even below. Since carbonate is the only additional introduced ligand (compared to the carbonate free system), this observation indicates a further complexation of Cm(III) by carbonate at the clay mineral surface.

Vibronic sideband spectroscopy

Vibronic sideband spectroscopy (VSB) was used to derive additional information on the coordination mode of the ligand and the structural order of the Cm(III) surface complexes. In previous studies this technique was only used for aqueous or dissolved organic systems [136, 137]. Different to the TRLFS experiments described before, VSB spectroscopy offers the chance to obtain information not only on the number, but also on the nature of ligands. For the first time the applicability was proven for sorption studies by measurements of aqueous suspensions in the present work. As described in section 4.1.2, the scissor vibration of H_2O is overlapping with stretching vibrations of the carbonate ligands. Therefore D_2O was used as solvent.

The VSB spectra for Cm(III) adsorbed onto montmorillonite under saline, deuterated conditions (3 M NaCl) in presence of carbonate (pD = 5.83, 7.02) and in absence of CO_2 (pD = 7.24, Figure 4.9) are displayed against wavelength (lower axis) and wavenumber (upper axis). These spectra are compared to an infrared spectrum of pure D_2O to identify solvent effects in the measured spectra.

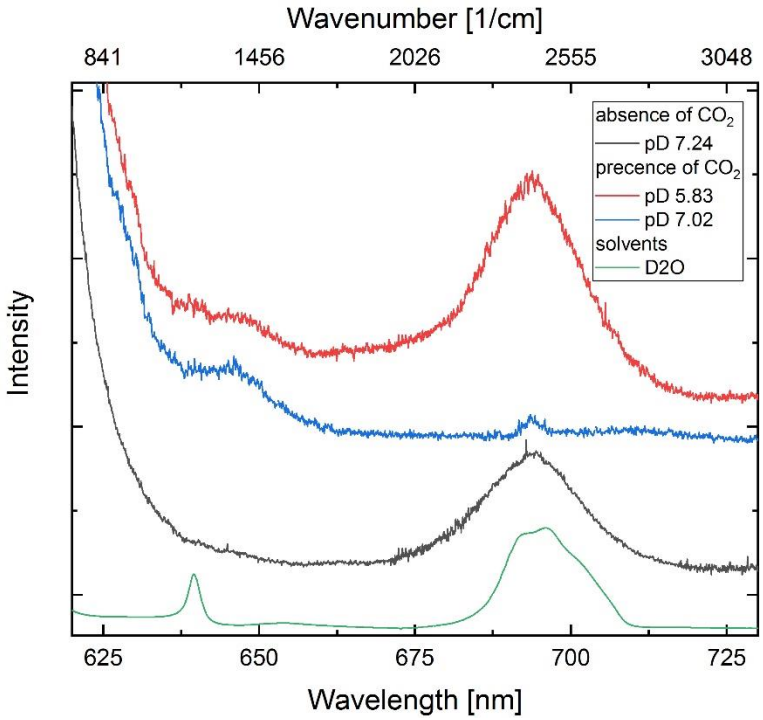

Figure 4.9: VSB spectra for Cm(III) adsorbed onto Na-SWy-2 in presence (red, blue) and absence of carbonate (black), compared to a D_2O infrared spectra (green).

In previous studies, VSB spectra, e.g. of extraction ligands [137], were normalized relative to the position of the maximum of the fluorescence emission (ZPL: zero phonon line). This is only possible for systems with a single predominant species. The here discussed Cm(III) emission spectra always represent a mixture of different species. For this reason all measurements were normalized to the Cm_{aq}^{3+} emission band at λ = 593.8 nm. The measured spectra in the absence of CO_2 (black line) show no significant VSB features between λ = 620-660 nm. The broad vibrational band between λ = 675-710 nm is assigned to the O-D stretching vibration of D_2O. The maximum of this feature is located at λ = 694 nm, which is in good agreement with that in the infrared spectrum for D_2O (green line). The scissor vibration of D_2O at λ = 639.5 nm is not resolved in the clay suspensions. This is explained by the lower intensity and the proximity to the main Cm(III) fluorescence emission band. In the presence of carbonate a second feature appears between λ = 642-640 nm (red, blue line). Since this feature is only present in carbonate containing systems, it can be attributed to adsorbed carbonate species close to adsorbed Cm(III). The position of

this feature (λ = 650 nm ≙ 1456 cm^{-1}) was previously identified as adsorbed carbonate on the clay mineral surface by ATR-IR spectroscopy (section 4.1.2, Figure 4.6).
From pD = 5.83-7.02 the feature attributed to the O-D stretching vibration (λ ~694 nm) is significantly reduced. This is indicating a reduction of the number of D_2O molecules in the first coordination sphere around the adsorbed Cm(III) with increasing pH. A reduction from ~ 4 to 1 coordinated H_2O molecules was previously indicated by fluorescence lifetime measurements. The results of VSB spectroscopy further supports these earlier findings.
Results of VSB spectroscopy, TRLFS measurements and ATR-IR measurements consistently point to the existence of a carbonate stabilized Cm(III) surface species starting from the slightly acidic pH range.

4.1.4. Theoretical calculations (DFT, AIMD)

To validate the indications of both, carbonate sorption on clay minerals and presence of carbonate stabilized surface species of An(III) based on spectroscopic and batch sorption experiments, a combined theoretical approach was applied using density functional theory and ab initio molecular dynamics (AIMD). The adsorption of carbonate onto clay mineral edges was studied with AIMD. Two different potential and reasonable structures (with carbonate sorption occurring on the clay edge sites) were calculated (Figure 4.10): A hydrated clay edge with a carbonate molecule in front, i.e. a layer of water molecules between carbonate and the clay surface (A) and the same clay edge with a carbonate substituting a hydroxyl group of the octahedral alumina in a mono-dentate fashion (B). The energy of the systems was monitored for 4 ns. Over the simulated period of time system B was by about 26.7 kJ/mol more stable. With this analysis, the stability of carbonate adsorbed to clay mineral surface is supported by theory and in-line with experimental findings from ATR-IR measurements (section 4.1.2).

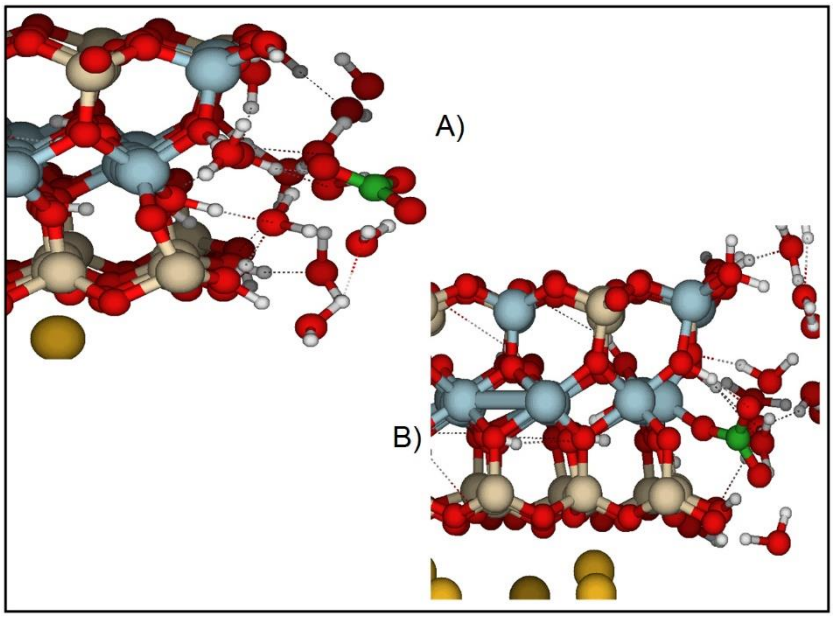

Figure 4.10: Theoretical consideration of carbonate binding to clay mineral edge surfaces via a kind of outer-sphere complexation (A) and inner-sphere adsorption to the surface (B). Atom colour code: O red, Al blue, Si beige, C green, H white, K yellow.

Possible surface complexes including An(III) and carbonate ligands (bound only to An(III) or bridging between clay and An(III)) were computed, the most stable structures are shown in Figure 4.11. The species A is coordinated in a monodentate fashion to different Al-OH, Si-OH groups and a carbonate entity which is adsorbed to the surface and will be denoted as ≡S-OCO_2-An^{2+}. The adsorbed metal ion exhibits monodentate bonding to the adsorbed carbonate an average coordination number of 2-3 to the mineral surface and 4-5 remaining coordinated water molecules and is thus in agreement with TRLFS results. The addition of a second carbonate ligand forms a stable surface species B termed hereafter as ≡S-OCO_2-$AnCO_3$. The second carbonate is coordinated in a bidentate mode via two oxygen atoms, replacing 2 coordinated H_2O molecules. A monodentate binding to surface adsorbed Carbonate, a bidentate binding to the second carbonate ligand and a three-fourfold coordination to the clay edge surface reduces the amount of coordinated water molecules to n(H_2O)= 2. TRLFS lifetime measurements confirm the decreasing number of OH entities in the first coordination sphere. Conversion of t via the Kimura equation into n(H_2O) results in a somewhat lower number of 1 H_2O equivalents.

The addition of the third carbonate ligand (formally "≡S-OCO_2-An$(CO_3)_2^-$") significantly changes the structure and forms a three times bidentate coordination of An(III) to carbonate (no binding to Al-OH or Si-OH surface groups) (surface species C). For this reason, species C is assumed to be desorb after sufficient simulation time. The effect is visualized by the development of the distance between An(III) and surfacial Al atoms as function of the number of carbonate ligands (Figure 4.11, D). Since clay edges are no plane surfaces, the An(III)-Al distance was taken as a measure for the space between adsorbate and adsorbent. With increasing number of coordinated carbonate ligands the An(III)-Al distance changes from 3.86 Å, to 4.18 Å and to 3.66 Å for n(CO_3^{2-}= 0, 1, 2) and to 5.65 Å for n(CO_3^{2-}= 3).

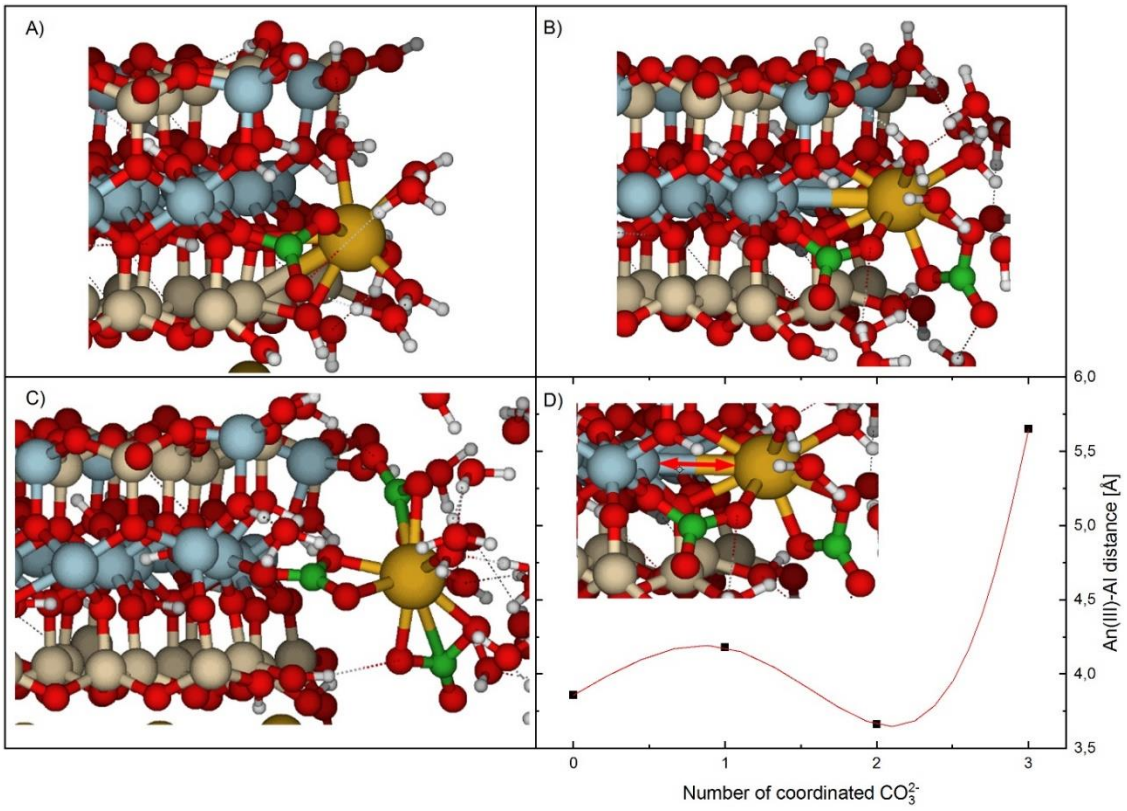

Figure 4.11: Calculated structure of potential carbonate stabilized An(III) surface complexes with n(CO_3^{2-}) = 1, 2, 3 (A, B, C) and an evaluation of the development of the An(III)-Al distance as function of n(CO_3^{2-}) with B-spline function (D). Atom colour code: O red, Al blue, Si beige, C green, H white, An(III) yellow.

The structure of the surface species B (Figure 4.11, B) was used to compute VSB spectra of the Cm(III) ion (Figure 4.14). Two different spectra were extracted: One for

the surface associated carbonate ligand (bridging the surface to the Cm(III); orange) and another for the coordinated carbonate ligand with no bonding to surface atoms (purple). The carbonate ligand coordinated to An(III) in a bidentate fashion (purple) shows 3 vibrational bands at λ = 626.0 nm, λ = 635.8 nm and λ = 641.2 nm. These vibrational bands are comparatively weak and partly overlaid by the tailing of the excitation band.

Beside small features of negligible intensity (e.g. at λ = 641.7 nm) a well separated signal at λ = 648.9 nm is computed for the carbonate directly located at the surface. This is clearly coinciding with the experimentally obtained vibronic sideband of the adsorbed carbonate (red and blues spectra). In general, theoretical spectra agree with measured data and their interpretation.

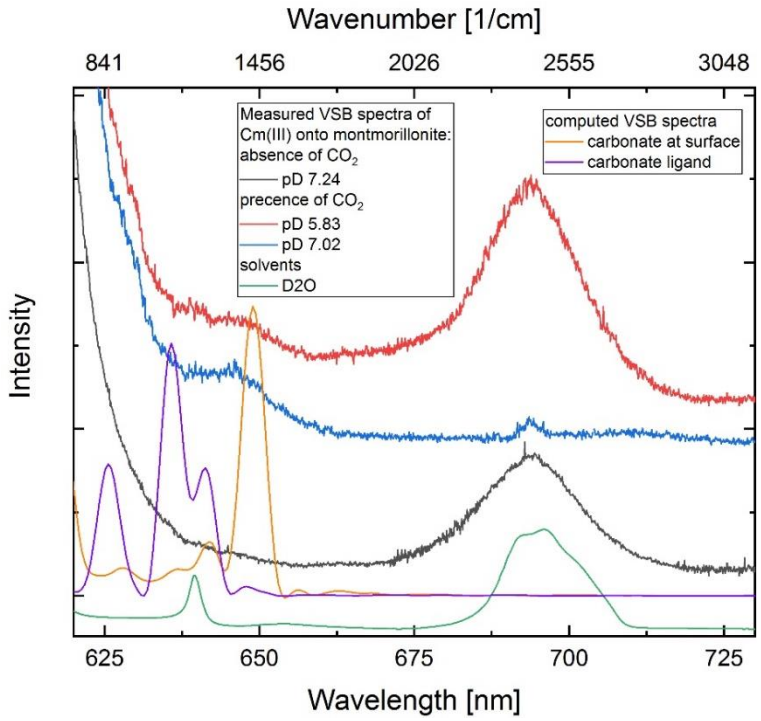

Figure 4.12: Computed VSB spectra (DFT) of An(III) adsorbed onto clay mineral edge sites of the stabilizing surface bound carbonate (≡S-OCO_2-$AnCO_3$, orange) and the additional coordinate carbonate ligand (≡S-OCO_2-$AnCO_3$, purple) are displayed as function of the wavelength (lower axis) and wavenumber (upper axis) and compared to measured vibronic side bands of Cm(III) adsorbed onto montmorillonite in the presence of carbonate (red, blue). A measured VSB spectra of Cm(III) adsorption onto montmorillonite in absence of CO_2 (black) and an infrared spectra of the solvents D_2O (green) are added for comparison.

4.1.5. Geochemical modelling

The results derived from batch sorption experiments, spectroscopic investigations and theoretical calculations were used to apply a surface complexation model. For this purpose, an established 2SPNE/CE [13] approach was modified as described below.

All experimental data collected in the present work for Eu(III) and Cm(III) will be indicated in the model as “Am(III) data”. The use of Am(III) as an representative for all Ln(III)/An(III) is a common practice for the applied 2SPNE/CE model from literature.

Figure 4.13 displays adsorption data of Eu(III) onto Illite du Puy in presence of ambient carbonate reported by Marques *et al.* (closed symbols, orange, p_{CO_2} = $10^{-3.5}$ bar, [113]) as well as data from the present work (black squares, p_{CO_2} = $10^{-3.3}$ bar). Data in the absence of carbonate was added for comparison (open symbols [17]).

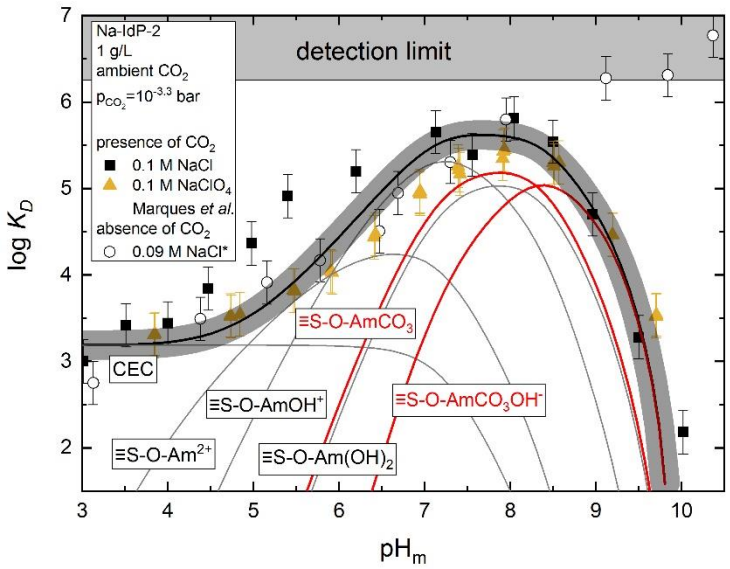

Figure 4.13: pH-depending sorption of Eu(III) onto Illite du Puy (1 g/L) in presence of equilibrium concentrations of carbonate related to a partial pressure of p_{CO2} = $10^{-3.3}$ bar, displayed as logarithmic distribution coefficient as function of pH. Three different data sets are shown, closed black symbols (0.1 M NaCl, this work) and closed yellow symbols (0.1 M $NaClO_4$, Marques *et al*. [113]) in presence of ambient CO_2 and a third series in absence of CO_2 (open black symbols, 0.09 M NaCl, Schnurr *et al.* [17]). An unmodified geochemical 2 SPNE/CE model was applied according to Marques *et al.* [113]. The relevant ternary surface species are plotted in red.

The 2SPNE/CE model developed by Bradbury and Baeyens, for systems in the absence of CO_2 [11, 16], was extended by Marques *et al.* [113] to describe the impact of carbonate on the retentions of An(III) onto clay mineral surfaces. By taking into account the aqueous carbonate complexation [22, 113], ternary An(III) carbonate surface species were needed for an description of the experimental data. Without considering these species, a strong underestimation of the experimental data is predicted by the model. Two carbonate containing surface complexes (≡S-O-Am-CO_3, ≡S-O-Am-CO_3OH^-) were assumed to describe the experimental finding. With that approach (considering 5 different adsorbed species and the cation exchange) a fully description of the experimental data was possible [22], despite no mixed hydroxo-carbonate species are reported in aqueous solution.

Due to the deviation of experimental data in the present work at slightly acidic pH compared the studies of Marques *et al.*, a modified geochemical model was applied based on the 2SPNE/CE model from Bradbury and Baeyens [11, 16], derived in the absence of CO_2. This new approach is also considering the adsorption of carbonate on clay mineral edge sites which was demonstrated ATR-IR spectroscopy and computational methods (DFT, AIMD). To describe the sorption of HCO_3^- and CO_3^{2-} onto the clay minerals a model proposed by Van Geen *et al.* [109] for HCO_3^- and CO_3^{2-} adsorption onto goethite was used. The parameters for the carbonate adsorption onto goethite were adopted without any modifications and are displayed in Table 16. A direct quantification of the adsorbed carbonate on clay minerals was not achieved during this work. For this reason the following assumptions has been made, knowing that the systems and models are not completely comparable. (1) Fe-OH sites of the goethite were substituted by the Al-OH sites of the clay mineral, more precisely the strong sites defined as ≡S^SOH. (2) Surface complexation constants of an electrostatic diffuse double-layer model (DLM) for the goethite system were used as parameters for the non-electrostatic 2SPNE/CE model. According to the applied model calculation, 100% of the strong sites are covered with carbonate (appendix 7.1). The carbonate adsorption, as implemented in the current model, show no pH dependency. To improve this insufficient description a quantification of the actual amount of adsorbed carbonate is needed. According to studies performed on the adsorption of carbonate onto goethite a significant pH dependency should be expected [106, 109, 145]. The importance and existence of ternary carbonate stabilized surface species was

previously discussed in several studies on the adsorption of U(IV) onto different mineral phases in presence of carbonate. While the existents and importance for geochemical modelling reported by Catalano *et al.* [155] (adsorbents: montmorillonite) and Müller *et al.* [156] (adsorbents: TiO_2), Tournassat *et al.* [157] (adsorbents: montmorillonite) reported in a recent study a modelling approach without the need of ternary surface complexes by including the spillover effect in a surface complexation model.

As the mineral surface is "covered" partly with carbonate, a modified surface is available for the adsorption of An(III). This results in the formation of ternary carbonate stabilized surface complexes, including the surface, the adsorbed carbonate and the actinide. According to the stoichiometry derived from DFT calculations two different surface species were assumed (Figure 4.11 A +B). The first species involves one surface connected carbonate ($\equiv S\text{-}O\text{-}CO_2Am^{2+}$), the second is formed by adding an additional carbonate ligand to the previous formed species ($\equiv S\text{-}O\text{-}CO_2AmCO_3$). The structure of both species is supported by spectroscopy and theoretical studies. By that it was possible to describe the sorption of Ln(III)/An(III) in presence of carbonate onto Illite du Puy (Na-IdP-2) and montmorillonite (Na-SWy-2) for ambient conditions (Figure 4.14) and an elevated partial pressure of CO_2 (Figure 4.15) consistently with one single set of constants (Table 16).

Table 16: Surface complexation reactions and stability constants describing the impact of carbonate sorption onto the clay surface [109] on Am(III) sorption.

Surface complexation reactions	log K
$\equiv S\text{-}OH + HCO_3^- \leftrightarrow \equiv S\text{-}O\text{-}CO_2H + OH^-$	20.78*
$\equiv S\text{-}OH + CO_3^{2-} \leftrightarrow \equiv S\text{-}O\text{-}CO_2^- + OH^-$	12.71*
$\equiv S\text{-}O\text{-}CO_2H + Am^{3+} \leftrightarrow \equiv S\text{-}O\text{-}CO_2Am^{2+} + H^+$	2.7
$\equiv S\text{-}O\text{-}CO_2H + Am(CO_3)^+ \leftrightarrow \equiv S\text{-}O\text{-}CO_2AmCO_3 + H^+$	0.3

The surface sorbed carbonate assisted sorption model was first applied to diluted systems in equilibrium with ambient CO_2 (Figure 4.14). A model description (black line) of the adsorption of Eu(III) onto illite (Na-IdP-2, left) and montmorillonite (right) was calculated using the geochemical code *PhreeqC* [45] and the *ThermoChimie* database [73]. The increased retention in presence of carbonate between pH ~ 4-7 is properly described by a first carbonate stabilized surface complex ($\equiv S\text{-}O\text{-}CO_2Am^{2+}$). This

surface complex is predominant between pH = 4-7. The characteristic decrease in sorption for pH > 8 is described by the competition of the second ternary surface species (≡S-O-CO_2AmCO_3) and the growing predominance of the dissolved $Cm(CO_3)_3^{3-}$ complex in the aquatic phase.

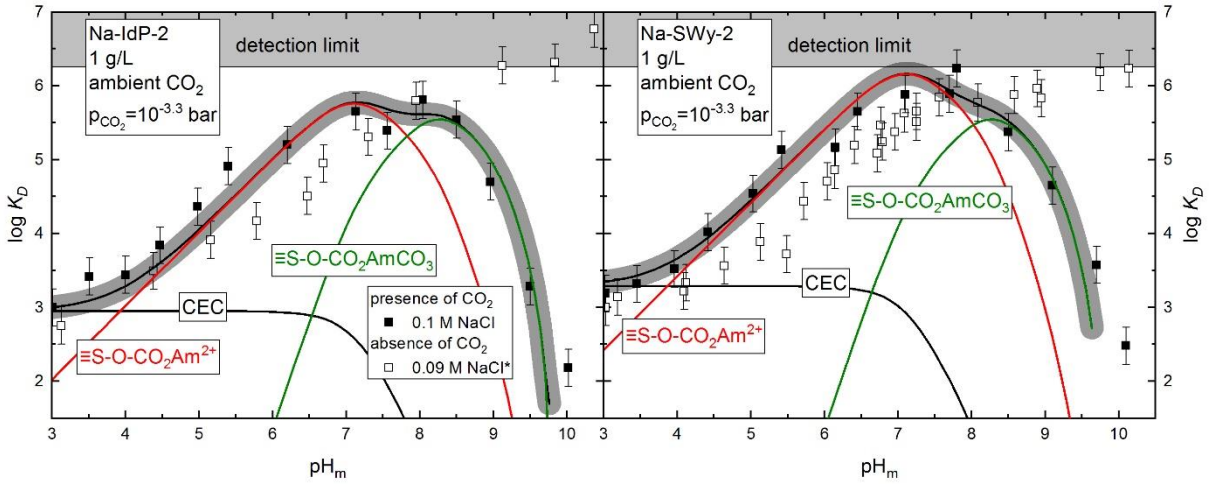

Figure 4.14: Model calculations (black line) for the Eu(III) sorption edge on Na-IdP-2 (left) and Na-SWy-2 (right), in equilibrium with ambient CO_2 (closed symbols) and in absence of CO_2 (open symbols, *Schnurr *et al.* [17]), in 0.1 M NaCl. Ternary surface species are highlighted in red and green.

To prove the applicability of the model to different experimental conditions the surface sorbed carbonate assisted sorption model was applied to systems at an elevated partial pressure of CO_2. The description of batch sorption experiments in equilibrium with an elevated partial pressure of CO_2 (1 % CO_2) is demonstrated in Figure 4.15. The adsorption of Eu(III) onto illite (left) and montmorillonite (right) in presence of carbonate (closed symbols) is displayed as log K_D vs. pH and compared to literature data in the absence of CO_2 (open symbols, Schnurr *et al.* [17]). As described for ambient conditions, the increase in Eu(III) retention in the slightly acidic to neutral pH range (pH ~ 4.5-7) and the characteristic decrease above pH > 8 are in good agreement with the model calculations. Furthermore, the general decrease of the maximum sorption compared to ambient conditions at pH ~ 7-8 is well described.

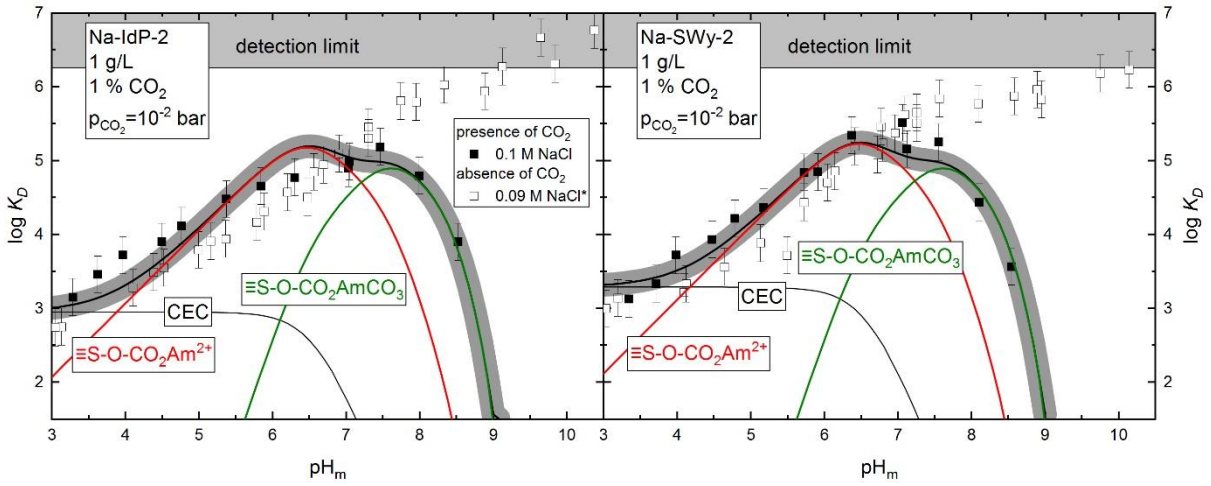

Figure 4.15: Model calculations (black line) for the Eu(III) sorption edge on Na-IdP-2 (left) and Na-SWy-2 (right), in equilibrium with an elevated partial pressure of 1% CO_2 (closed symbols) and in absence of CO_2 (open symbols, *Schnurr *et al.* [17]), in 0.1 M NaCl. Ternary surface species are highlighted in red and green.

The variation from low to high ionic strength (I = 0.1-3 M) is covered by the applied surface complexation model by including the SIT approach for ionic strength correction. The model calculation is limited by a steep increase in ionic strength caused by the predominance of dissolved CO_3^{2-} (section 2.1) at high pH in equilibrium with a partial pressure of CO_2. The model is applicable to systems in equilibrium with ambient CO_2 in a range of pH ≤ 9.5. For those systems being equilibrated with an elevated partial pressure of CO_2 (1 % CO_2) the model applicability is limited to pH ≤ 9.0. The description of the Eu(III) retention onto Illite du Puy (left) and montmorillonite (right) in equilibrium with ambient CO_2 (Figure 4.16) and an elevated partial pressure of 1 % CO_2 (Figure 4.17) are presented for diluted and concentrated electrolyte systems (closed symbols, [NaCl] = 0.1, 1, 3 M) and compared to experimental data in absence of carbonate (open symbols, Schnurr *et al.* [17]). As demonstrated for diluted systems, the decrease of the Eu(III) retention under alkaline conditions is covered by the current model description. Also Batch sorption experiments performed in 3 M NaCl (ambient conditions) are in good agreement with the model calculation. While the adsorption of Eu(III) onto montmorillonite in 1 M NaCl electrolyte solution (ambient CO_2) is covered by the model description, a deviation is observed for the retention of Eu(III) onto illite under the same conditions. In case of illite the increased adsorption of Eu(III) between pH ~ 4.5-6.5 is significantly underestimated. Apart from this deviation, the

experimental data is consistent over all experimental conditions. For this reason an experimental error might be the most likely explanation.

The model description at 1 % CO_2 is in good agreement with the experimental data under all applied experimental conditions for both selected clay minerals (Figure 4.17).

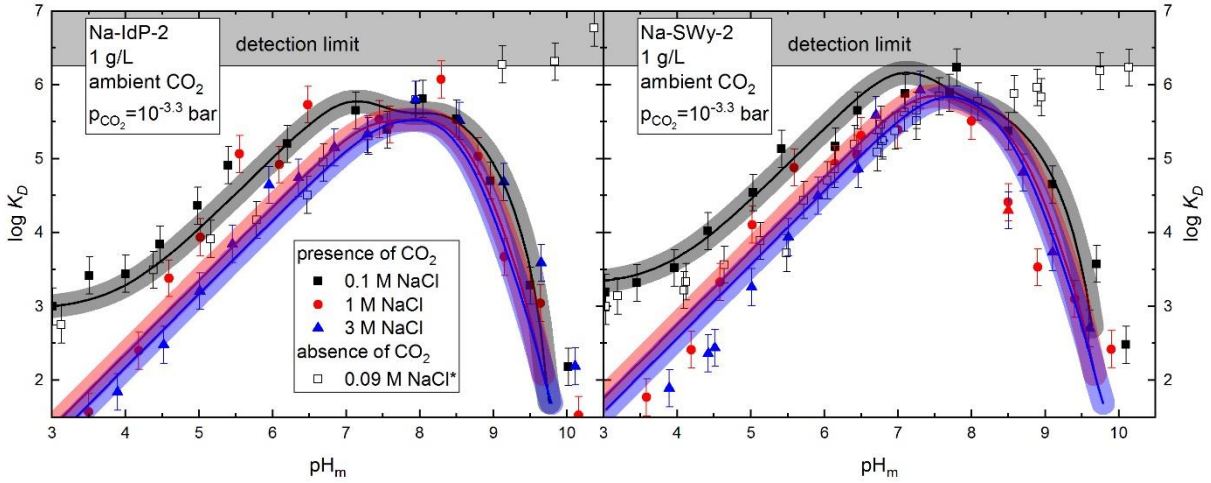

Figure 4.16: Model calculations (solid lines) for the Eu(III) sorption edge on Na-IdP-2 (left) and Na-SWy-2 (right), in equilibrium with an ambient CO_2 partial pressure (closed symbols) and in absence of CO_2 (open symbols, *Schnurr *et al.* [17]), in different saline media ([NaCl] = 0.1, 1, 3 M).

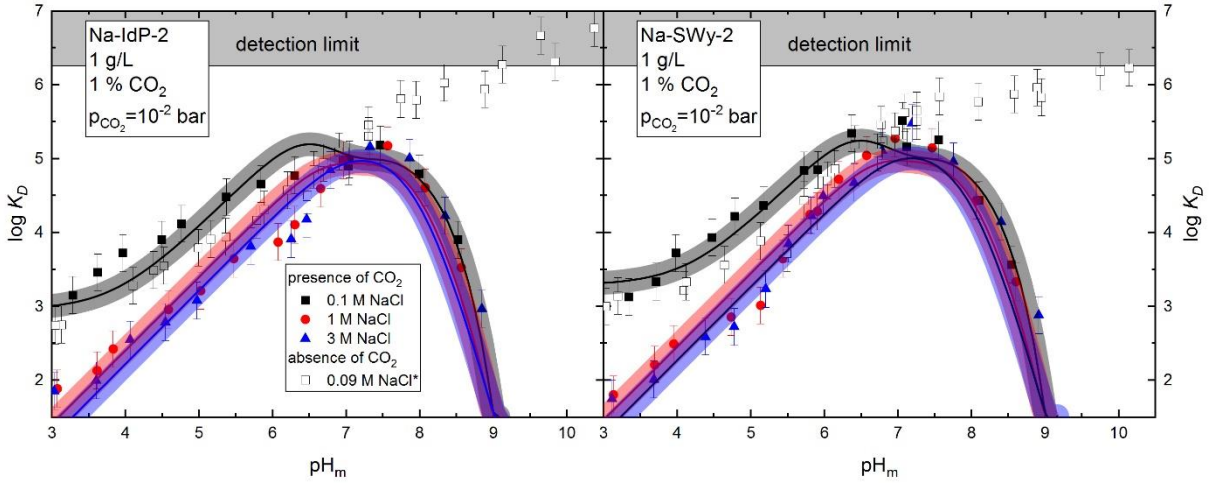

Figure 4.17: Model calculations (black line) for the Eu(III) sorption edge on Na-IdP-2 (left) and Na-SWy-2 (right), in equilibrium with an elevated partial pressure of 1 % CO_2 (closed symbols) and in absence of CO_2 (open symbols, *Schnurr *et al.* [17]), in different saline media ([NaCl] = 0.1, 1, 3 M).

Beside experiments in equilibrium with a partial pressure of CO_2, a study on the adsorption of Eu(III) onto Na-IdP-2 was conducted at a constant carbonate concentration of 0.1 M Na_2CO_3/$NaHCO_3$ (red symbols Figure 4.18). The surface sorbed carbonate assisted sorption model was used to describe these experimental results. Only a small deviation between the model description and the experimental data is observed from pH = 7-9.5. The applied model describes the steady decrease from log K_D = 4-3.3, but the predicted retention slightly overestimates the experimental data. The following increase in retention is qualitatively described, but the predicted retention is significantly overestimated by applied model. Possible explanations for these deviations are the following: At high pH > 10 CO_2 in-diffusion might increase the carbonate concentration and thus decrease sorption. It can also not be excluded that at high pH, the surface speciation of Am(III) may change. For instance it is well known that dissolution of clay minerals becomes relevant and impact the surface site concentration and their chemical nature. A decreasing surface site concentration might explain the observed divergence of calculated and measured sorption data.

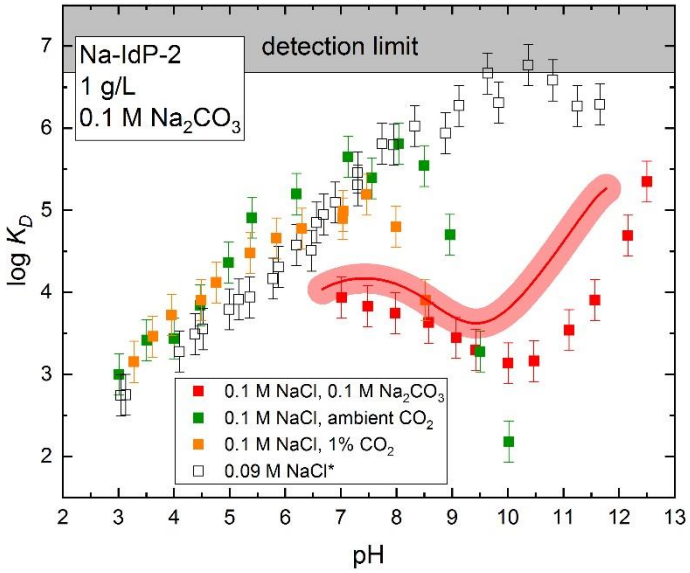

Figure 4.18: Model calculations (red line, I_{tot}= 0.4 M) for the Eu(III) sorption edge in the presence of Na-IdP-2 at constant Na_2CO_3/$NaHCO_3$ concentration (closed, red symbols), compared to experimental data in equilibrium with different partial pressures of CO_2 (closed symbols: ambient CO_2 green, 1 % CO_2 orange) and in absence of CO_2 (open symbols, *Schnurr *et al.* [17]), in 0.1 M NaCl.

The present model is able to reproduce the experimental data for the Ln(III)/An(III) adsorption on two of the most relevant clay minerals in the context of nuclear waste disposal, illite and montmorillonite to pH = 10 and for a large variety of experimental conditions (ambient to 1 % CO_2, 0.1-3 M NaCl ionic strength etc.). Moreover, the model approach is fully consistent with molecular scale information on surface speciation derived by spectroscopic and computational investigations. The existence of CO_3^{2-} adsorbed at the clay mineral surface was proven for the first time by ATR-IR measurements and confirmed by AIMD simulations. The structure and number of ternary An(III) carbonate surface complexes were interpreted from pH dependent spectroscopic (TRLFS) speciation studies supported by further theoretical studies. For the first time VSB spectroscopy was successfully applied to unravel speciation of surface complexes of actinides. By combining these information and adding the surface sorbed carbonate assisted sorption model to otherwise an unmodified 2SPNE/CE model from Bradbury and Baeyens [11, 16] a consistent surface complexation model was derived. Accordingly, it was possible to describe the majority of the experimental results of the present work with a single set of surface complexations constants for the An(III) retention onto Illite du Puy and montmorillonite. From this study it clearly could be shown that the adsorption of carbonate ($p_{CO_2} \geq 10^{-3.3}$ bar) onto clay mineral surfaces is dominating the sorption of An(III) by the formation of carbonate stabilized surface complexes from slightly acidic to neutral pH conditions.

4.2. Impact of gluconate on the sorption of Eu(III) and Cm(III) onto clay minerals

4.2.1. Batch sorption experiments

NaCl electrolyte system

The retention of Eu(III) at trace concentrations onto Illite du Puy (Figure 4.19, left) and montmorillonite (right) in presence of sodium gluconate is presented as the logarithmic distribution coefficient in dependence of pH for diluted and concentrated sodium chloride electrolyte solutions (0.1 M black, 1 M blue, 3 M red). Data obtained in the absence of gluconate are added for comparison (open black symbols, Schnurr *et al.* [17]).

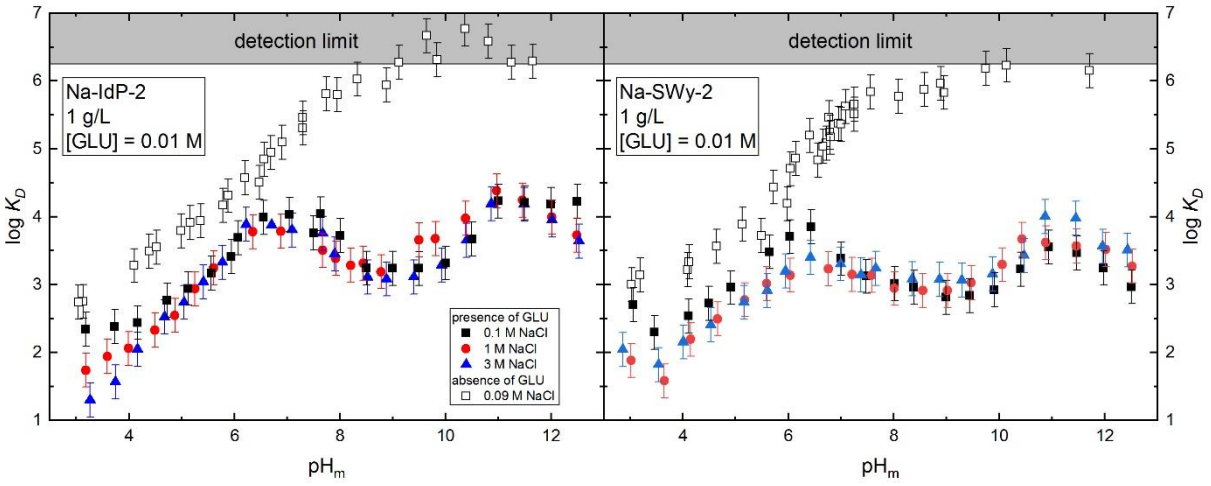

Figure 4.19: Eu(III) sorption onto Illite du Puy (left) and montmorillonite (right), in presence of 0.01 M Na-Gluconate, in different NaCl electrolytes solutions (0.1 M black, 1 M blue, 3 M red) shown as logarithmic distribution coefficient (log K_D) vs. pH. To estimate the effect of gluconate, an experimental series from Schnurr *et al.* in absence of any competing ligand was added (open black symbols, 0.09 M NaCl [17]).

In presence of 0.01 M Na-Gluconate, the retention of Eu(III) is reduced within the whole investigated pH range of this study in comparison to the gluconate free system. From pH = 3-6.5 a linear increase in sorption from log K_D ~ 2-3 is observed. In the higher pH range of pH = 7-9 the distribution coefficient decreases by about half an order in magnitude and increases again between pH = 9 to 11 up to log K_D = 4, were it reaches

a stable plateau. For pH > 11 a slight decrease about half an order in magnitude is observed for the Eu(III) adsorption onto montmorillonite. For the two other investigated ionic strengths (1, 3 M NaCl) the derived log K_D-values are matching with the values for 0.1 M NaCl within the experimental error and over the whole investigated pH range (slight deviations only at pH < 4).

It is obvious that the Eu(III) adsorption onto of illite and montmorillonite in presence of gluconate is quite comparable. The shape of the adsorption edge is strongly affected by the competition of stable aqueous Eu(III)-gluconate complexes with sorption processes. In the acidic pH range the effect of cation exchange on the basal plane which is the dominating retention process at low pH is significantly supressed. This can be explained by the formation of stable aqueous Eu(III) gluconate complexes. Sorption of gluconate on the negatively charged basal planes and blocking these sites is not very likely. The latter effect can potentially occur at the edge sites at protonated or uncharged surface hydroxyl groups. Therefore, Eu(III) sorption in this pH range up to around pH = 6 could be impacted by adsorbing gluconate. Binding of monocarboxylic acids to mineral surfaces is usually assumed to occur via the carboxylic group which then is no longer available for metal ion complexation. As a consequence, sorption of monocarboxylic acids will not increase metal ion sorption to minerals by forming additional (or stronger) sorption sites which is possible for ligands with more than 1 complexing unit (e.g. dicarboxylic acids) if we exclude binding to OH groups. Above pH = 6 no further increase in Eu(III) retention in presence of gluconate is observed. Due to the completely negative charge of clay platelets (basal and edge sites) in the neutral to alkaline pH-range, the adsorption of anionic ligands is unlikely. The strong impact of stable aqueous Eu(III) gluconate species is likely, as the retention of Eu(III) reduces from nearly quantitative sorption in the absence of gluconate (log K_D > 5.5) to a log K_D > 3±0.5 in presence of gluconate. The adsorption of gluconate itself to the clay mineral surface was not determined during this study.

Ca-Gluconate system

The cement additive gluconate interacts strongly with metal cations. This includes not only the trivalent actinides, but also divalent cations like Ca^{2+}. Calcium can form stable complexes with gluconate and is a relevant and omnipresent cation in natural groundwater and especially in cementitious systems (section 2.2.4). Therefore the effect of gluconate on the retention of Ln(III)/An(III) on clay mineral surface has to be studied as well in $CaCl_2$ electrolyte solutions. Batch sorption experiments with Eu(III) and the clay minerals illite (Figure 4.20, left) and montmorillonite (right) in presence of gluconate ([GLU] = 0.01 M) were conducted in calcium containing electrolytes ([$CaCl_2$] = 0.06 M black, 0.6 M red, 2 M blue). The retention of Eu(III) is shown as distribution coefficient vs. pH in Figure 4.20. Data in the absence of gluconate were added for comparison (open black symbols, Schnurr *et al.* [17]).

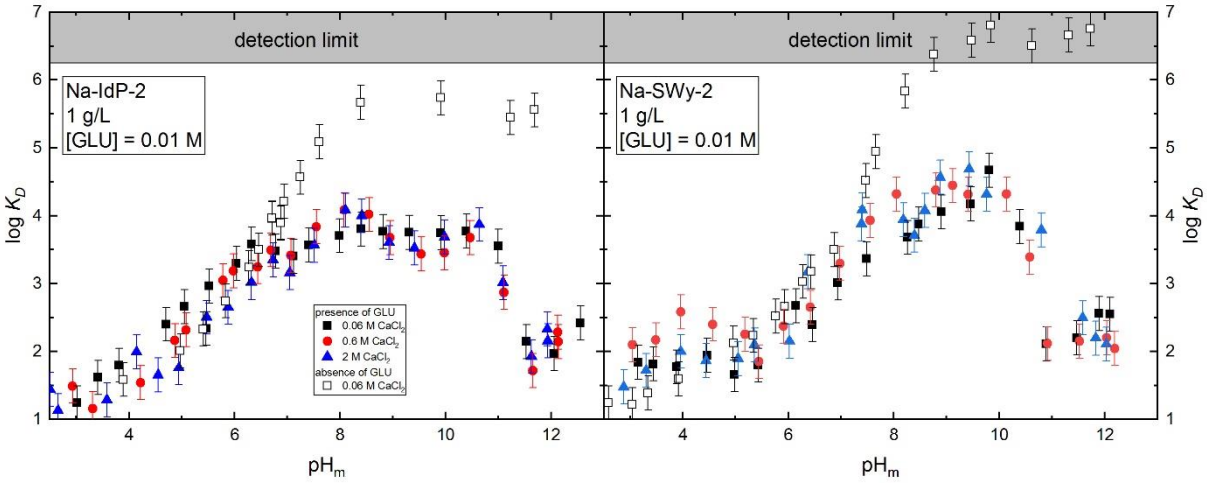

Figure 4.20: Eu(III) sorption onto Illite du Puy (left) and montmorillonite (right), in presence of 0.01 M Ca-Gluconate, in different $CaCl_2$ electrolytes solutions (0.06 M black, 0.6 M blue, 2 M red) shown as logarithmic distribution coefficient log K_D vs. pH. To estimate the effect of gluconate, experimental data from Schnurr *et al.* [17] in absence of any competing ligand was added (open symbols, 0.06 M $CaCl_2$).

In the acidic pH range (pH = 3-6.5) a steady increase from log K_D = 1-3.5 is observed for the illite case (identical to the gluconate free system) followed by a small plateau region and a further increase up to pH = 8.2 with log K_D = 4.

A plateau scatter around log K_D = 2 is observed for montmorillonite in the acid range. Above pH = 6 an increase in retention is observed with a maximum at pH 10 and a log K_D = 4.5.

As reported before for NaCl electrolyte solutions (see Figure 4.22) increase in retention is observed for the adsorption of Eu(III) onto montmorillonite in presence of gluconate between pH = 8.5-11. The retention of Eu(III) onto illite is in the range of log K_D = 3.5-4 Overall, the retention of Eu(III) on both clay minerals between pH = 6.5-10.5 for illite and pH = 7.5-10.5 for montmorillonite is reduced by gluconate up to Δlog K_D ~ 2. The strongest impact of gluconate in calcium containing systems is observed by a step like decrease of additional Δlog K_D ~ 2 above pH > 11. Compared to data in absence of gluconate (open symbols) a decrease of Δlog K_D = 3.5-4 is observed in highly alkaline solutions.

The log K_D values determined in the acidic pH range of 3-6.5 for illite and 3-7.5 for montmorillonite are in good agreement with literature data in absence of gluconate (Schnurr et al, [17]) only a minor effect (Δlog K_D < 0.5) is observed for montmorillonite at low pH. As in the NaCl electrolyte solution (see above), no significant effect of ionic strength on the Eu(III) retention is observed also in different calcium electrolyte solutions over the whole investigated pH range. At pH ~ 7 the predominance of stable aqueous Eu(III) gluconate species starts to significantly decrease Eu(III) retention. The step like decrease in Eu(III) retention in the high-pH region indicates the formation of very strong aqueous Eu(III)-gluconate complexes. The absence of this feature in sodium chloride systems indicates the participation of Ca in the aqueous Eu speciation. This species can't be defined by the formation of ternary Ca-Eu-OH complexes [17], because it's not observed in the absence of gluconate. For this reason a quaternary Ca-Eu-OH-GLU complex can be assumed. Quaternary Ca-Th^{IV}-OH-GLU complexes were previously reported in the literature [75].

GLU – concentration dependent sorption:

To investigate the effect to the ligand concentration on the Eu(III) adsorption onto clay minerals, a batch sorption study focusing on the concentration of gluconate was conducted (montmorillonite, Figure 4.21; illite, appendix 7.1) The concentration of gluconate was increased from [GLU] = $1 \cdot 10^{-4}$ - $5 \cdot 10^{-3}$ M at fixed pH values (pH = 9, 10.5, 12). These pH values were selected to monitor a region with a significant amount of adsorbed Eu(III) and the strong decrease in Eu(III) retention in presence of Ca^{2+}. The adsorption of Eu(III) is displayed as log K_D versus pH and compared to experimental data in presence of a constant gluconate concentration (0.01 M GLU, closed black symbols) and in absence of gluconate (open black symbols, Schnurr *et al.* [17]).

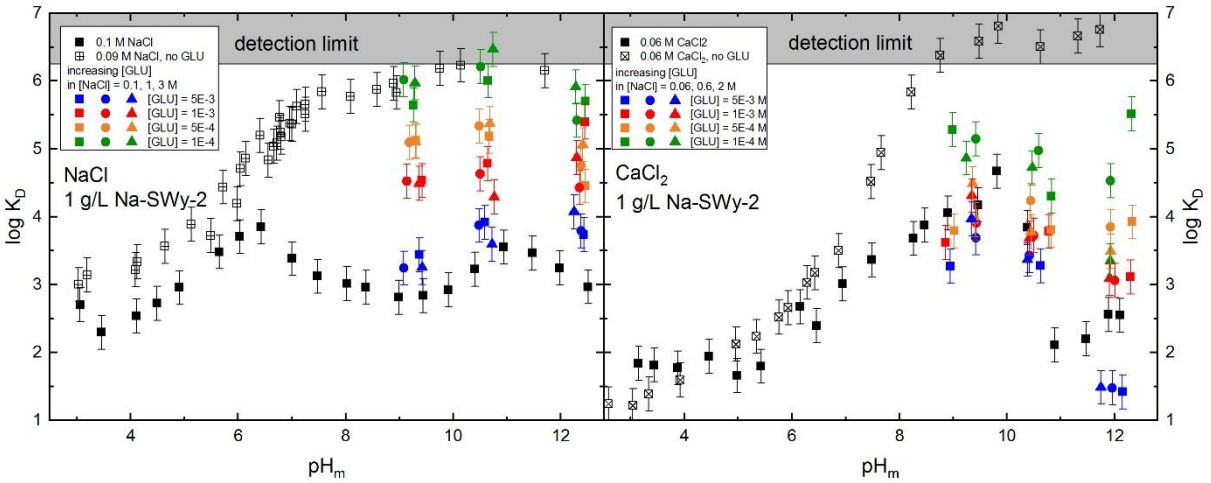

Figure 4.21: Eu(III) sorption onto montmorillonite under variation of the gluconate concentration in diluted and concentrated NaCl (left, 0.1 M squares, 1 M circles, 3 M triangles) and $CaCl_2$ (right, 0.1 M squares, 0.6 M circles, 2 M triangles) solutions at pH = 9, 10.5, 12. Data with constant gluconate concentration ([GLU] = 0.01 M, closed black symbols) and in absence of gluconate (open symbols, 0.09 M NaCl / 0.06 M $CaCl_2$ Schnurr *et al.* **[17]**) are added for comparison. Equal ligand concentrations are highlighted with the same colours and equal ionic strength with the same shape of symbols.

In sodium chloride solutions (Figure 4.21, left) no clear effect of gluconate on the retention of Eu(III) on montmorillonite is observed at [GLU] = $1 \cdot 10^{-4}$ M (green). At [GLU]= $5 \cdot 10^{-4}$ M (orange) a clear decrease of Eu(III) sorption is found which further decreases with increasing gluconate concentration. At [GLU] = $5 \cdot 10^{-3}$ M (blue) the log K_D*'s* are only slightly different to the results determined at [GLU] = $1 \cdot 10^{-2}$ M (see

above). In addition, the derived log K_D*'s* show no significant effect of ionic strength. The shape of the adsorption edges at the varying gluconate concentrations is very comparable to each other. Thus, it can be assumed that the same aqueous Eu(III)-gluconate species occur within the whole range of investigated ligand concentrations. A more complex picture is obvious for the adsorption of Eu(III) onto montmorillonite in presence of different concentrations of gluconate in calcium chloride solutions (Figure 4.21, right). The addition of [GLU] = $1 \cdot 10^{-4}$ M (green) already reduces the retention of Eu(III) by about $\Delta \log K_D$ = 1-1.5 at pH = 9 and up to $\Delta \log K_D$ = 1-3.5 at pH = 12. The lowest effect at pH 12 is observed at the lowest Ca concentration pointing to a stabilization of aqueous Eu(III)-gluconate species by a further association of Ca^{2+} cations under these conditions. This is in good agreement to literature data regarding the complexation of Th(IV) by GLU in $CaCl_2$ solution [75]. It can be assumed that ternary Eu(III)-OH-GLU complexes are bearing a highly negative charges. With the high affinity of Ca^{2+} to carboxylic acids, a partly compensation of this charge by the formation of Ca-Eu(III)-OH-GLU complexes can be assumed.

4.2.1. Time resolved laser fluorescence spectroscopy (TRLFS)

To gain a deeper insight into the complexation of trivalent actinides with gluconate, the aqueous Cm(III)-gluconate system was studied by TRLFS in diluted NaCl and $CaCl_2$ electrolyte solutions and in absence of CO_2. The investigation of the aqueous system was necessary to derive reference spectra in the absence of clay minerals that had been studied in addition in a second step. In the latter case the adsorption of Cm(III) onto the clay minerals illite and montmorillonite was spectroscopically examined in the presence of 0.01 M gluconate and in 0.1 M NaCl or 0.06 M $CaCl_2$ to assure the same conditions as applied in the batch sorption experiments. Results for illite and montmorillonite are quite comparable. Therefore, in the following section only the results for montmorillonite will be discussed in detail. The findings for the illite system are given in the appendix (7.3). All displayed emission spectra were area normalized to assure comparability.

Aqueous Cm(III) gluconate systems

The complexation of Cm(III) with gluconate was studied by TRLFS at a fixed ligand concentration of 0.01 M gluconate and a metal ion concentration of $1 \cdot 10^{-7}$ M Cm(III) as a function of pH. Spectroscopic measurements were conducted in diluted NaCl (0.1 M, Figure 4.22 left) and $CaCl_2$ (0.06 M, Figure 4.22 right) to study the effects of the electrolyte composition.

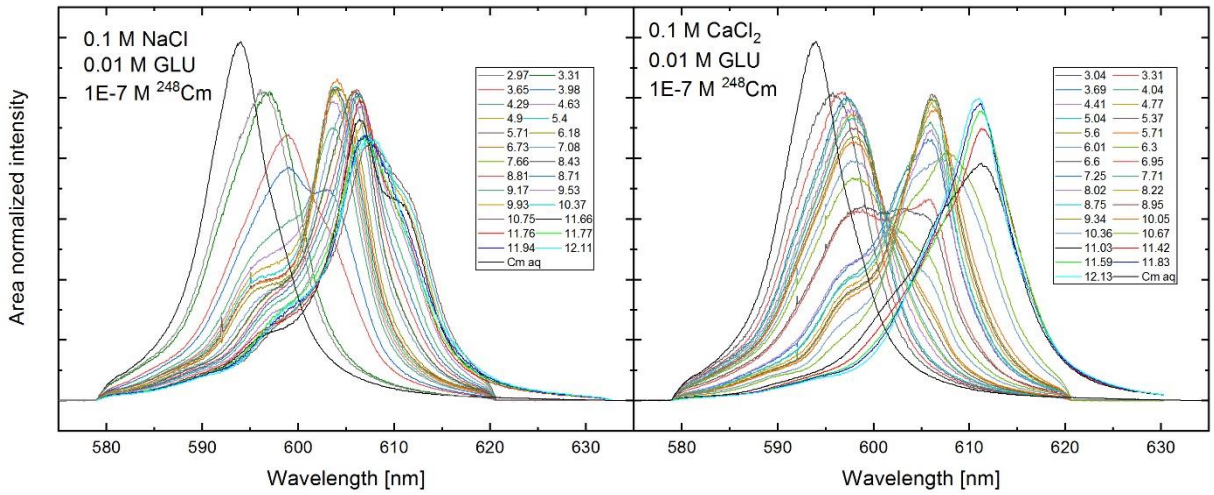

Figure 4.22: Fluorescence spectra of dissolved Cm(III) as a function of pH in presence of 0.01 M gluconate in 0.1 M NaCl (left) and 0.06 M $CaCl_2$ (right).

A presentation of a reduced amount of spectra is given in Figure 4.23 (0.1 M NaCl left, 0.06 M $CaCl_2$ right) to highlight the relevant peak maxima, which indicate the presence of different species. A strong red shift of the emission band is observed with increasing pH in both electrolyte systems, starting from the lowest pH value (pH ~ 3). Besides the uncomplexed Cm(III) aquo ion located at λ = 593.8 nm, a first peak maximum is found at λ = 596 nm. A further increase of the pH results in a shift to λ = 599 nm in NaCl (pH = 3.65) and to λ = 598 nm in $CaCl_2$ solution (pH = 5.60). An additional maximum at λ = 604 nm is observed in NaCl electrolyte occurring at pH = 5.71. This feature is not observed in $CaCl_2$ solutions. A further increase in pH leads to the appearance of a distinct peak maximum at λ ~606 nm at pH > 8.5. In the highly alkaline pH-range and in NaCl solutions a shoulder is observed at λ = 611 nm above pH = 11.5. At the same position a well separated peak is observed in $CaCl_2$ electrolyte solution. It has to be mentioned that similar or even identical spectra must not correspond to identical

species. The similar spectra only reflect a similar ligand field in the first coordination sphere of the central cation. In contrary, different peak positions clearly point to different species. The association of Ca^{2+} in the second coordination sphere of Cm(III) has no direct impact on the peak position of the fluorescence emission. However, a stabilization by Ca^{2+} may have an indirect effect on the first coordination sphere of Cm(III) (e.g. by a change of the nature or number of ligands), resulting in a shift of the peak position.

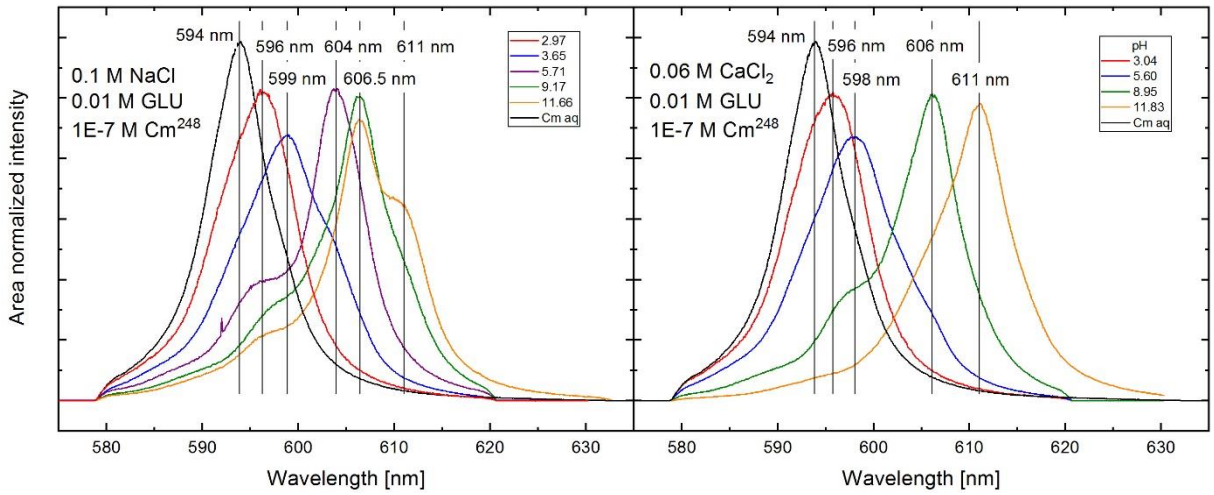

Figure 4.23: Selected fluorescence spectra of dissolved Cm(III) at different pH values in presence of 0.01 M gluconate in 0.1 M NaCl (left) and 0.06 M $CaCl_2$ (right). With highlighted distinct peak positions indicating the presence of different species.

With this qualitative, pH depending spectroscopic study and without performing a detailed peak deconvolution procedure (at least) 5 different species could clearly be differentiated in the NaCl and 4 in the $CaCl_2$ electrolyte system. It is assumed that calcium is capable to stabilize negatively charged An(III) hydroxo gluconate species $An^{III}(OH)_x(GLU)_z^{3-x-z}$. This stabilizing Ca^{2+} effect on Cm(III) species was already reported for hydrolysed species the trivalent Cm(III) ($CaCm(OH)_3^{2+}$, $Ca_2Cm(OH)_4^{3+}$ [58]), hexavalent U(VI) ($Ca_2UO_2(CO_3)_3$, [158]) the tetravalent Th(IV) ($CaTh(OH)_4(GLU)_2$, [75]) and Pu(IV) ($CaPu(OH)_3ISA_{-H}^{+}$ and $CaPu(OH)_3ISA_{-2H}$, [159]). The strong increase of the emission band at λ = 611 nm (pH > 11.5) in presence of Ca^{2+} is a clear indication of the mentioned stabilization effect.

Precipitation of $Cm(OH)_3$ cannot be excluded at the relatively high Cm(III) concentration (10^{-7} M) applied in this study in presence of gluconate [34]. However, due to extremely low fluorescence intensity of colloidal $Cm(OH)_3$ (concentration quenching) [160], recorded fluorescence spectra still can be assigned to dissolved species. Adsorption of Cm(III) onto montmorillonite in presence of gluconate

To study the mechanistic adsorption of Ln(III)/An(III) onto clay minerals in presence of gluconate a comprehensive TRFLS studied was conducted as a function of pH in diluted NaCl and $CaCl_2$ electrolyte solutions. A set of fluorescence emission spectra of Cm(III) adsorbed onto montmorillonite (and illite, appendix 7.3) in presence of 0.01 M gluconate is shown in Figure 4.24 for 0.1 M NaCl (left) and 0.06 M $CaCl_2$ (right). The spectra of a Cm^{3+} aquo ion is added for comparison. Presentation of a reduced amount of spectra is given in Figure 4.25 (NaCl left, $CaCl_2$ right) to point out the different peak positions more precisely.

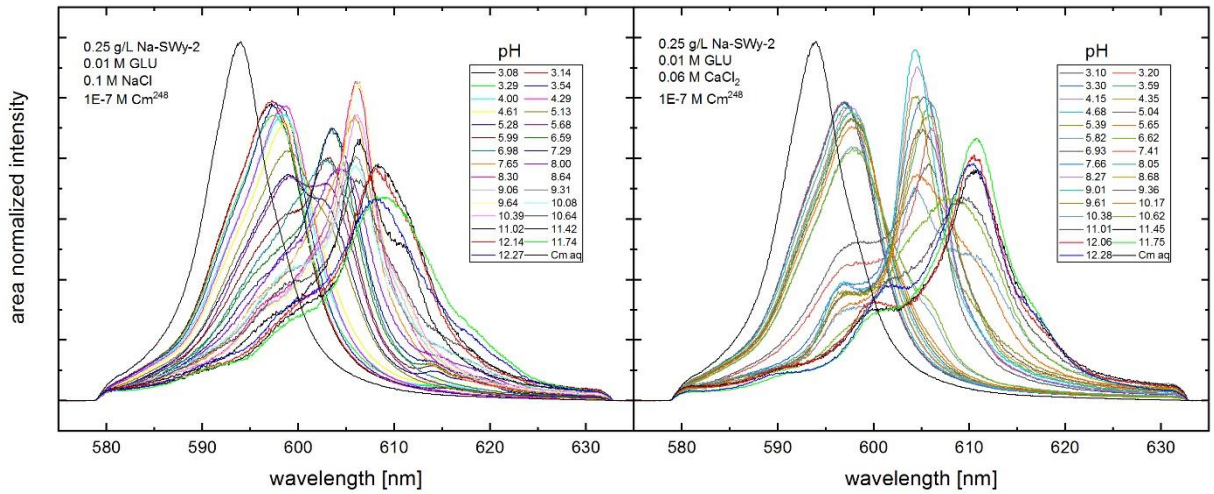

Figure 4.24: Fluorescence spectra of Cm(III) adsorbed onto montmorillonite as function of the pH in presence of 0.01 M gluconate in 0.1 M NaCl (left) and 0.06 M $CaCl_2$ (right).

In the NaCl system and at low pH values (pH = 3.08) the maximum of the Cm(III) fluorescence emission is located above λ = 596 nm. A small shoulder at λ = 594 nm indicates a small amount of free Cm^{3+} aquo ion. A successive shift from λ = 597 to 598.5 nm is observed in the pH range from pH = 3-5. The formation of a second distinct peak maximum at λ = 603.5 nm is observed in the neutral pH-range. At pH ~ 9 another feature is observed with a relatively sharp peak at λ = 606 nm. Above pH = 11 a shoulder forms at λ ~ 611 nm.

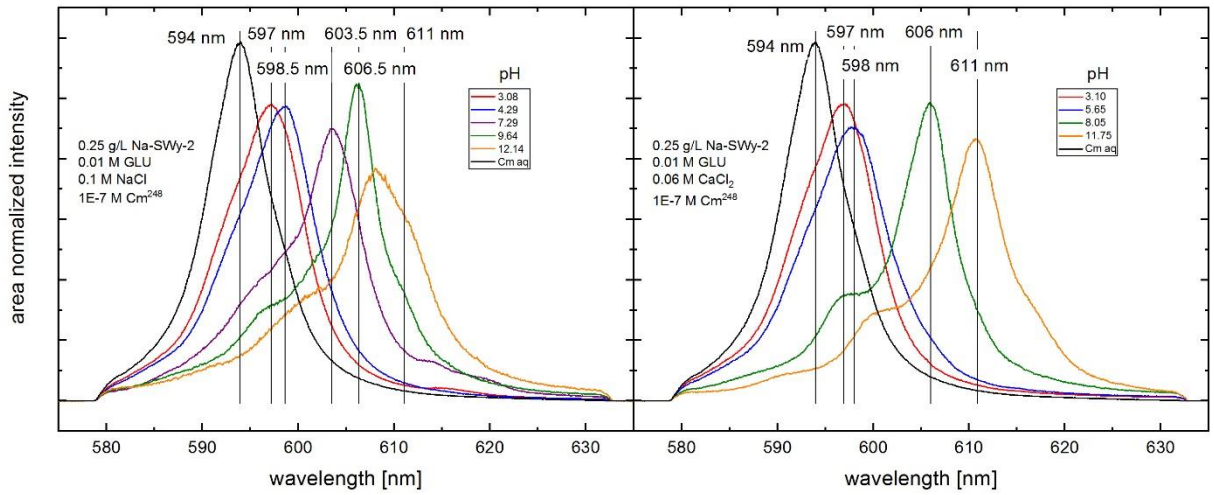

Figure 4.25: Selected fluorescence spectra of Cm(III) adsorbed onto montmorillonite as function of the pH in presence of 0.01 M gluconate in 0.1 M NaCl (left) and 0.06 M $CaCl_2$ (right). With highlighted distinct peak positions indicating the presence of different species.

In presence of Ca^{2+}, the same features are observed, except of the one at λ = 603.5 nm. This feature is missing, which is in good agreement with the aqueous systems described above. It is also remarkable that the main features of the Cm(III) clay gluconate system can be attributed to the pure aqueous Cm(III) gluconate species. This effect may be explained by a superimposition of the emission bands of adsorbed and aqueous species. Another possibility could be that the sorbed species are not very much different compared to dissolved species, i.e. the denticity to the surface may be reduced compared to strong surface complexes of e.g. pure hydrolysed species. A comparison of the fluorescence intensity factors (FI) of aqueous systems and clay containing systems in absence and presence of gluconate (Figure 4.26) shows a significant decrease in fluorescence intensity, if clay minerals are present (mainly by light scattering effects on colloidal particles of the incident laser beam as well as the fluorescent light). More important, an increased fluorescence intensity is observed for sorption experiments in presence of gluconate compared to experiments in the absence of gluconate. The stronger intensity of Cm-gluconate complexes as compared to that of Cm-clay surface complexes suggests that the spectra in Figure 4.25 can be assigned predominantly to dissolved Cm-gluconate species.

Similar as for the pure Cm(III) aqueous complexation in presence of gluconate a detailed peak deconvolution and assignment of well-defined surface species is simply

not possible due to the huge number of potentially adsorbed and aqueous Cm(III) species being present in this system simultaneously.

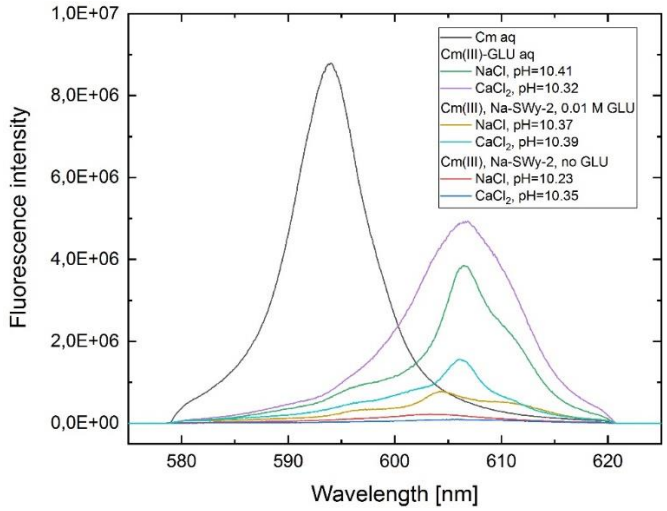

System	FI-factor
$NaCl_{(aq)}$	0.49
$CaCl_{2,\ (aq)}$	0.77
NaCl, SWy, GLU	0.13
$CaCl_2$, SWy, GLU	0.21
NaCl, SWy, no GLU	0.04
$CaCl_2$, SWy, no GLU	0.02

Figure 4.26: Selected Cm(III) fluorescence emission spectra of aqueous and suspended clay sample in the presence of 0.01 M gluconate compared to suspended clay samples in the absence of gluconate (left). Relative fluorescence intensity factors (FI) of each system (right).

A qualitative separation of the observed influence of gluconate on the adsorption of Eu(III) onto montmorillonite is shown in Figure 4.27 for NaCl (left) and $CaCl_2$ (right) electrolytes. Both show 3 regions (blue boxes) of different influencing factors. In the absence of Ca^{2+} a small decrease in Eu(III) retention is observed in 0.1 M NaCl solution from log K_D =2.8-2.3 (pH = 3-3.5), above pH = 3.5 the observed log K_D is comparable to studies under saline condition. Between pH = 3.5-6.5 a comparable retention is found for all investigated ionic strengths (Figure 4.27, left, (1) blue box). The small, but observable decrease in the acidic pH indicates a competition between the formation of aquatic Eu(III)-gluconate species and the cation exchange of Eu^{3+} on the basal planes of the clay minerals. As observed by pH dependent TRLFS measurements, a complexation of Eu(III) with gluconate starts already below pH = 3. The formation of complexed species gets more dominant with increasing pH, the availability of Eu^{3+} is reduced and the relevance of the cation exchange effect decreases. A second explanatory approach might be an adsorption of gluconate to the clay mineral surface. This adsorption could block a decent number of surface sites, which are no longer available for a further adsorption of Eu(III). From pH = 6.5-10 (Figure 4.27, left, (2) blue

box) a competition between aqueous Eu(III)-gluconate species and inner sphere sorption processes is the most reasonable explanation for the reduced Eu(III) retention. Above pH = 10 (Figure 4.27, left, (3) blue box) stable gluconate containing aquatic complexes are formed, as indicated by TRLFS measurements. In addition, an instability of the clay mineral is expected in the hyperalkaline pH. The dissolution of the mineral phase is related with the release of its components (Si, Al, Fe, Mg) into the electrolyte solution. This change of the chemical composition can also influence the speciation and adsorption of An(III)/Ln(III) as reported by Schnurr *et al.* and Huittinen *et al*. [17, 114].

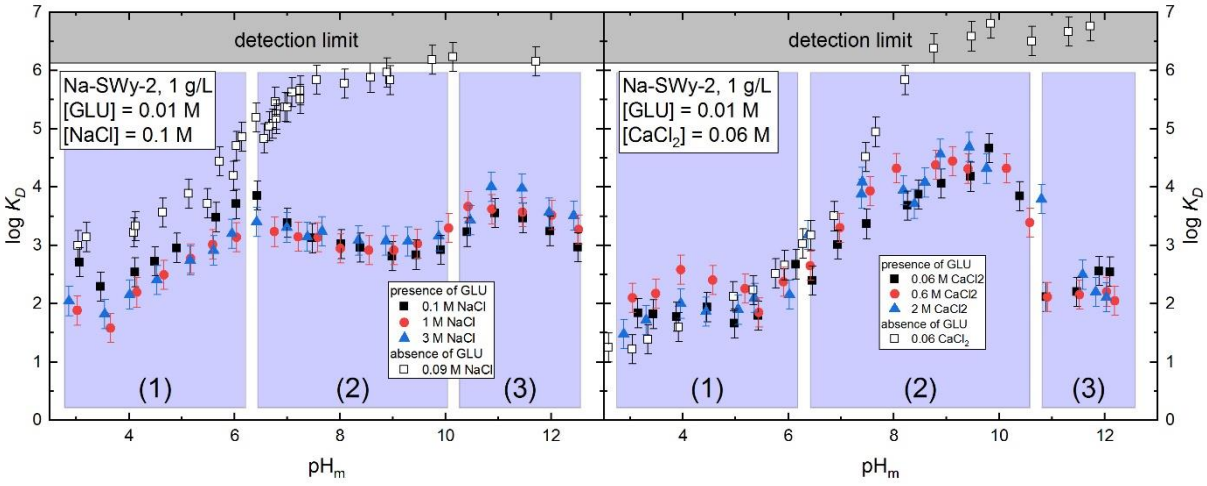

Figure 4.27: Retention of the Eu(III) sorption onto montmorillonite as function of pH, in presence of 0.01 M gluconate (closed symbols) and absence of gluconate (open symbols, Schnurr *et al.* [17]), in different NaCl (left) and $CaCl_2$ (right) electrolyte solutions (0.1 M black, 1 M blue, 3 M red). To estimate the effect of gluconate, an experimental series from Schnurr *et al.* in absence of any competing ligand was added (open black symbols, 0.09 M NaCl or 0.06 M CaCl [17]).

The adsorption of Eu(III) onto montmorillonite in presence of gluconate and Ca^{2+} (Figure 4.27, right) could also be separated into 3 regions with different impact of the organic ligand. In the acidic pH a low adsorption of Eu(III) is observed in presence of gluconate (Figure 4.27, right, (1) blue box). This was also reported for experimental data in the absence of gluconate [17]. According to spectroscopic results (TRLFS) similar Cm(III) gluconate species are present, as shown by the same shift in wavelength (λ = 597 nm) for both NaCl and $CaCl_2$ solution. The already reduced retention of Eu(III) in $CaCl_2$ systems is unaffected by processes in the aquatic phase.

This difference between NaCl and $CaCl_2$ electrolyte systems supports the assumption of a competition between the formation of aquatic complexes and the cation exchange, which is supressed in Ca^{2+} containing systems and at high ionic strength [17]. A steady increase up to log K_D =4.5 (pH = 10) characterizes the region from pH = 6.5-10.5 (Figure 4.27, right, (2) blue box). Compared to systems in the absence of Ca^{2+} (and presence of gluconate) a significant increase in Eu(III) adsorption is observed. A reduction of the available free gluconate in solution, by the formation of a $Ca(HGlu)^+$ species could explain the weakening of the impact of gluconate on the Eu(III) retention. According to TRLFS measurements, a significant amount of complexed species is still observed in the aquatic phase. This can explain the lowered retention of Eu(III) onto montmorillonite in presence of gluconate as compared to data in the absence of gluconate. A third observed effect is a strong decrease in adsorption at pH ≥ 11 (Figure 4.27, right, (2) blue box). As discussed above, the formation of aquatic quaternary, Ca^{2+} stabilized Ca-An(III)-OH-GLU in the hyperalkaline pH range is the most likely explanation for this decrease [58, 75, 158, 159]. A stabilization of An(III)/Ln(III)-GLU species in the hyperalkaline pH is also supported by TRLFS measurements.
In general an oversaturation of the investigated systems with respect to the solubility of $Eu(OH)_3$ and $Cm(OH)_3$ could not be excluded. As already discussed at p. 89, In presence of clay mineral surfaces the formation of surface complexes and surface precipitation , thus cannot be excluded at above pH ~ 9. Due to extremely low fluorescence intensity of $Cm(OH)_3$ colloids (concentration quenching) [160], recorded fluorescence spectra can be correlated with dissolved species.

4.3. Impact of citrate on the sorption of Eu(III) and Cm(III) onto clay minerals

4.3.1. Batch sorption experiments

NaCl-electrolyte system

The impact of citrate on the retention of Eu(III) adsorbed onto the clay minerals Illite du Puy (Figure 4.28, left) and montmorillonite (right) was studied in NaCl solutions. The experimental data is presented as logarithmic distribution coefficient log K_D versus

pH_m. Experiments were conducted with a ligand concentration of 0.001 M citrate in diluted and concentrated NaCl electrolyte solutions (closed symbols: 0.1 M black, 1 M red, 3 M blue NaCl) and compared to a study in the absence of citrate (open symbols: 0.1 M black, 1 M red, 3 M blue NaCl, Schnurr *et al.* [17]).

In diluted NaCl the retention of Eu(III) is slightly decreasing from pH = 3-4 ($\Delta \log K_D \sim 1.5$) for illite and less pronounced for montmorillonite. Contrary, in concentrated NaCl solutions a more or less constant $\log K_D \sim 1.5\text{-}2$ is observed in this pH range for both clays. Between pH = 4-8 a steady increase in the adsorption of Eu(III) onto illite is observed in diluted and concentrated NaCl solutions. Compared to data in the absence of citrate, this increase is about 2 logarithmic units lower for 0.1M NaCl and 1.5 log units for the higher ionic strengths in presence of citrate. Above pH > 8.5 a retention higher than $\log K_D > 5.5$ is observed for all studied ionic strengths.

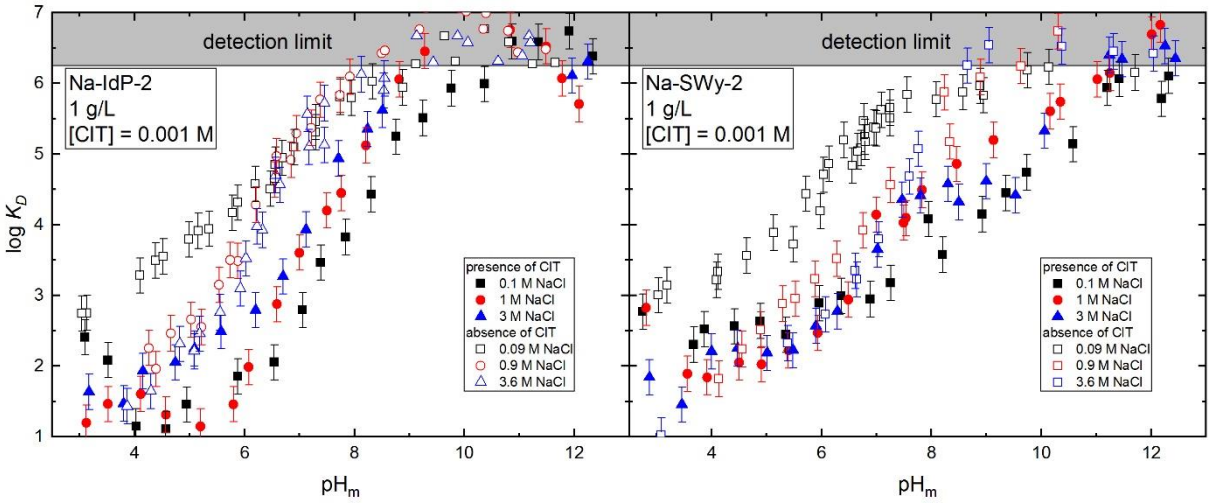

Figure 4.28: Eu(III) sorption onto Illite du Puy (left) and montmorillonite (right), in presence of 0.001 M Na-Citrate as function of the pH, in different NaCl electrolyte solutions (closed symbols: 0.1 M black, 1 M blue, 3 M red). To estimate the effect of citrate, data in absence of any competing ligand is added (open black symbols, 0.09 M black, 0.9 red, 3.6 M NaCl Schnurr *et al.* [17]).

In case of montmorillonite, a nearly linear increase in adsorption is observed between pH = 5-11, with a final retention of $\log K_D > 5.5$ for diluted and concentrated NaCl solutions. The total deviation between the $\log K_D$ values in presence and absence of citrate is $\Delta \log K_D \sim 1.5\text{-}2$ for diluted systems. No significant deviation is observed for saline systems between pH = 4-8. In absence of citrate a $\log K_D > 6$ is reached for pH > 8, while in presence of citrate this level of retention is reached for pH > 11. An

increased retention of Eu(III) is observed with increasing ionic strength in a pH range from 4 to 9.

A general decrease in Eu(III) retention in presence of citrate is observed for both clay minerals, illite and montmorillonite, but with a different ionic strength dependence. It is assumed that the formation of strong aqueous Eu(III)-citrate complexes, especially $Eu(Cit)_2^{-3}$ (section 2.2.4), outcompetes surface complexation reactions over a broad range of pH. The predominance of anionic aqueous species also suppresses the electrostatic attraction of cations like Eu^{3+} to the negatively charged basal planes of the clay minerals. With increasing pH inner sphere surface complexes of Eu(III) on the clay mineral sites gain more importance, leading to an increase in Eu(III) retention.

$CaCl_2$-electrolyte systems

The adsorption of Eu(III) onto illite (Figure 4.29, left) and montmorillonite (right) in presence of 0.001 M citrate (right) was investigated in different $CaCl_2$ electrolyte solutions (closed symbols: 0.06 M black, 0.6 M red, 2 M blue $CaCl_2$). To estimate the effect of this strong complexing ligand, data in absence of citrate were added for comparison (open symbols: 0.06 M, 0.6 M, 2 M $CaCl_2$, Schnurr *et al.* [17]).

In deviation to the NaCl system an increase in Eu(III) retention is observed in $CaCl_2$ electrolyte solutions (Figure 4.29) in presence of 0.001 M citrate for both clay minerals. The adsorption of Eu(III) increases from log K_D ~ 1-6 (illite, left) and log K_D ~ 2-5.5 (montmorillonite, right) between pH = 3-9. Above pH > 9 the retention of Eu(III) remains high (log K_D > 5.5). Almost no influence of ionic strength is observed within the experimental conditions from pH = 3-12.5. Only in case of the Eu(III) adsorption onto illite in 2 M $CaCl_2$ the presence of citrate causes a reduction of the log K_D by 0.5-1 logarithmic units between pH = 7.5-9.5. In contrast to the NaCl system, the formation of aqueous Ca-citrate complexes reduces the concentration of the free citrate ligand in solution and with this the predominance of the previously dominating $Eu(Cit)_2^{3-}$ complex (section 2.2.4). The reduction of competing complexes in solution can also support the formation of surface complexed species.

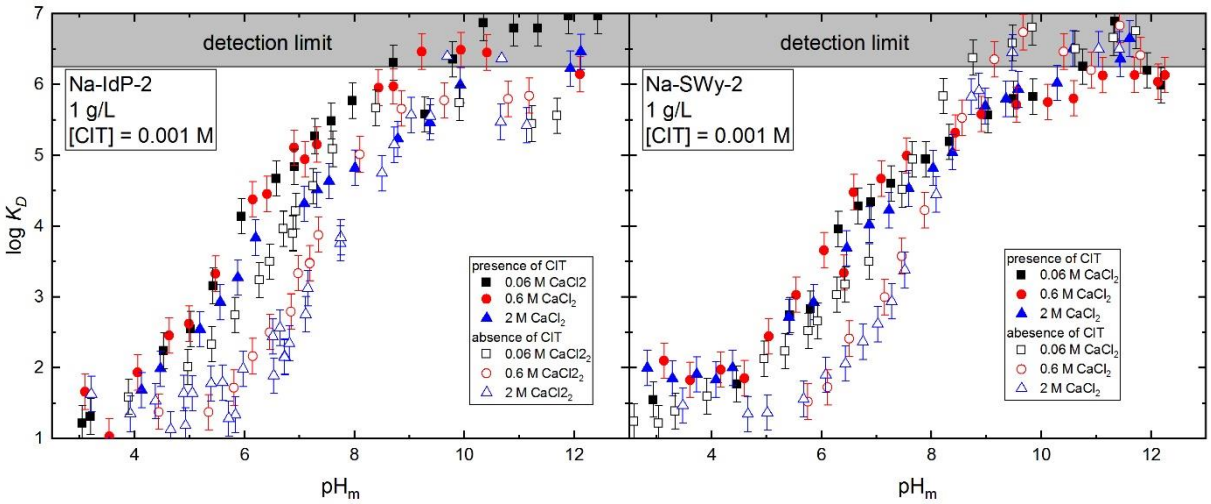

Figure 4.29: Eu(III) sorption onto Illite du Puy (left) and montmorillonite (right), in presence of 0.001 M Na-Citrate as function of the pH, in different $CaCl_2$ electrolytes solutions (closed symbols: 0.06 M black, 0.6 M blue, 2 M red). To estimate the effect of citrate, data in absence of any competing ligand is added (open symbols: 0.06 M black, 0.6 M blue, 2 M red $CaCl_2$ Schnurr *et al.* [17]).

4.3.2. Time resolved laser fluorescence spectroscopy (TRLFS)

The adsorption of Cm(III) onto illite (Figure 4.30) in presence of 0.001 M citrate was studied as function of the pH in diluted NaCl (left) and $CaCl_2$ solutions using TRLFS. To highlight relevant peak positions a presentation with a reduced number of spectra is shown in Figure 4.31.

In 0.1 M NaCl a shift to higher wavelengths is observed for all pH values compared to the Cm aquo ion at λ = 593.8 nm. A first species is observed at λ = 597.1 nm (pH = 3.13) and a second at λ = 599.9 nm (pH = 5.26). In the alkaline pH range another species is observed at λ = 602.5 nm at pH = 9.01. Two shoulders indicate further species with larger peak shifts at pH = 10.08 with a wavelength of λ = 605.8 nm and for pH > 11.51 around λ = 610.2 nm. According to Heller *et al.* [35] the first species at λ = 597.1 nm is attributed to the neutral CmHCit complex. The peak maximum at λ = 599.9 nm is attributed to the 1:2 complex $Cm(HCitH)HCit^{2-}$. While the appearance of the first species is in excellent agreement with Heller *et al.* [35] regarding pH and wavelength, the second species is reported at slightly higher wavelength of λ = 600.4 nm in the same pH range. With respect to the increasing retention for pH > 7 the observed species at λ = 602.5 nm (pH = 9.01), λ = 605.8 nm (pH = 10.08) and

λ = 610.2 nm (pH = 11.51) in the alkaline pH range are assigned to adsorbed Cm(III) surface complex without the participation of citrate as described by Schnurr *et al.* [17]. Although the comparable peak positions support this assumption, the formation of citrate containing surface complexes settled by spectroscopy.

According to the spectroscopic findings the decrease in An(III)/Ln(III) retention in the acidic pH range is related to the predominance of aqueous Cm-Citrate complexes. The following increase in retention is caused by the formation of Cm(III) surface complexes.

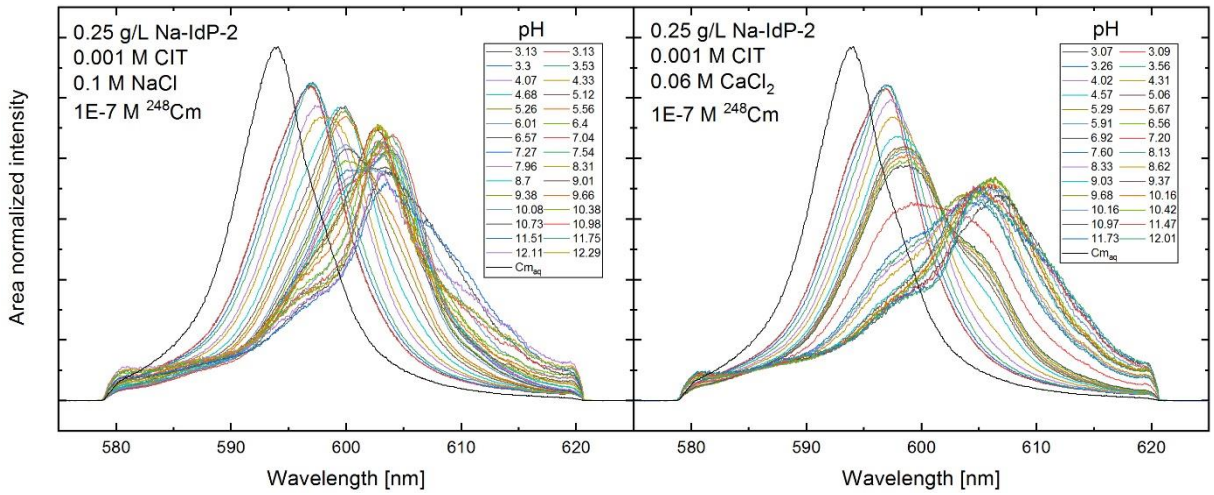

Figure 4.30: Fluorescence spectra of Cm(III) adsorbed onto illite in presence of 0.001 M citrate as function of the pH, in 0.1 M NaCl (left) and 0.06 M $CaCl_2$ (right).

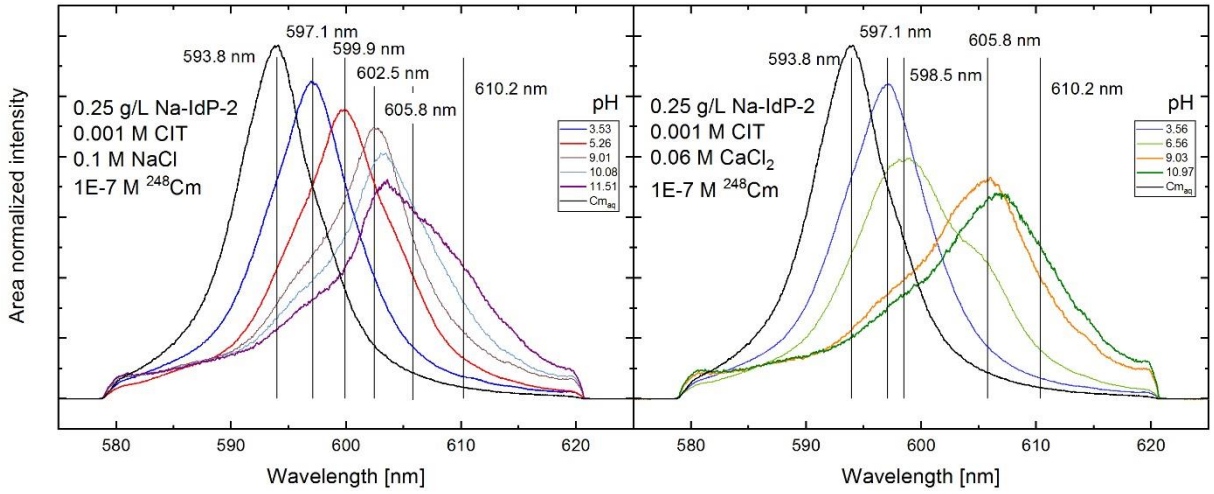

Figure 4.31: Selected fluorescence spectra of Cm(III) adsorbed onto illite in presence of 0.001 M citrate as function of the pH in 0.1 M NaCl (left) and 0.06 M $CaCl_2$ (right). Highlighted distinct peak positions indicate the presence of different species.

The retention of Cm(III) onto illite in presence of 0.001 M citrate was investigated in diluted $CaCl_2$ electrolyte solution (0.06 M $CaCl_2$, Figure 4.30, right). Relevant peak maxima are highlighted in Figure 4.31. Already at pH = 3 a significant shift of the emission band to higher wavelengths (λ = 597.1 nm, pH = 3.53) compared to the Cm^{3+} aquo ion is observed. A second feature with a broad half width (more than one species involved) and a central wavelength of λ = 598.5 nm is detected at pH = 6.56. In the alkaline region around pH = 9.03 a feature is observed at λ = 605.8 nm, with a shoulder at λ = 610.2 nm forming at pH ≥ 10.97. As discussed for the NaCl electrolyte systems, the band at λ = 597.1 nm can be attributed to an aqueous 1:1 Cm citrate complex (Heller *et al.* [35]). The two bands at λ = 605.8 nm and λ = 610.2 nm are identified as two adsorbed surface species as reported by Schnurr *et al.* [17]. The participation of citrate in Cm(III) surface complexes was neither confirmed nor excluded. As batch sorption experiments (section 4.3.1) show an increased retention of Eu(III) (pH = 6.5) the feature at λ = 598.5 nm can also be attributed to an adsorbed Cm species.

As discussed in section 2.2.4, cement additives like citrate have the potential to adsorb to calcium containing surfaces in CSH phases and similarities between silicate structures in CSH phases and basal planes of clay minerals are reported [161]. Because citrate is known for its high affinity to Ca^{2+} ions, adsorption of Cm(III) to a calcium bridged citrate seems to be possible. It is unlikely that all three carboxylic groups will be bound to a single adsorbed Ca^{2+} ion. For this reason, the formation of ternary Clay-Ca-Citrate-Cm(III) surface species might be located at the basal plan of the clay mineral. This ternary Cm(III) surface species could explain the observed increase of the total An(III)/Ln(III) retention above the level of the ligand free case in slightly acidic pH.

5. Summary

Within the framework of this PhD thesis the adsorption of trivalent lanthanides and actinides onto the clay minerals Illite du Puy (Na-IdP-2) and montmorillonite (Na-SWy-2) was studied under the influence of competing anions from low to high ionic strength. The main focus was set on the impact of carbonate on the adsorption of Ln(III)/An(III). Beside this natural occurring ligand also gluconate, as an analogue for the cellulose degradation product isosaccharinic acid, and citrate as a natural occurring ligand and commercial decontamination agent were investigated. In addition both ligands are commonly used as cement additive. In the following section a short summary is given for the different systems and effects of the competing ligands.

Adsorption of Ln(III)/An(III) onto clay minerals in presence of carbonate:

The adsorption of Eu(III) / Cm(III) onto different clay minerals (illite, montmorillonite) was studied in NaCl electrolyte solutions (0.1, 1, 3 M) in equilibrium with ambient CO_2 and 1 % CO_2. Depending on the applied CO_2 partial pressure the retention measured as pH dependent distribution coefficient log K_D decreases between pH = 9-10 (ambient CO_2) or pH = 8-9 (1 % CO_2) over more than 2 logarithmic units. This significant decrease is explained by an increasing carbonate concentration in the alkaline region and hence the formation of the predominant 1:3 carbonate species of Ln(III)/An(III) in solution. These finding is in good agreement with previous studies by Marques *et al.* [22, 113]. Beside this effect a second effect was identified, which leads to an increasing adsorption in the slightly acidic pH-range between pH = 4-6 by about $\Delta\log K_D \sim 1.5$ (ambient conditions) and $\Delta\log K_D \sim 1$ (1 % CO_2) compared to the carbonate free system (Schnurr *et al.* [17]). This increasing effect was also observed in presence of selenite, as an analogue for carbonate. To explain this effect a comprehensive theoretical computational study using DFT and AIMD was conducted to derive further insights in the structural properties of adsorbed species on a molecular scale. In a first step the stability of adsorbed carbonate on clay mineral edge sites was proven. The sorption mechanism was explained by a ligand exchange reaction between surface hydroxyl groups and dissolved carbonate. This is in good agreement with literature reported on the adsorption of carbonate onto iron and aluminium hydroxides [108, 109]. Surface

sensitive ATR-IR measurements were performed on montmorillonite suspended in carbonate containing electrolyte solutions. The results clearly show that carbonate binds to the clay mineral surface and has to be considered as a further surface binding site for metal ions. The structures of ternary Cm(III)-carbonate surface complexes were determined by DFT and AIMD simulations. Localised infrared spectra of the first coordination shall of the adsorbed Ln(III) were extracted and compared with vibronic sideband spectra. Using time resolved laser fluorescence spectroscopy two different surface sorbed species were revealed by peak deconvolution and fluorescence lifetime measurements. For both sorbed species vibronic sidebands were recorded and compared to computed IR spectra and reference systems in the absence of carbonate. As this technique only probes the first coordination shell of the excited metal ion, the presence of carbonate in the VSB spectra indicates ternary Cm(III)-carbonate surface complexes. This confirms the previous findings. The adsorption of An(III) on clay minerals is dominated by the formation of carbonate stabilized surface species from slightly acidic to alkaline pH conditions.

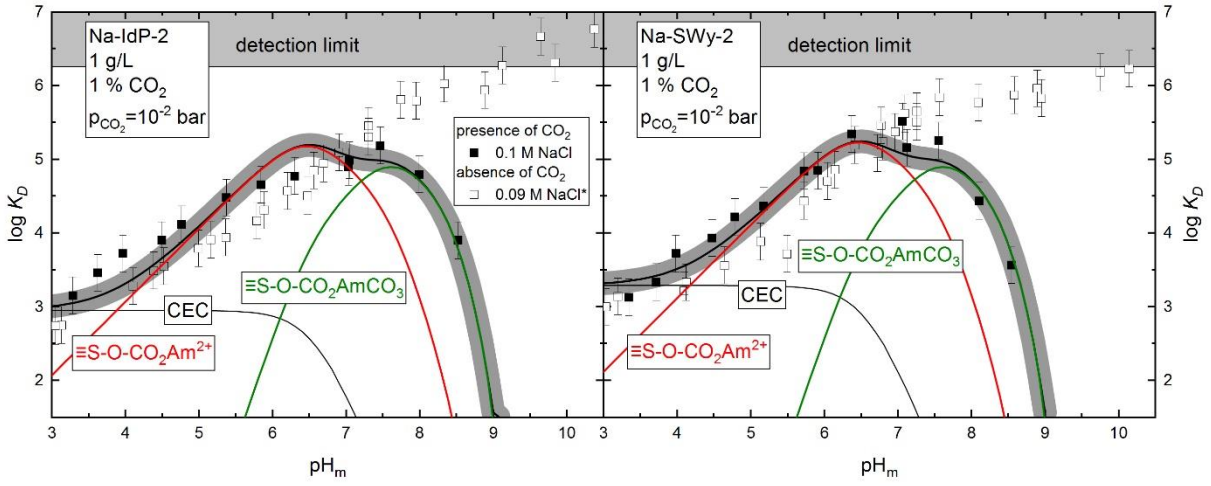

Figure 5.1: Surface sorbed carbonate assisted sorption model (black line) of the Eu(III) sorption edge on Na-IdP-2 (left) and Na-SWy-2 (right), in equilibrium with an elevated partial pressure of 1% CO_2 (closed symbols) and in absence of CO_2 (open symbols, *Schnurr *et al.* [17]), in 0.1 M NaCl. Ternary surface species are highlighted in red and green.

Combining the results of batch sorption experiments, time resolved laser fluorescence and vibronic sideband measurements, ATR infrared spectroscopy and theoretical computations a 2SPNE/CE model was successfully applied (Figure 5.1). The

adsorption of carbonate to the clay mineral could not be quantified experimentally within the present study. A electrostatic dynamic double-layer model of Van Geen *et al.* [109] for the carbonate adsorption onto goethite was adopted in a nonelectrostatic 2SPNE/CE model. Although this approach holds some uncertainties, an accurate description of the experimental findings was achieved. The two ternary Cm(III) carbonate surface species ≡S-O-CO_2Am^{2+} and ≡S-O-CO_2AmCO_3 were added to the 2SPNE/CE model of Bradbury and Baeyens [13, 118], which then was able to describe the adsorption of Eu(III) onto montmorillonite and illite under different partial pressures of CO_2 and from diluted to concentrated sodium chloride electrolyte systems. For the first time, the impact of carbonate on Eu/Cm(III) sorption was described by the applied geochemical model considering consistently batch sorption experiments, spectroscopic results from TRLFS, VSB, ATR-FTIR measurements and theoretical DFT and AIMD calculations.

Adsorption of Ln(III)/An(III) onto clay minerals in presence of gluconate:

In NaCl solution the Eu(III) retention in presence of 0.01 M gluconate is reduced by about 2 orders of magnitude over the whole pH-range, compared to gluconate free systems (log K_D> 6 to log K_D~ 4, Schnurr *et al.* [17]). Gluconate acts as a competing ligand. Hence, a lower limit of the gluconate concentration was derived to estimate its impact on the sorption. Below [GLU] < $1 \cdot 10^{-4}$ M, gluconate shows no significant effect on the Eu(III) retention onto Illite du Puy.

Between pH = 7-11, a similar Eu(III) retention is observed in presence of Ca^{2+}, as reported for NaCl electrolyte systems. Above pH = 11 an even further decreased log K_D~ 2 is observed. A significant effect of ionic strength isn't observed neither for NaCl nor for $CaCl_2$ electrolyte systems.

Time resolved laser fluorescence spectroscopy was used to study the behaviour of adsorbed Cm(III) and aquatic species in presence of gluconate. Due to higher fluorescence intensity factors of dissolved Cm(III)-gluconate species, no distinct surface species could be identified. Nevertheless, a qualitative description of the competition of adsorbed and aquatic species was derived. In addition to that, a

stabilizing effect of Ca^{2+} on the formation of quaternary Ca-Cm-OH-GLU species was identified at high pH values.

Adsorption of Ln(III)/An(III) onto clay minerals in presence of citrate:

The influence of citrate on the sorption behaviour of Eu(III) onto Illite du Puy and montmorillonite was studied in NaCl and $CaCl_2$ electrolyte solutions in the pH range of pH = 3-12.5. In NaCl electrolyte solutions the retention of Eu(III) onto Illite du Puy is significantly reduced from the acidic to neutral pH. Under alkaline conditions a quasi-quantitative sorption is reached. Experiments performed in $CaCl_2$ electrolyte solutions show an increased retention in the pH-range of 3 to 8, also reaching quasi-quantitative retention in the alkaline pH. A time resolved laser fluorescence study was performed on suspended clay samples containing Cm(III) and citrate in NaCl and $CaCl_2$ electrolyte systems. In the absence of calcium, aquatic Cm(III) citrate complexes dominate the speciation in the acidic pH range. Adsorbed species were observed similar to studies in the absence of competing ligands from neutral to alkaline. Unfortunately, the association of citrate to these surface species could not be clarified. The enhanced retention of Eu(III) in $CaCl_2$ electrolyte systems may be explained by the formation of a ternary Ln(III)/An(III)-citrate surface complex.

The influence of the different competing anionic ligands used in this study on the adsorption of trivalent lanthanides and actinides on clay minerals has been proven to be very complex. Not only a competition between adsorbed Ln(III)/An(III) surface species and aquatic species is taking place. Also, the adsorption of the competing ligands onto clay mineral surface can affect the adsorption behaviour of trivalent lanthanide and actinides significantly. While the presence of carbonate (or the analogue selenite) and citrate increases the Ln(III)/An(III) adsorption in the slightly acidic and neutral pH, gluconate is generally decreasing the retention. A possible explanations could be the number of carboxylic acid groups of the ligand (citrate 3, gluconate 1), the lower reactivity of alcohol groups and steric hindrance of the organic rest.

6. Literature

1. Däuper, O. and A. von Bernstorff, *Gesetz zur Suche und Auswahl eines Standortes für die Endlagerung radioaktiver Abfälle–zugleich ein Vorschlag für die Agenda der „Kommission Lagerung hoch radioaktiver Abfallstoffe".* Zeitschrift für Umweltrecht, 2014: p. 24-31.
2. SKB, *Long-term safety for KBS-3 repositories at Forsmark and Laxemar - a first evaluation; Main report of the SR-Can project. SKB Technical report TR-06-09*. 2006, Svensk Kärnbränslehantering AB: Stockholm, Sweden. p. 620.
3. Swiss Standard, S., *670 010b.* Characteristic Coefficients of soils, Association of Swiss Road and Traffic Engineers, 1999.
4. Blume, H.-P., et al., *Scheffer/schachtschabel: Lehrbuch der bodenkunde*. 2016: Springer-Verlag.
5. Nagra, *Project Opalinus Clay - Safety Report - Demonstration of disposal feasibility for spent fuel, vitrified high-level waste and long-lived intermediate level waste (Entsorgungsnachweis)*. 2003, Nagra: Wettingen (Switzerland). p. 360.
6. Ondraf/Niras, *SAFIR 2: Safety assessment and feasibility report 2*. 2002.
7. ONDRAF/NIRAS, *Technical overview of the SAFIR 2 report*. 2001.
8. Hoth, P., Wirth, H., Reinhold, K., Bräuer, V., Krull, P., Feldrappe, H., *Endlagerung radioaktiver Abfälle in tiefen geologischen Formationen Deutschlands - Untersuchung und Bewertung von Tongesteinsformationen* in *BGR-Bericht*. 2007: Berlin/Hannover.
9. Nagra, *Projekt Opalinuston -Konzept für die Anlage und den Betrieb eines geologischen Tiefenlagers- Entsorgungsnachweis für abgebrannte Brennelemente, verglaste hochaktive sowie langlebige mittelaktive Abfälle*. 2002, Nagra: Wettingen (Switzerland). p. 150.
10. Brewitz, W., *Zusammenfassender Zwischenbericht.* GSF T, 1980. **114**.
11. Baeyens, B., Bradbury, M. H., *A mechanistic description of Ni and Zn sorption on Na-montmorillonite Part I: Titration and sorption measurements.* Journal of Contaminant Hydrology, 1997. **27**(3–4): p. 199-222.
12. Baeyens, B. and M.H. Bradbury, *Cation exchange capacity measurements on illite using the sodium and cesium isotope dilution technique: Effects of the index cation, electrolyte concentration and competition: Modeling.* Clays and Clay Minerals, 2004. **52**(4): p. 421-431.
13. Bradbury, M.H., Baeyens, B., Geckeis, H., Rabung, T., *Sorption of Eu(III)/Cm(III) on Ca-montmorillonite and Na-illite. Part 2: Surface complexation modelling.* Geochimica Et Cosmochimica Acta, 2005. **69**(23): p. 5403-5412.
14. Bradbury, M.H., Baeyens, B., *Sorption modelling on illite. Part II: Actinide sorption and linear free energy relationships.* Geochimica Et Cosmochimica Acta, 2009. **73**(4): p. 1004-1013.
15. Bradbury, M.H., Baeyens, B., *Sorption modelling on illite Part I: Titration measurements and the sorption of Ni, Co, Eu and Sn.* Geochimica Et Cosmochimica Acta, 2009. **73**(4): p. 990-1003.
16. Bradbury, M.H. and B. Baeyens, *A mechanistic description of Ni and Zn sorption on Na-montmorillonite Part II: modelling.* Journal of Contaminant Hydrology, 1997. **27**(3–4): p. 223-248.

17. Schnurr, A., *Untersuchungen zur Radionuklidsorption an Tonmineraloberflächen bei hohen Ionenstärken*, in *Institut für Nukleare Entsorgung (INE)*. 2015, Karlsruher Institut für Technologie (KIT): Karlsruhe. p. XIV, 147 Seiten.
18. Schnurr, A., et al., *Sorption of Cm(III) and Eu(III) onto clay minerals under saline conditions: Batch adsorption, laser-fluorescence spectroscopy and modeling.* Geochimica et Cosmochimica Acta, 2015. **151**: p. 192-202.
19. Schnurr, A., et al., *Sorption studies of actinides onto clay minerals under saline conditions.* Abstracts of Papers of the American Chemical Society, 2014. **248**.
20. Turner, D.R., R.T. Pabalan, and F.P. Bertetti, *Neptunium (V) sorption on montmorillonite: An experimental and surface complexation modeling study.* Clays and Clay Minerals, 1998. **46**(3): p. 256-269.
21. Wendt, S., *Sorption and direct speciation of neptunium (V) on aluminium oxide and montmorillonite*. 2009, Citeseer.
22. Fernandes, M.M., B. Baeyens, and M.H. Bradbury, *The influence of carbonate complexation on lanthanide/actinide sorption on montmorillonite.* Radiochimica Acta International journal for chemical aspects of nuclear science and technology, 2008. **96**(9-11): p. 691-697.
23. Fernandes, M.M., et al., *U (VI) sorption on montmorillonite in the absence and presence of carbonate: a macroscopic and microscopic study.* Geochimica et Cosmochimica Acta, 2012. **93**: p. 262-277.
24. Fernandes, M.M., A.C. Scheinost, and B. Baeyens, *Sorption of trivalent lanthanides and actinides onto montmorillonite: Macroscopic, thermodynamic and structural evidence for ternary hydroxo and carbonato surface complexes on multiple sorption sites.* Water Research, 2016. **99**(Supplement C): p. 74-82.
25. Fernandes, M.M., et al., *Spectroscopic Identification of Ternary Cm-Carbonate Surface Complexes.* Environmental Science & Technology, 2010. **44**(3): p. 921-927.
26. Kadhim, Z.N., A.K. Ibraheem, and M.J. Al-assadi, *Effect of Citrate Salts of Li+, Na+ and K+ on Some Physical Properties of Ordinary Portland Cement (OPC).* 2017.
27. Stroh, J., et al., *Time-resolved in situ investigation of Portland cement hydration influenced by chemical admixtures.* Construction and Building Materials, 2016. **106**(Supplement C): p. 18-26.
28. Bessaies-Bey, H., et al., *Organic admixtures and cement particles: Competitive adsorption and its macroscopic rheological consequences.* Cement and Concrete Research, 2016. **80**(Supplement C): p. 1-9.
29. Plank, J., et al., *Chemical admixtures — Chemistry, applications and their impact on concrete microstructure and durability.* Cement and Concrete Research, 2015. **78**(Part A): p. 81-99.
30. Kutus, B., et al., *Formation of mono-and binuclear neodymium (iii)–gluconate complexes in aqueous solutions in the pH range of 2–8.* Dalton Transactions, 2017. **46**(18): p. 6049-6058.
31. Zhang, Z., et al., *Complexation of gluconic acid with Nd (III) in acidic solutions: A thermodynamic study.* Journal of Alloys and Compounds, 2007. **444**: p. 470-476.
32. Giroux, S., et al., *Complexes of praseodymium(III) with d-gluconic acid.* Polyhedron, 2000. **19**(13): p. 1567-1574.

33. Svoronos, D.-R., et al., *Citric complexes and neodymium citrate: NdCit, 3H2O.* Journal of Inorganic and Nuclear Chemistry, 1981. **43**(7): p. 1541-1545.
34. Rojo, H., et al., *Nd (III)/Cm (III) complexation with gluconate in NaCl and CaCl 2 alkaline solutions: solubility and TRLFS studies.* 2014.
35. Heller, A., et al., *Curium (III) citrate speciation in biological systems: a europium (III) assisted spectroscopic and quantum chemical study.* Dalton Transactions, 2012. **41**(45): p. 13969-13983.
36. Wall, N.A., et al., *Complexation of americium with humic, fulvic and citric acids at high ionic strength.* Radiochimica Acta, 2002. **90**(9-11): p. 563-568.
37. Lackovic, K., et al., *Modeling the adsorption of citric acid onto Muloorina illite and related clay minerals.* Journal of Colloid and Interface Science, 2003. **267**(1): p. 49-59.
38. Ramos, M.E., et al., *Modeling the Adsorption of Oxalate onto Montmorillonite.* Langmuir, 2015. **31**(43): p. 11825-11834.
39. Ramos, M.E. and F.J. Huertas, *Adsorption of lactate and citrate on montmorillonite in aqueous solutions.* Applied Clay Science, 2014. **90**(Supplement C): p. 27-34.
40. Zhao, H., et al., *Adsorption of organic molecules on mineral surfaces studied by first-principle calculations: A review.* Advances in Colloid and Interface Science, 2018.
41. Bradbury, M.H., Baeyens, B., *Experimental and Modelling Investigations on Na-illite: Acid-Base Behaviour and the Sorption of Strontium, Nickel, Europium and Uranyl*, in *PSI Bericht Nr. 05-02*. 2005.
42. Bradbury, M.H. and B. Baeyens, *Sorption of Eu on Na- and Ca-montmorillonites: Experimental investigations and modelling with cation exchange and surface.* Geochimica Et Cosmochimica Acta, 2002. **66**(13): p. 2325-2334.
43. Macpherson, G., *CO2 distribution in groundwater and the impact of groundwater extraction on the global C cycle.* Chemical Geology, 2009. **264**(1-4): p. 328-336.
44. Sigg, L. and W. Stumm, *Aquatische Chemie: Einführung in die Chemie natürlicher Gewässer*. 2016: vdf Hochschulverlag AG.
45. Parkhurst, D.L., Appelo, C.A.J., *Description of input and examples for PHREEQC ersion 3 – A computer program for speciation, batch-reaction, one-dimensional transport and inverse geochemical calculations* 2012: USGS.
46. *Brookhaven Instruments Corp. Data Analysis Software (BI-ISDA), version 8.0, Brookhaven Instruments Corp. (www.bic.com), Holtsville, NY, 1990*.
47. Buckau, G., *Komplexierung von Americium (III) mit Huminstoffen in natürlichen Grundwässern*. 1991, Freie Universität Berlin: Berlin.
48. Katz, J. and G. Seaborg, *„Morss, LR: The Chemistry of the Actinide Elements, vol. 2*. 1986, Chapman and Hall, New York.
49. Persson, I., *Hydrated metal ions in aqueous solution: How regular are their structures?* Pure and Applied Chemistry, 2010. **82**(10): p. 1901-1917.
50. Choppin, G.R., *Solution chemistry of the actinides.* Radiochimica acta, 1983. **32**(1-3): p. 43-54.
51. Choppin, G.R. and E.N. Rizkalla, *Solution chemistry of actinides and lanthanides.* Handbook on the physics and chemistry of rare earths, 1994. **18**: p. 559-590.

52. Hixon, A.E. and B.A. Powell, *Plutonium environmental chemistry: mechanisms for the surface-mediated reduction of Pu (v/vi).* Environmental Science: Processes & Impacts, 2018. **20**(10): p. 1306-1322.
53. Pearson, R.G., *Hard and soft acids and bases.* Journal of the American Chemical Society, 1963. **85**(22): p. 3533-3539.
54. Guillaumont, R., et al., *Update on the chemical thermodynamics of uranium, neptunium, plutonium, americium and technetium*. 2003, Amsterdam, The Netherlands: Elsevir B.V.
55. Moll, H., V. Brendler, and G. Bernhard, *Aqueous curium (III) phosphate species characterized by time-resolved laser-induced fluorescence spectroscopy.* Radiochimica Acta International journal for chemical aspects of nuclear science and technology, 2011. **99**(12): p. 775-782.
56. Panak, P.J., et al., *Complexation of Cm(III) with aqueous silicic acid.* Radiochimica Acta, 2005. **93**(3): p. 133-139.
57. Lindqvist-Reis, P., Klenze, R., Schubert, G., Fanghanel, T., *Hydration of Cm3+ in aqueous solution from 20 to 200 degrees C. A time-resolved laser fluorescence spectroscopy study.* Journal of Physical Chemistry B, 2005. **109**(7): p. 3077-3083.
58. Rabung, T., et al., *A TRLFS study of Cm(III) hydroxide complexes in alkaline CaCl2 solutions.* Radiochimica Acta, 2008. **96**(9-11): p. 551-559.
59. Neck, V., et al., *Thermodynamics of trivalent actinides and neodymium in NaCl, MgCl2, and CaCl2 solutions: Solubility, hydrolysis, and ternary Ca-M(III)-OH complexes.* Pure and Applied Chemistry, 2009. **81**(9): p. 1555-1568.
60. Fanghanel, T., et al., *Thermodynamics of Cm(III) in concentrated electrolyte solutions. Carbonate complexation at constant ionic strength (1 m NaCl).* Radiochimica Acta, 1998. **82**: p. 47-53.
61. Shi, K., et al., *Solubility of Eu2(SeO3)3 and sorption of Eu(III) onto TiO2 in the presence of Se(IV).* Journal of Radioanalytical and Nuclear Chemistry, 2012. **292**(3): p. 1277-1283.
62. Schmeide, K., et al., *Interaction of uranium(VI) with various modified and unmodified natural and synthetic humic substances studied by EXAFS and FTIR spectroscopy.* Inorganica Chimica Acta, 2003. **351**: p. 133-140.
63. Schmeide, K., et al., *Plutonium(III) complexation by humic substances studied by X-ray absorption fine structure spectroscopy.* Inorganica Chimica Acta, 2006. **359**(1): p. 237-242.
64. Rabung, T., et al., *The Influence of Anionic Ligands on the Sorption Behaviour of Eu(III) on Natural Hematite.* Radiochim. Acta, 1998. **82**: p. 243.
65. Schüßler, W., et al. *Influence of humic substances on the actinide migration: Applicability of laboratory results to natural systems*. in *5. Workshop zur Sanierung der Hinterlassenschaften des Uranbergbaus "Chancen und Grenzen der geochemischen und Transportmodellierung bei der Verwahrung von Uranbergwerken und bei der Endlagerung radioaktiver Stoffe"*. 2000. Dresden, 18-19th May 2000.
66. Fröhlich, D.R., et al., *A thermodynamical and structural study on the complexation of trivalent lanthanides with a polycarboxylate based concrete superplasticizer.* Dalton Transactions, 2017. **46**(12): p. 4093-4100.
67. Fröhlich, D.R., et al., *A spectroscopic study of the complexation reaction of trivalent lanthanides with a synthetic acrylate based PCE-superplasticizer.*

Spectrochimica Acta Part A: Molecular and Biomolecular Spectroscopy, 2019. **207**: p. 270-275.
68. Lippold, H. and M. Becker, *Complexation of Eu (III) with a polymeric cement additive as a potential carrier of actinides*. 2017.
69. Kitamura, A., et al., *Thorium and americium solubilities in cement pore water containing superplasticiser compared with thermodynamic calculations.* Journal of Radioanalytical and Nuclear Chemistry, 2013. **298**(1): p. 485-493.
70. Tits, J., E. Wieland, and M.H. Bradbury, *The effect of isosaccharinic acid and gluconic acid on the retention of Eu(III), Am(III) and Th(IV) by calcite.* Applied Geochemistry, 2005. **20**(11): p. 2082-2096.
71. appliquée, U.i.d.c.p.e., *Stability Constants of Metal-ion Complexes, with Solubility Products of Inorganic Substances: Part I. Organic Ligands*. 1957: Chemical Society.
72. Perrin, D.D., *Dissociation constants of organic bases in aqueous solution: supplement 1972*. 1972: Butterworths.
73. Giffaut, E., et al., *Andra thermodynamic database for performance assessment: ThermoChimie.* Applied Geochemistry, 2014. **49**(Supplement C): p. 225-236.
74. Tits, J., et al., J. Colloid Interface Sci., 2011. **359**: p. 248.
75. Gaona, X., et al., *Review of the complexation of tetravalent actinides by ISA and gluconate under alkaline to hyperalkaline conditions.* Journal of Contaminant Hydrology, 2008. **102**(3-4): p. 217-227.
76. Hufner, S., *Optical Spectra of Transparent Rare.* Earth Compounds (Academic Press. Inc, London, 1978), 1978.
77. Carnall, W. and H. Crosswhite, *Optical spectra and electronic structure of actinide ions in compounds and in solution*, in *The Chemistry of the Actinide Elements*. 1986, Springer. p. 1235-1277.
78. Richardson, F.S., *Vibronic coupling model for the intensities of f-f transitions in octahedral lanthanide (III) complexes AU - Faulkner, Thomas R.* Molecular Physics, 1978. **35**(4): p. 1141-1161.
79. Panak, P., R. Klenze, and J.I. Kim, *Untersuchung von intramolekularen Energietransferprozessen in Cm(III)- und Tb(III)-Komplexen mit organischen Liganden mit Hilfe der zeitaufgelösten Laserfluoreszenzspektrokopie*. 1996, Institute of Radiochemistry, Technical University of Munich: Munich.
80. Carnall, W. and K. Rajnak, *Electronic energy level and intensity correlations in the spectra of the trivalent actinide aquo ions. II. Cm3+.* The Journal of Chemical Physics, 1975. **63**(8): p. 3510-3514.
81. Beitz, J.V., *Laser-induced fluorescence studies of Cm3+ complexes in solution.* Radiochimica Acta, 1991. **52**(1): p. 35-40.
82. Cotton, S., *Lanthanide and actinide chemistry*. 2013: John Wiley & Sons.
83. Edelstein, N.M., et al., *Optical properties of Cm(III) in crystals and solutions and their application to Cm(III) speciation.* Coordination Chemistry Reviews, 2006. **250**(7): p. 948-973.
84. Horrocks, W.D. and D.R. Sudnick, *Lanthanide ion probes of structure in biology. Laser-induced luminescence decay constants provide a direct measure of the number of metal-coordinated water molecules.* Journal of the American Chemical Society, 1979. **101**(2): p. 334-340.
85. Kimura, T., et al., *Determination of the hydration number of Cm(III) in various aqueous solutions.* Radiochimica Acta, 1996. **72**(2): p. 61-64.

86. Panak, P., et al., *A Study of Intramolecular Energy-Transfer in Cm(Iii) Complexes with Aromatic Ligands by Time-Resolved Laser Fluorescence Spectroscopy.* Journal of Alloys and Compounds, 1995. **225**(1-2): p. 261-266.
87. Ewald, H., *Die Analyse und Deutung der Neodymsalzspektren.* Annalen der Physik, 1939. **426**(3): p. 209-236.
88. Iben, I.E., et al., *Gd3+ vibronic side band spectroscopy. New optical probe of Ca2+ binding sites applied to biological macromolecules.* Biophysical Journal, 1991. **59**(5): p. 1040-1049.
89. Chodos, S.L. and R. Satten, *Model calculation of vibronic sidebands in Cs2UBr6.* The Journal of Chemical Physics, 1975. **62**(6): p. 2411-2417.
90. Freed, S., *Spectra of ions in fields of various symmetry in crystals and solutions.* Reviews of Modern Physics, 1942. **14**(2-3): p. 105.
91. Lindqvist-Reis, P., et al., *Optical Spectra and Crystal-Field Levels of [Cm (H2O) 9] 3+ Ions with C 3 h Symmetry in Isotypic Rare-Earth Triflate and Ethyl Sulfate Salts.* The Journal of Physical Chemistry C, 2008. **113**(1): p. 449-458.
92. *Grimsel Test Site Investigation Phase V: The CRR final project report series II: Supporting laboratory experiments with radionuclides and bentonite colloids.*, in *Nagra Technical Report*, H. Geckeis and T. Missana, Editors. 2006, NAGRA: Wettingen.
93. Grim, R.E., *Clay mineralogy*. 1968, McGraw-Hill.
94. Bauer, A., et al., *The fate of smectite in KOH solutions.* American Mineralogist, 2006. **91**(8-9): p. 1313-1322.
95. Grindrod, P., M. Peletier, and H. Takase, *Mechanical interaction between swelling compacted clay and fractured rock, and the leaching of clay colloids.* Engineering Geology, 1999. **54**(1-2): p. 159-165.
96. Segad, M., et al., *Ca/Na Montmorillonite: Structure, Forces and Swelling Properties.* Langmuir, 2010. **26**(8): p. 5782-5790.
97. Montoya, V., et al., *Sorption of Sr, Co and Zn on illite: Batch experiments and modelling including Co in-diffusion measurements on compacted samples.* Geochimica et Cosmochimica Acta, 2018. **223**: p. 1-20.
98. Bauer, A. and G. Berger, *Kaolinite and smectite dissolution rate in high molar KOH solutions at 35 degrees and 80 degrees C.* Applied Geochemistry, 1998. **13**(7): p. 905-916.
99. Gaucher, E.C. and P. Blanc, *Cement/clay interactions – A review: Experiments, natural analogues, and modeling.* Waste Management, 2006. **26**(7): p. 776-788.
100. Altmann, S., Tournassat, C. Goutelard, F., Parneix, J.-C., Gimmi, T., Maes, N., , *Diffusion-driven transport in clayrock formations.* Applied Geochemistry, 2012. **27**(2): p. 463-478.
101. Glaus, M.A., Frick, S., Rossé, R., Van Loon, L. R., *Comparative study of tracer diffusion of HTO, 22Na and 36Cl in compacted kaolinite, illite and montmorillonite.* Geochim. Cosmochim. Acta, 2010. **74**(7): p. 1999.
102. Tournassat, C., et al., *The titration of clay minerals: II. Structure-based model and implications for clay reactivity.* Journal of Colloid and Interface Science, 2004. **273**(1): p. 234-246.
103. Tournassat, C., et al., *The titration of clay minerals: I. Discontinuous backtitration technique combined with CEC measurements.* Journal of Colloid and Interface Science, 2004. **273**(1): p. 224-233.
104. Helfferich, F.G., *Ion exchange kinetics--evolution of a theory*, in *Mass transfer and kinetics of ion exchange*. 1983, Springer. p. 157-179.

105. Hartmann, E., *Sorption von Ln (III)-An (III) und U (VI) an Tonmineralen und natürlichen Tongesteinen*. 2010, Karlsruher Inst. für Technologie, Diss., 2010.
106. Brechbühl, Y., et al., *Competitive sorption of carbonate and arsenic to hematite: combined ATR-FTIR and batch experiments.* Journal of colloid and interface science, 2012. **377**(1): p. 313-321.
107. Hiemstra, T., R. Rahnemaie, and W.H. van Riemsdijk, *Surface complexation of carbonate on goethite: IR spectroscopy, structure and charge distribution.* Journal of Colloid and Interface Science, 2004. **278**(2): p. 282-290.
108. Su, C.M. and D.L. Suarez, *In situ infrared speciation of absorbed carbonate on aluminum and iron oxide.* Clays and Clay Minerals, 1997. **45**(6): p. 814-825.
109. VAN GEEN, A., A.P. ROBERTSON, and J.O. LECKIE, *Complexation of Carbonate Species at the Goethite Surface - Implications for Adsorption of Metal Ions in Natural Waters.* Geochim. Cosmochim. Acta, 1994. **58**(9): p. 2073-2086.
110. Golubev, S.V., A. Bauer, and O.S. Pokrovsky, *Effect of pH and organic ligands on the kinetics of smectite dissolution at 25 °C.* Geochimica et Cosmochimica Acta, 2006. **70**(17): p. 4436-4451.
111. Noerpel, M.R. and J.J. Lenhart, *The impact of particle size on the adsorption of citrate to hematite.* Journal of Colloid and Interface Science, 2015. **460**: p. 36-46.
112. Nalet, C. and A. Nonat, *Ionic complexation and adsorption of small organic molecules on calcium silicate hydrate: Relation with their retarding effect on the hydration of C3S.* Cement and Concrete Research, 2016. **89**: p. 97-108.
113. Marques Fernandes, M., N. Vér, and B. Baeyens, *Predicting the uptake of Cs, Co, Ni, Eu, Th and U on argillaceous rocks using sorption models for illite.* Applied Geochemistry, 2015. **59**: p. 189-199.
114. Huittinen, N., et al., *New insight into Cm(III) interaction with kaolinite – Influence of mineral dissolution.* Geochimica Et Cosmochimica Acta, 2012. **99**(0): p. 100-109.
115. Stumpf, T., et al., *Spectroscopic study of Cm(III) sorption onto gamma-alumina.* Journal of Colloid and Interface Science, 2001. **238**(1): p. 219-224.
116. Hartmann, E., et al., *A Spectroscopic Characterization and Quantification of M(III)/Clay Mineral Outer-Sphere Complexes.* Environmental Science & Technology, 2008. **42**(20): p. 7601-7606.
117. Bradbury, M.H.B.B. and J. Lützenkirchen, *Surface Complexation Modelling*. 2006.
118. Bradbury, M.H. and B. Baeyens, *Modelling the sorption of Mn(II), Co(II), Ni(II), Zn(II), Cd(II), Eu(III), Am(III), Sn(IV), Th(IV), Np(V) and U(VI) on montmorillonite: Linear free energy relationships and estimates of surface binding constants for some selected heavy metals and actinides.* Geochimica Et Cosmochimica Acta, 2005. **69**: p. 875-892.
119. Geckeis, H., et al., *Mineral–Water Interface Reactions of Actinides.* Chemical Reviews, 2013. **113**(2): p. 1016-1062.
120. Fröhlich, D., et al., *Sorption of neptunium (V) on Opalinus Clay under aerobic/anaerobic conditions.* Radiochimica Acta International journal for chemical aspects of nuclear science and technology, 2011. **99**(2): p. 71-77.
121. Fröhlich, D.R., et al., *Speciation of Np (V) uptake by Opalinus Clay using synchrotron microbeam techniques.* Analytical and bioanalytical chemistry, 2012. **404**(8): p. 2151-2162.

122. Marsac, R., et al., *Neptunium redox speciation at the illite surface.* Geochimica et Cosmochimica Acta, 2015. **152**: p. 39-51.
123. Altmaier, M., et al., *THEREDA. Thermodynamic reference database. Summary of final report*. 2011, Gesellschaft fuer Anlagen-und Reaktorsicherheit mbH (GRS).
124. Poinssot, C., Baeyens, B.,Bradbury, M.H., *Experimental studies of Cs, Sr, Ni and Eu sorption on Na-illite and the modelling of Cs sorption*, in *PSI Bericht Nr. 99-06* 1999.
125. Reinholdt, M., et al., *Fluorine Route Synthesis on Montmorillonite Containing Mg or Zn and Characterization by XRD, Thermal Analysis, MAS NMR, and EXAFS Spectroscopy.* Eur. J. Inorg. Chem., 2001. **11**: p. 2831.
126. Soltermann, D., et al., *Competitive Fe(II)–Zn(II) Uptake on a Synthetic Montmorillonite.* Environmental Science & Technology, 2013. **48**(1): p. 190-198.
127. Atkins, P.W. and J. De Paula, *Physikalische chemie*. 2013: John Wiley & Sons.
128. Altmaier, M., et al., *Solid-liquid equilibria of Mg(OH)2(cr) and Mg2(OH)3Cl·4H2O(cr) in the system Mg-Na-H-OH-Cl-H2O at 25°C.* Geochimica et Cosmochimica Acta, 2003. **67**(19): p. 3595-3601.
129. Neethirajan, S., D. Jayas, and S. Sadistap, *Carbon dioxide (CO 2) sensors for the agri-food industry—a review.* Food and Bioprocess Technology, 2009. **2**(2): p. 115-121.
130. Chukanov, N.V. and A.D. Chervonnyi, *Infrared spectroscopy of minerals and related compounds*. 2016: Springer.
131. Brunauer, S., P.H. Emmett, and E. Teller, J. Am. Chem. Soc., 1938. **60**: p. 309.
132. Churakov, S.V., *Ab Initio Study of Sorption on Pyrophyllite: Structure and Acidity of the Edge Sites.* The Journal of Physical Chemistry B, 2006. **110**(9): p. 4135-4146.
133. LIPPERT, B.G., J.H. PARRINELLO, and MICHELE, *A hybrid Gaussian and plane wave density functional scheme.* Molecular Physics, 1997. **92**(3): p. 477-488.
134. VandeVondele, J., et al., *Quickstep: Fast and accurate density functional calculations using a mixed Gaussian and plane waves approach.* Computer Physics Communications, 2005. **167**(2): p. 103-128.
135. Hutter, J., et al., *cp2k: atomistic simulations of condensed matter systems.* Wiley Interdisciplinary Reviews: Computational Molecular Science, 2014. **4**(1): p. 15-25.
136. Adam, N., et al., *Incorporation of transuranium elements: coordination of Cm (III) to human serum transferrin.* Dalton Transactions, 2018. **47**(41): p. 14612-14620.
137. Trumm, M., et al., *A closer look on the coordination of soft nitrogen-donor ligands to Cm (iii): SO 3-Ph-BTBP.* Dalton Transactions, 2016. **45**(31): p. 12308-12311.
138. Harvie, C.E., N. Møller, and J.H. Weare, *The prediction of mineral solubilities in natural waters: The Na-K-Mg-Ca-H-Cl-SO4-OH-HCO3-CO3-CO2-H2O system to high ionic strengths at 25°C.* Geochimica et Cosmochimica Acta, 1984. **48**(4): p. 723-751.
139. Pitzer, K.S., *Ion interaction approach: theory and data correlation.* Activity coefficients in electrolyte solutions, 1991. **2**: p. 75-153.
140. Ciavatta, L., *The specific interaction theory in evaluating ionic equilibria.* Ann. Chim.(Rome), 1980. **70**: p. 551.

141. Fernandes, M.M., B. Baeyens, and M.H. Bradbury, *The influence of carbonate complexation on lanthanide/actinide sorption on montmorillonite.* Radiochimica Acta, 2008. **96**(9-11): p. 691-697.
142. BRADBURY, M.H. and B. BAEYENS, *A general application of surface complexation to modeling radionuclide sorption in natural systems.* Journal of Colloid and Interface Science, 1993. **158**: p. 364-371.
143. Rabung, T., et al., *Sorption of Eu(III)/Cm(III) on Ca-montmorillonite and Na-illite. Part 1: Batch sorption and time-resolved laser fluorescence spectroscopy experiments.* Geochimica Et Cosmochimica Acta, 2005. **69**(23): p. 5393-5402.
144. Missana, T., U. Alonso, and M. García-Gutiérrez, *Experimental study and modelling of selenite sorption onto illite and smectite clays.* Journal of Colloid and Interface Science, 2009. **334**(2): p. 132-138.
145. Villalobos, M. and J.O. Leckie, *Surface complexation modeling and FTIR study of carbonate adsorption to goethite.* Journal of colloid and interface science, 2001. **235**(1): p. 15-32.
146. Wijnja, H. and C. Schulthess, *ATR–FTIR and DRIFT spectroscopy of carbonate species at the aged γ-Al2O3/water interface.* Spectrochimica Acta Part A: Molecular and Biomolecular Spectroscopy, 1999. **55**(4): p. 861-872.
147. Wijnja, H. and C. Schulthess, *Carbonate adsorption mechanism on goethite studied with ATR–FTIR, DRIFT, and proton coadsorption measurements.* Soil Science Society of America Journal, 2001. **65**(2): p. 324-330.
148. Alliot, C., et al., *Effect of aqueous acetic, oxalic and carbonic acids on the adsorption of americium onto α-alumina.* Radiochimica Acta, 2005. **93**(8): p. 435-442.
149. Roonasi, P. and A. Holmgren, *An ATR‐FTIR study of carbonate sorption onto magnetite.* Surface and Interface Analysis, 2010. **42**(6‐7): p. 1118-1121.
150. Romanov, V.N., *Evidence of irreversible CO2 intercalation in montmorillonite.* International Journal of Greenhouse Gas Control, 2013. **14**: p. 220-226.
151. Karakassides, M.A., D. Gournis, and D. Petridis, *An Infrared Reflectance Study of Si–O Vibrations in Thermally Treated Alkali- Saturated Montmorillonites*, in *Clay Minerals*. 1999. p. 429.
152. Su, C. and D.L. Suarez, *IN SITU INFRARED SPECIATION OF ADSORBED CARBONATE ON ALUMINUM AND IRON OXIDES.* Clays and Clay Minerals, 1997. **45**(6): p. 814-825.
153. Hartmann, E., Brendebach, B., Polly, R., Geckeis, H., Stumpf, T., *Characterization and quantification of Sm(III)/ and Cm(III)/clay mineral outer-sphere species by TRLFS in D2O and EXAFS studies.* Journal of Colloid and Interface Science, 2011. **353**(2): p. 562-568.
154. Marques Fernandes, M., et al., *Spectroscopic identification of ternary Cm - Carbonate surface complexes.* Environmental Science and Technology, 2010. **44**(3): p. 921-927.
155. Catalano, J.G. and G.E. Brown, *Uranyl adsorption onto montmorillonite: Evaluation of binding sites and carbonate complexation.* Geochimica Et Cosmochimica Acta, 2005. **69**(12): p. 2995-3005.
156. Müller, K., et al., *Sorption of U (VI) at the TiO2–water interface: An in situ vibrational spectroscopic study.* Geochimica et Cosmochimica Acta, 2012. **76**: p. 191-205.
157. Tournassat, C., et al., *Modeling uranium (VI) adsorption onto montmorillonite under varying carbonate concentrations: A surface complexation model*

accounting for the spillover effect on surface potential. Geochimica et Cosmochimica Acta, 2018. **220**: p. 291-308.
158. Bernhard, G., et al., *Uranyl(VI) carbonate complex formation: Validation of the Ca2UO2(CO3)(3)(aq.) species.* Radiochimica Acta, 2001. **89**(8): p. 511-518.
159. Tasi, A., et al., *Thermodynamic description of the plutonium – α–d–isosaccharinic acid system ii: Formation of quaternary Ca(II)–Pu(IV)–OH–ISA complexes.* Applied Geochemistry, 2018. **98**: p. 351-366.
160. Stumpf, T., et al., *Uptake of trivalent actinides (curium(III)) by hardened cement paste: a time-resolved laser fluorescence spectroscopy study.* Journal of Colloid and Interface Science, 2004. **276**(1): p. 118-124.
161. Grangeon, S., et al., *Structure and reactivity of nanocrystalline calcium silicate hydrates: the parallel with clay minerals.* Calcium-Silicate Hydrates Containing Aluminium: CASH II, 2018: p. 11.
162. Geckeis, H., et al., *Annual Report 2013/Institute for Nuclear Waste Disposal.(KIT Scientific Reports; 7664)*. Vol. 7664. 2015: KIT Scientific Publishing.
163. Geckeis, H., M. Altmaier, and S. Fanghänel, *Annual Report 2015/Institute for Nuclear Waste Disposal.(KIT Scientific Reports; 7725)*. Vol. 7725. 2017: KIT Scientific Publishing.

7. Appendix

7.1. Carbonate coverage of strong sites

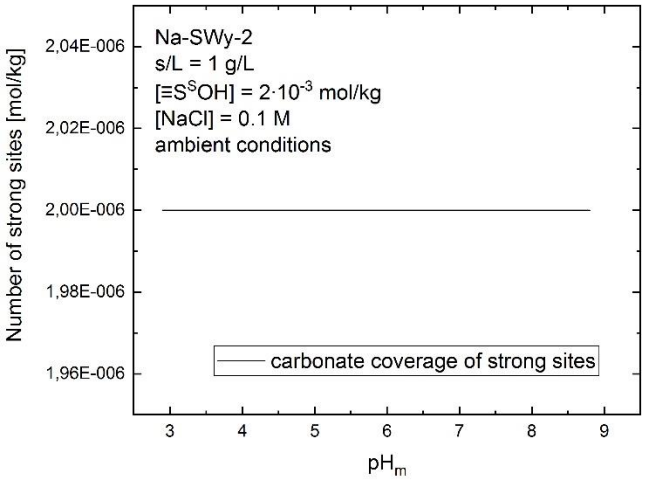

Figure 7.1: Model calculation of the carbonate coverage of clay mineral strong sites as function of pH_m in equilibrium with ambient CO_2 ($p_{CO2} = 10^{-3.3}$ bar), according to the surface complexation model developed in the present work. With respect to the s/l ratio 100 % of the available strong sites are loaded with carbonate.

7.2. Concentration depending studies Eu(III)-GLU-illite

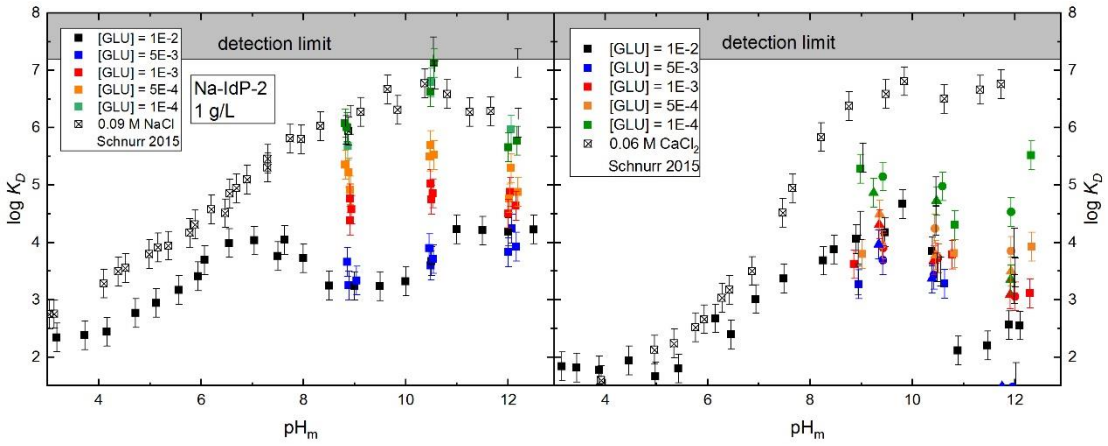

Figure 7.2: Eu(III) sorption onto illite under variation of the gluconate concentration in diluted and concentrated NaCl (left, 0.1 M squares, 1 M circles, 3 M triangles) and $CaCl_2$ (right, 0.1 M squares, 0.6 M circles, 2 M triangles) solutions at pH = 9, 10.5, 12. Data with constant gluconate concentration ([GLU] = 0.01 M, closed black symbols) and in absence of gluconate (open symbols, 0.09 M NaCl / 0.06 M $CaCl_2$ Schnurr *et al.* **[17]**) are added for comparison. Equal ligand concentrations are highlighted with the same colours and equal ionic strength with the same shape of symbols.

7.3. TRFLS spectra of the Cm(III)-GLU-Illite system

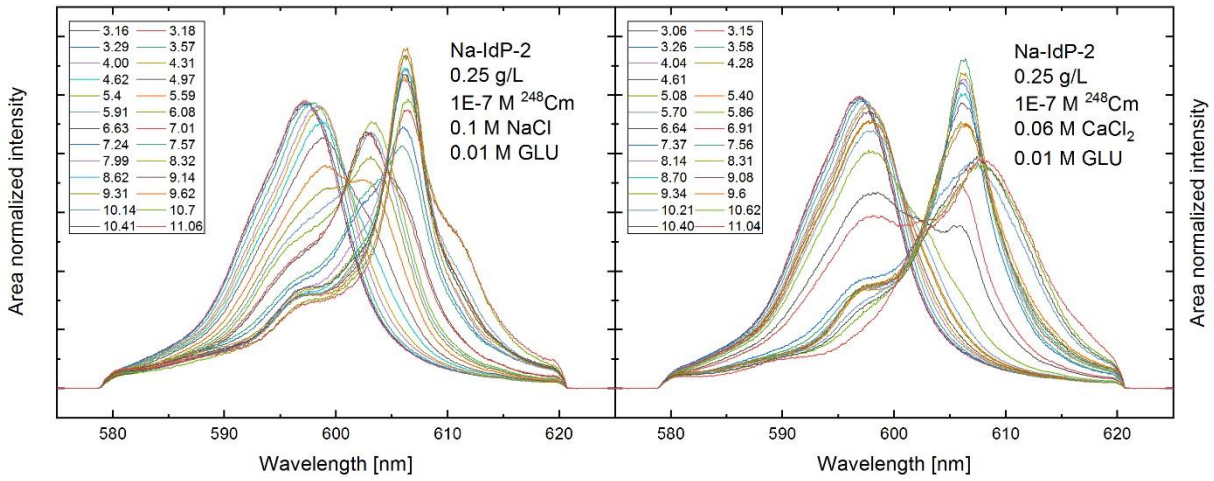

Figure 7.3: Fluorescence spectra of Cm(III) adsorbed onto montmorillonite as function of the pH in presence of 0.01 M gluconate in 0.1 M NaCl (left) and 0.06 M $CaCl_2$ (right).

7.4. $Ca_3(Cit)_2{:}4{\cdot}H_2O$ solubility

The total citrate concentration in calcium containing solutions is controlled by a binary Ca-Citrate phase (Ca3(Cit)2:4H2O(s)). The pH dependent solubility of Ca3(Cit)2:4H2O(s) was calculated as a function of pH using the geochemical code *PhreeqC* [45] with the *Thermochimie* database [73]. The lowest solubility of calcium citrate appears between pH = 7-10.1 resulting in a citrate concentration of 2.48 mM citrate. To avoid precipitation effects during batch sorption experiments the total citrate concentration was limited to 0.001 M.

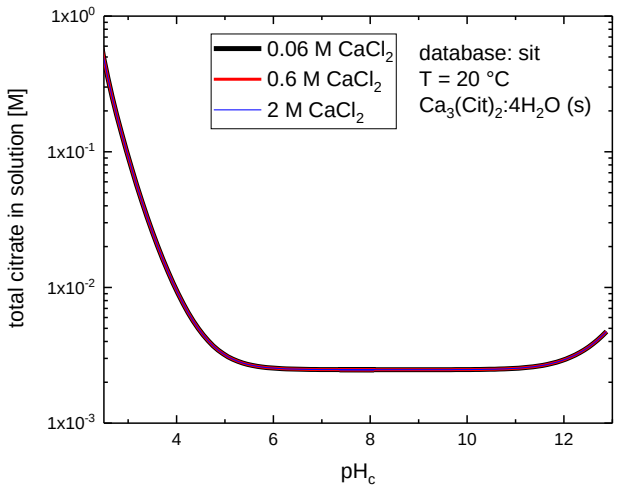

Figure 7.4: Calculated solubility of $Ca_3(Cit)_2{:}4H_2O$ as a function of pH in 0.06, 0.6, 2 M $CaCl_2$ electrolyte solutions. The calculation was performed using *PhreeqC* [45] and *Thermochimie* [73].

7.5. Long-term study: Evolution of batch sorption experiments at high pH

The adsorption of Eu(III) and Cm(III) onto montmorillonite, illite and iron free montmorillonite was studied for 930 day under portlandite pore water conditions (sat. $Ca(OH)_2$, pH_{start}= 12.3) and a 0.1 M NaCl solution (pH_{start}= 12.3). This was to investigate the alteration of clay surfaces and their sorption capability when in contact with alkaline cement porewaters. A slight decrease in pH was observed, ΔpH ~ 0.3 in NaCl and ΔpH ~ 0.2 in $Ca(OH)_2$ electrolyte systems. A high retention of Eu(III) (log K_D > 5.5) was still observed over 930 days.

TRLFS

The adsorption of Cm(III) onto the different clay minerals was studied by TRLFS. In NaCl solution, a shift of the fluorescence emission wavelength to λ = 603.9 nm (illite), λ = 603 nm (montmorillonite) and λ = 608.2 nm (iron free montmorillonite, IFM) is observed (Figure 7.5, left). Comparable, but slightly lower (Δλ = 1-2 nm) peak positions were reported for adsorbed species onto illite and IFM within “short term” (48 h) sorption studies by Schnurr *et al.* [17]. A shift to higher wavelength (λ = 602.5-604 nm) after the addition of [Si] = $1 \cdot 10^{-3}$ M was also described in the same study and may explain a slight deviations in the present study. A significant difference between the natural clay minerals illite and montmorillonite is observed by a strong shift to higher wavelength (λ = 608.2 nm) observed for Cm(III) adsorbed to the synthetic iron free montmorillonite (IFM). It can be assumed that the high content of structural Mg^{2+} tends to dissolve and reprecipitates as Brucite ($Mg(OH)_2$). Studies in pure Cm(III)-Brucite systems by Wiedemann *et al.* are supporting this assumption, a fluorescence emission at λ = 608.1 nm for Cm(III) in Brucite containing systems [162]. Measured fluorescence lifetimes are very short: for illite τ = 67±1 µs and for montmorillonite τ = 71±1 µs. The fluorescence lifetime measurements of IFM show biexponential decay with a short fluorescence lifetime of τ = 93±5 µs and a longer lifetime of τ = 248±5 µs. The shortening of the fluorescence lifetime of Cm(III) adsorbed to iron bearing illite at high pH was described by Rabung *et al.* [143] and is in good agreement with the present

study. The short lifetimes were explained by the alteration of the clay mineral at high pH, formation of FeOOH or Fe silicate secondary phases with Cm(III) associated to. In this case fluorescence quenching is known to occur resulting in short fluorescence emission lifetimes. In studies on the adsorption and incorporation of Cm(III) into Brucite a lifetime of τ >> 210 µs is reported [163]. This is supporting the assumption of the formation of Brucite in IFM containing samples after. The shorter lifetime of τ = 93±5 µs could not be explained by a comparison with literature data.

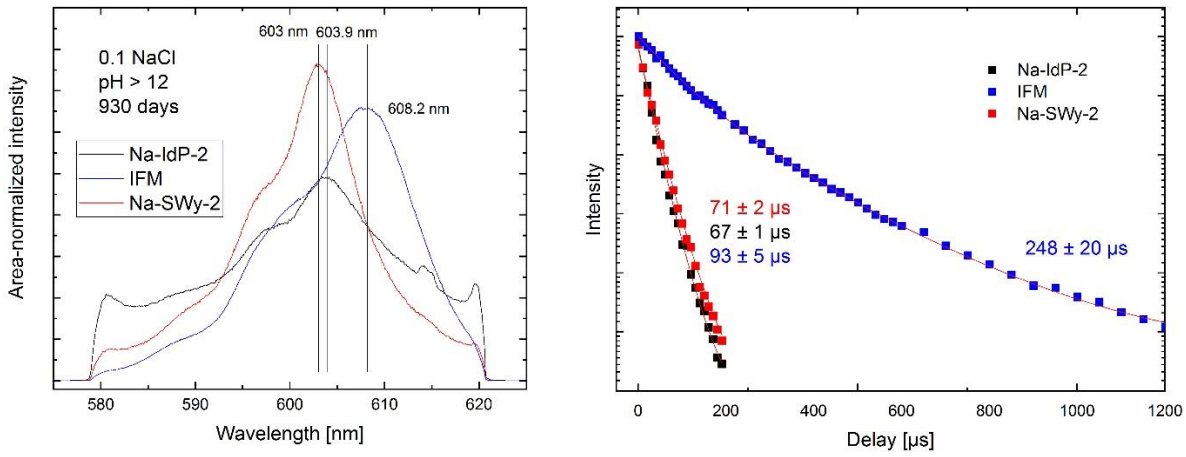

Figure 7.5: Fluorescence spectra of adsorbed Cm(III) onto illite (black), montmorillonite (red) and iron free montmorillonite (blue) after 930 days contacted with a 0.1 M NaCl solution at pH > 12 (left), corresponding fluorescence lifetime measurements (right).

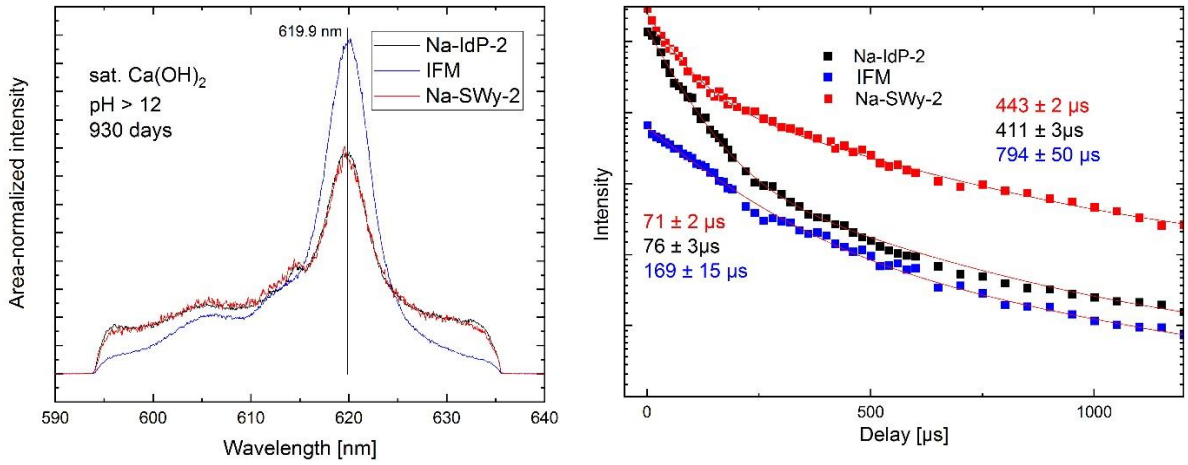

Figure 7.6: Fluorescence spectra of adsorbed Cm(III) onto illite (black), montmorillonite (red) and iron free montmorillonite (blue) after 930 days contacted with a saturated $Ca(OH)_2$ solution at pH > 12 (left), corresponding fluorescence lifetime measurements (right).

In presence of Ca^{2+} and under portlandite pore water conditions only a single feature is observed at λ = 619.9 nm for Cm(III) adsorbed onto the different clay minerals. The similar spectra were reported for Cm(III)-CSH (calcium silicate hydrates) sorption species by Stumpf *et al.* [160] and Rabung *et al.* [143]. Due to a partly dissolution of the clay mineral in the hyperalkaline pH range [97], silicate as main component of the mineral and calcium from the electrolyte can form CSH phase. The adsorption or incorporation of Cm(III) to these phases is then possible.

XRD

XRD measurements were performed on untreated samples (c) and on samples contacted with hyperalkaline solutions (a: $Ca(OH)_2$; b: 0.1 M NaCl) as described above (Figure 7.7, Figure 7.8, Figure 7.9). In the absence of Ca^{2+} no significant changes in diffractograms are observed. Crystalline halite particles originate from dried electrolyte solution. In presence of Ca^{2+} a number of sharp signal are observed, which can't be attributed to the formation of crystalline Portlandite. The signal could be partly assigned to Levyne, a calcium aluminium silicate hydrate (CASH). But it can be assumed that not only one secondary phase forms but rather a mixture of solid, partly amorphous, phases.

SEM-EDS

SEM images and EDS analysis of untreated clay samples (Figure 7.10, Figure 7.11, Figure 7.12) and samples contacted with 0.1 M NaCl show no significant differences (Figure 7.13, Figure 7.14, Figure 7.15) over the period of 2 years. Samples contacted with $Ca(OH)_2$ solution show a change in morphology (SEM image, left : Figure 7.16, Figure 7.17, Figure 7.18) and chemical composition (EDS analysis, right). These analyses verify a change from clay mineral structures to CASH phases, where the secondary phase is partly overgrowing the initial clay mineral (Figure 7.18).

Conclusion

With the combination of batch sorption experiments over more than 2 years and spectroscopic techniques it was possible to observe structural changes on clay minerals in presence of Ca^{2+} ions. In the absence of Ca^{2+} no significant change in morphology were observed. The mineral phases in the Ca-system, originating from dissolution and reprecipitation processes, were partly identified as CASH phases. A distinct identification of specific CASH phases was not possible, due to the heterogeneity of the sample. Unaffected from structural changes of the solid a high retention of Eu(III) was observed under all applied conditions. As indicated by TRLFS measurements adsorbed Cm(III) species in sodium chloride systems and adsorbed or incorporated Cm(III) species in calcium chloride solution are observed. Both mechanisms, sorption and incorporation, are known for their capability to immobilize Ln(III)/An(III) sufficiently.

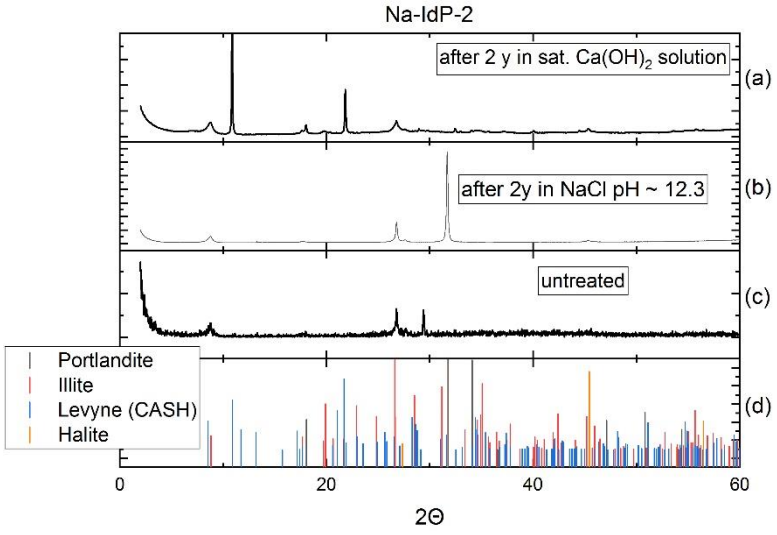

Figure 7.7: XRD measurements of illite du puy, contacted with a saturated $Ca(OH)_2$ solution (a) or 0.1 M NaCl pH=12.3 for 740 d (b) and untreated (as received). XRD pattern of portlandite, illite, Levyne (CASH) and halite are added for comparison from the PDF-2 database (d).

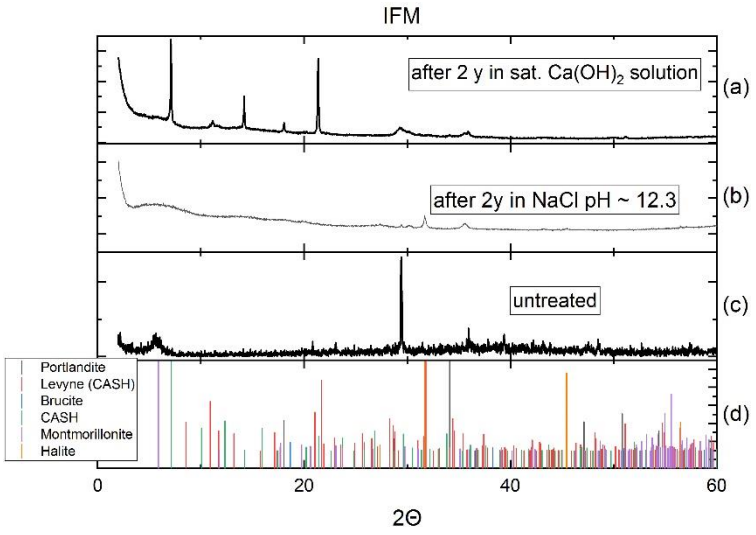

Figure 7.8: XRD measurements of iron free montmorillonite, contacted with a saturated $Ca(OH)_2$ solution (a) or 0.1 M NaCl pH=12.3 for 740 d (b) and untreated (as received). XRD pattern of portlandite, illite, Levyne (CASH) and halite are added for comparison from the PDF-2 database (d).

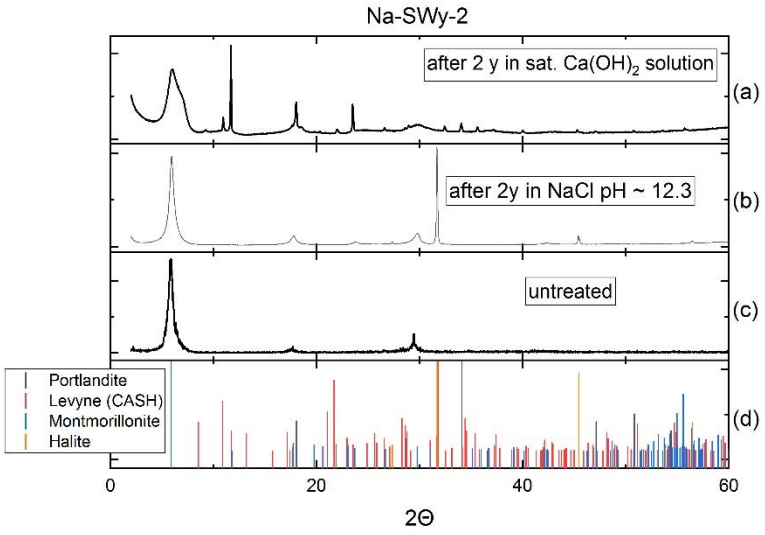

Figure 7.9: XRD measurements of illite du puy, contacted with a saturated $Ca(OH)_2$ solution (a) or 0.1 M NaCl pH=12.3 for 740 d (b) and untreated (as received). XRD pattern of portlandite, illite, Levyne (CASH) and halite are added for comparison from the PDF-2 database (d).

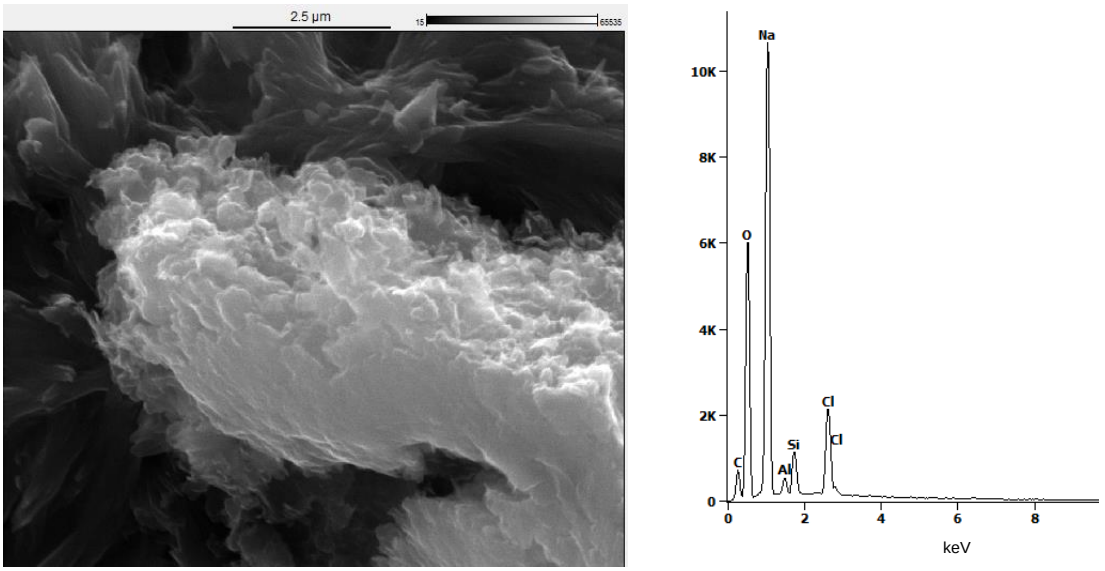

Figure 7.10: SEM image (left) and EDS analysis (right) of untreated illite du puy.

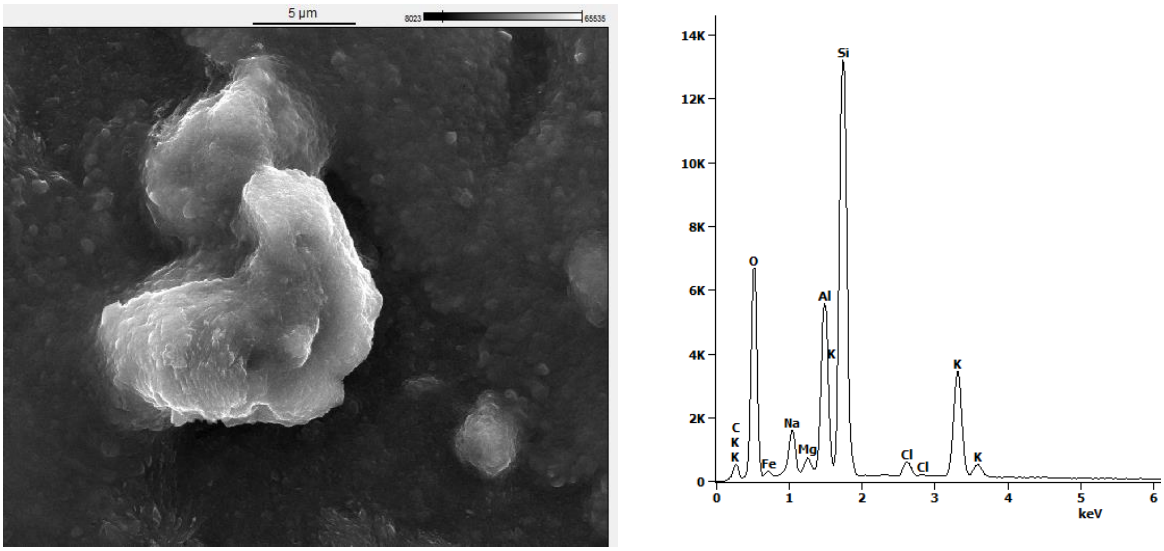

Figure 7.11: SEM image (left) and EDS analysis (right) of untreated iron free montmorillonite.

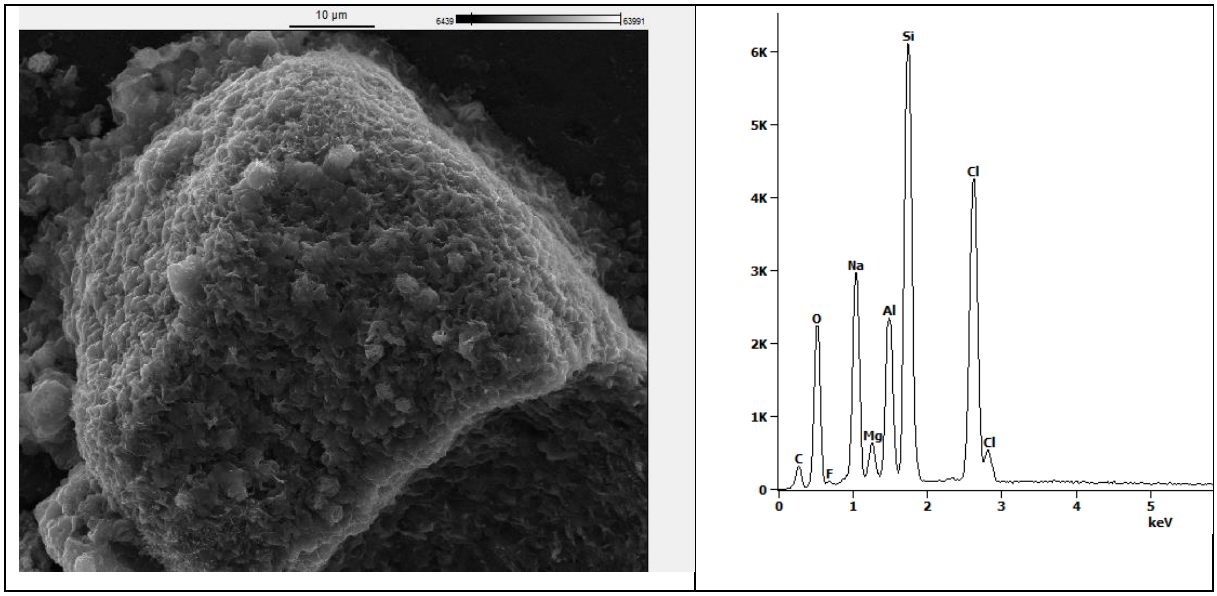

Figure 7.12: SEM image (left) and EDS analysis (right) of untreated montmorillonite.

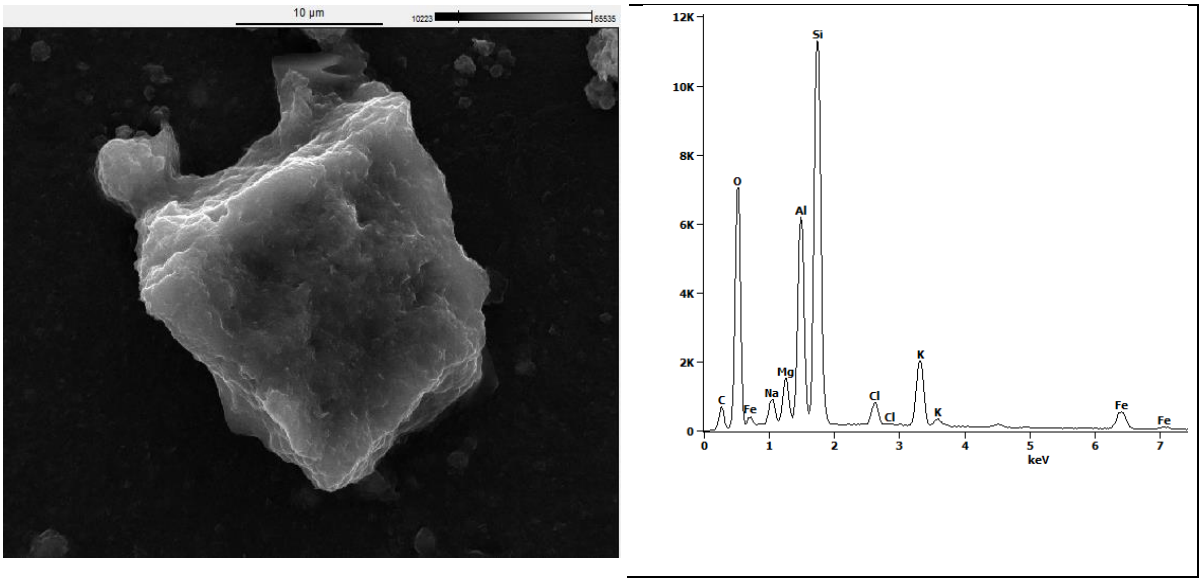

Figure 7.13: SEM image (left) and EDS analysis (right) of illite du puy contacted with 0.1 M NaCl for 740 days at pH > 12.

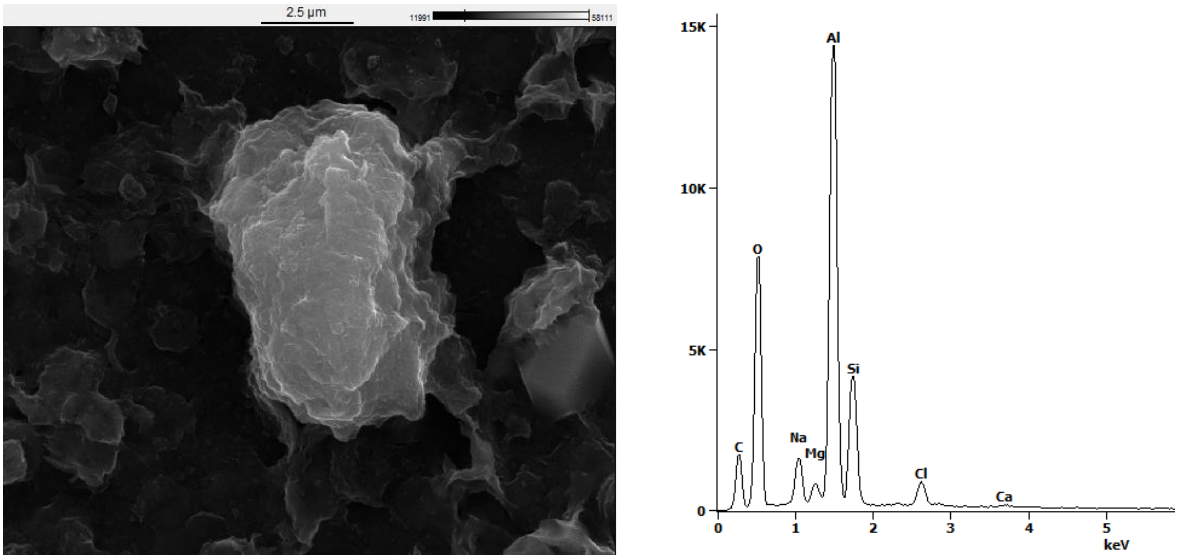

Figure 7.14: : SEM image (left) and EDS analysis (right) of iron free montmorillonite contacted with 0.1 M NaCl for 740 days at pH > 12.

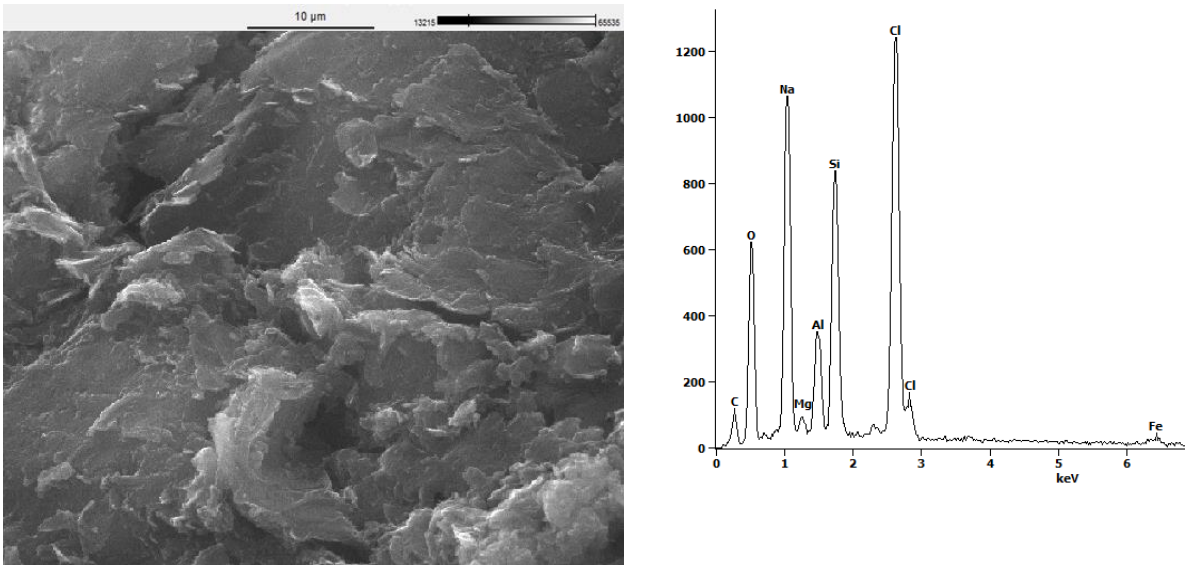

Figure 7.15: SEM image (left) and EDS analysis (right) of montmorillonite contacted with 0.1 M NaCl for 740 days at pH > 12.

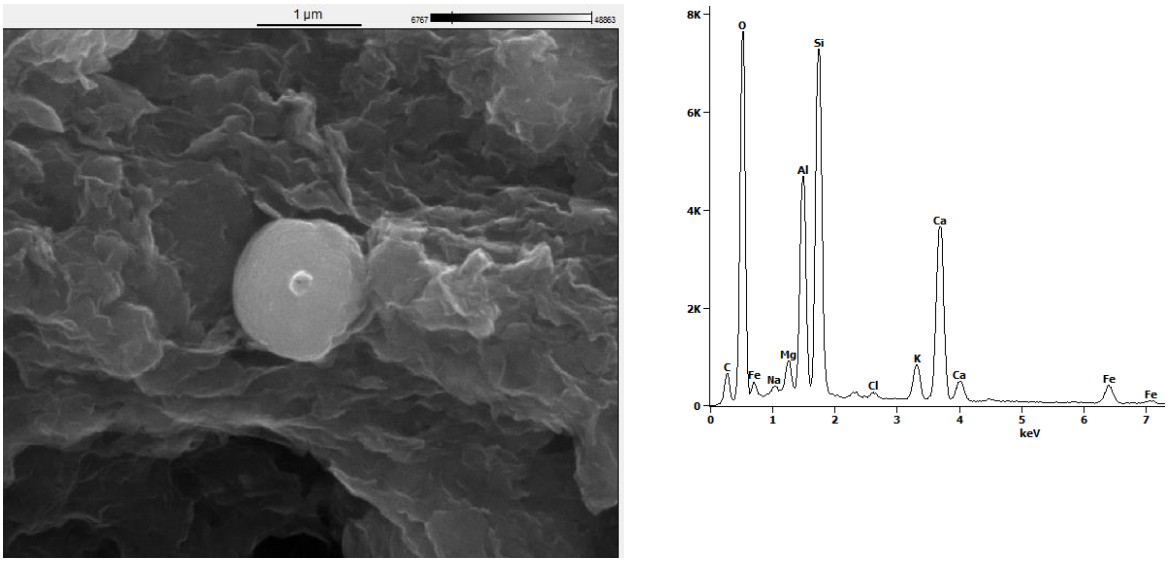

Figure 7.16: SEM image (left) and EDS analysis (right) of illite du puy contacted with sat. $Ca(OH)_2$ solution for 740 days at pH > 12.

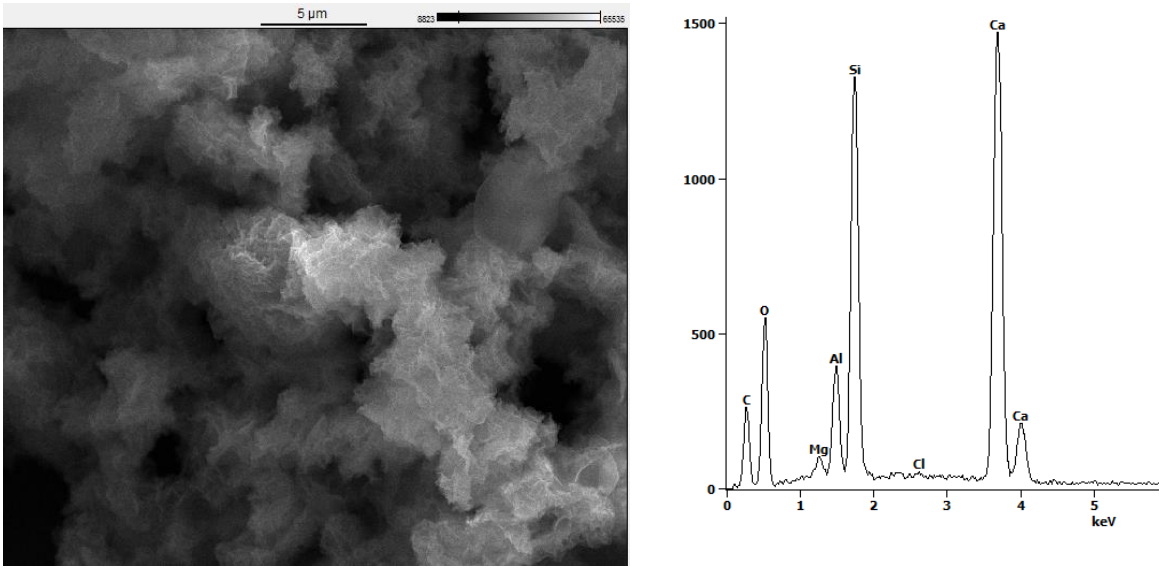

Figure 7.17: SEM image (left) and EDS analysis (right) of iron free montmorillonite contacted with sat. $Ca(OH)_2$ solution for 740 days at pH > 12.

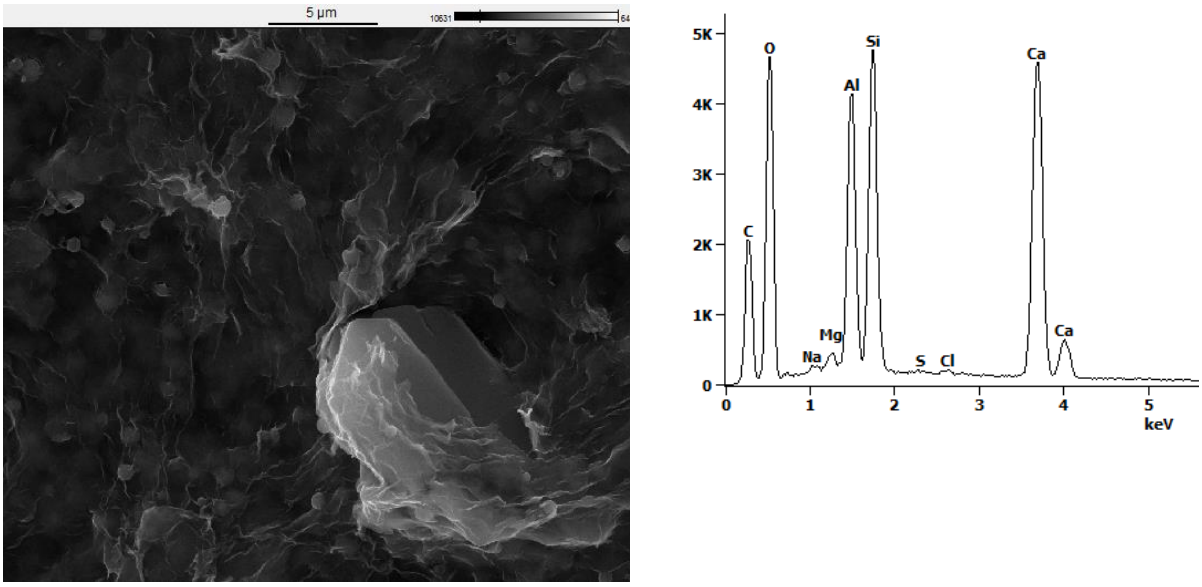

Figure 7.18: SEM image (left) and EDS analysis (right) of montmorillonite contacted with sat. $Ca(OH)_2$ solution for 740 days at pH > 12.

8. List of Figures

9. List of Tables

10. List of Publications

Peer Reviewes Publikationen:

F. Rieder, M. Trumm, N. Adam, A Skerencak-Frech, T. Rabung, P. J. Panak, & H. Geckeis “Probing clay mineral surfaces with vibronic side-band spectroscopy: experiment & theory of Cm(III) carbonate systems”, in preparation.

Oral Presentation:

F. Rieder, N. Adam, K. Hinz, M. Trumm, X. Gaona, T. Rabung, C. Marquardt, M. Altmaier, P. Panak & H. Geckeis „Rückhaltung von Radionukliden unter dem Einfluss von Zementadditiven: Löslichkeits-und Sorptionsstudien“ 13. Projektstatusgespräch zu BMWi-geförderten FuE-Arbeiten zur Entsorgung radioaktiver Abfälle, June 21, 2018, Karlsruhe, Germany.

Poster Presentation:

F. Rieder, T. Rabung & H. Geckeis „Influence of carbonate and gluconate on th Eu(III)/Cm(III) sorption onto clay minerals” 16th International Conference on the Chemistry and Migration Behaviour of Actinides and Fission Products in the Geo-sphere, September 10 - 15, 2017, Barcelona, Spain.